https://doi.org/10.5194/egusphere-2026-3434
Preprint. Discussion started: 9 September 2026

Physical and glaciochemical signals of the ~25.3 ka Ōruanui supereruption in ice cores across Antarctica

Alexander Mattin[1,2], Simon J. Barker[1], V. Holly L. Winton[2], Andrea Burke[3], Will Hutchison[3], Patrick Sugden[3], Kirstin Krüger[4], Alexa R. Van Eaton[5], Larry G. Mastin[5], Michael Sigl[4], Eric W. Wolff[6], Shuji Fujita[7,8], Kumiko Goto-Azuma[7], Ikumi Oyabu[7,8], Motohiro Hirabayashi[7], Anders Svensson[9], Magali Verkerk[10], Colin J. N. Wilson[1], Stephen B. Piva[1], Nels A. Iverson[11], Nelia W. Dunbar[11], Helle A. Kjær[9], Nancy A. N. Bertler[2,12], Mirko Severi[13], Andrei V. Kurbatov[14], and Dominic A. Winski[14]

[1]School of Geography, Environment and Earth Sciences, Victoria University of Wellington, Wellington, 6140, New Zealand
[2]Antarctic Research Centre, Victoria University of Wellington, Wellington, 6140, New Zealand
[3]School of Earth and Environmental Sciences, University of St Andrews, St Andrews, KY16 9AJ, UK
[4]Department of Geosciences, University of Oslo, Oslo, NO-0316, Norway
[5]U.S. Geological Survey, Cascades Volcano Observatory, U.S. Geological Survey, Vancouver, Washington, 98683, USA
[6]Department of Earth Sciences, University of Cambridge, Cambridge, CB2 3EQ, UK
[7]National Institute of Polar Research, Tokyo, 190-8518, Japan
[8]Polar Science Program, Graduate Institute for Advanced Studies (SOKENDAI), Tokyo 190-8518, Japan
[9]Physics of Ice Climate and Earth, Niels Bohr Institute, University of Copenhagen, Copenhagen, 2200, Denmark
[10]Department of Earth and Environmental Sciences, University of Oxford, Oxford, OX1 3AN, UK
[11]Department of Earth and Environmental Science, Mexico Institute of Mining and Technology, Socorro, NM 87801, USA
[12]Earth Sciences New Zealand, National Isotope Centre, Lower Hutt, 5010, New Zealand
[13]Department of Chemistry "Ugo Schiff", University of Florence, Florence, 50121, Italy
[14]Climate Change Institute, University of Maine, Orono, 04469, USA

Correspondence to: Alexander Mattin (alexander.mattin@vuw.ac.nz)

Abstract

Supereruptions are the largest-scale explosive volcanic events, injecting large amounts of sulfate, halogens, and ash into the stratosphere, yet their resulting impacts on global climate and the environment remain uncertain. Polar ice cores can preserve glaciochemical anomalies (sulfate and conductivity) and volcanic glasses from past eruptions, providing hightemporal resolution records of their timing, source, and potential impacts on the climate and environment. We examined nine Antarctic ice cores to evaluate the variability in preservation of glaciochemical signatures from the youngest known supereruption, the ~25.3 ka Ōruanui event, from Taupō

https://doi.org/10.5194/egusphere-2026-3434
Preprint. Discussion started: 9 September 2026

volcano, New Zealand. We identified glaciochemical anomalies related to the eruption in six of these cores, and fingerprinted Ōruanui volcanic glass shard populations in three cores: West Antarctic Ice Sheet Divide (WDC06A), EPICA Dronning Maud Land (EDML) and Dome Fuji 2 (DF2). Shard sizes and abundances vary between sites, which we attribute to spatially heterogeneous dispersal of the volcanic plume due to varying transport and settling processes in the atmosphere, supported by model simulations of ash deposition across the Southern Hemisphere (SH). Glaciochemical signals also vary substantially between cores and are best explained by broadly uniform stratospheric sulfate transport followed by heterogeneous tropospheric deposition pathways, and varying site-specific post-depositional processes. We use ice core sulfate concentrations to refine estimates of sulfate deposition over Antarctica to ~270 kg km^{-2}, estimate a stratospheric sulfur injection of ~114 ± 33 Tg S, and estimate a maximum monthly global radiative forcing from the Ōruanui event of -8.6 W m^{-2}, suggesting that there were severe short-term global climatic impacts. Coupled chemistry climate model simulations (CESM2/WACCM6), constrained by stratospheric sulfur and variable halogen injection scenarios, indicate global average cooling of up to 3 K and stratospheric increases of aerosol optical depth (AOD) lasting 4-5 years, with ozone impacts potentially lasting beyond 5 years. However, consistent with other recent supereruption impact studies, our results suggest that the eruption likely did not trigger decadal-centennial scale climate shifts.

1 Introduction

Explosive volcanic eruptions are potentially important natural drivers of abrupt changes in Earth's climate and environment. Large-scale injection of sulfuric gases (e.g., SO_2) into the stratosphere results in the formation of sulfate aerosols that backscatter incoming solar radiation, reducing the amount reaching the surface. This can result in several degrees of global cooling in the years that follow, with the potential for widespread impacts on society (e.g., Robock, 2000; Oppenheimer, 2003; Sigl et al., 2015; Büntgen et al., 2020; Marshall et al., 2022). Our current understanding of volcanic-induced climatic cooling is mainly based on observations and reconstructions of climate from tree rings following the largest historic explosive eruptions in the past 2000 years (e.g., Rampino and Self, 1982; McCormick et al., 1995; Esper et al., 2013; Sigl et al., 2014, 2015; Stoffel et al., 2015; Wilson et al., 2016). For example, the 1991 Mount Pinatubo (7 – 11 Tg stratospheric S injection; Bluth et al., 1992; Guo et al., 2004) and 1815 Tambora (~ 30 Tg stratospheric S injection; Gao et al., 2008; Stoffel et al.,

https://doi.org/10.5194/egusphere-2026-3434
Preprint. Discussion started: 9 September 2026

2015; Fasullo et al., 2017) eruptions demonstrate the global climate impacts of some historic events, with up to two years of cooling of ~0.5 ºC and ~0.4–0.8 ºC, respectively (Stothers, 1984; McCormick et al., 1995; Parker et al., 1996; Self et al., 1996; Raible. et al., 2016). However, the geological record displays evidence of far larger eruptions, including those of supereruption magnitude (i.e., venting >450 km^3 of magma: Sparks et al., 2005; Self, 2006). By extrapolation, it has been suggested that such events may have had severe and long-lasting impacts on Earth's climate (Self, 2006; Self and Blake, 2008; Robock et al., 2009; Timmreck et al., 2010; Sigl et al., 2015; Brenna et al., 2020). But as no supereruptions have occurred in the historic era, and the number of well-preserved supereruption deposits is limited, opportunities to study the global impacts of such events are rare.

In the absence of direct observations, high-resolution proxy records are essential for improving our understanding of past volcanic eruptions and their impacts, Earth system feedbacks, and for constraining the potentially severe global consequences of future large magnitude explosive eruptions. Polar ice cores can provide high-resolution records of volcanic gas and ash emissions, preserving semi-continuous volcanic fallout signals through sulfate, electrical conductivity, and insoluble particle anomalies (e.g., Sigl et al., 2015; Lin et al., 2023; Piva et al., 2023a; Plunkett et al., 2023; Abbott et al., 2024). The presence and strength of these chemical and physical anomalies at any one ice core site can be highly variable depending on many factors including setting (e.g., coastal vs inland), climate and weather conditions at the time of eruption, accumulation rate and volcanic source region (e.g., Wolff et al., 2005; Gao et al., 2007, 2008; Gautier et al., 2016). Strong and widespread volcanic anomalies in ice cores have become a key tool for dating and linking individual ice core records (Sigl et al., 2015; Toohey & Sigl, 2017; Cole-Dai et al., 2021; Lin et al., 2022; Plunkett et al., 2023; Abbott et al., 2024). However, pinpointing volcanic signals becomes more challenging in deep ice, with increasing age uncertainties, high diffusion rates, and a lack of existing volcanic tie-points.

https://doi.org/10.5194/egusphere-2026-3434
Preprint. Discussion started: 9 September 2026

Volcanic events are commonly identified in ice cores using sulfate and/or conductivity anomalies, which act to link ice core chronologies within and between the polar ice sheets (Lemieux-Dudon et al., 2010; Buizert et al., 2018; Svensson et al., 2026); however, these anomalies cannot pinpoint an exact source. Enrichments of coarse-mode insoluble particles (3 - 10 µm) coinciding with volcanic acid anomalies have been recognised to be diagnostic for the presence of volcanic glass in ice cores (Plunkett et al., 2023, and references therein). These insoluble particle anomalies represent distinct glass shard horizons preserved in ice which can be geochemically characterised to elucidate the source volcano forming these fallout deposits (e.g., Dunbar et al., 2017; Abbott et al., 2021; Cook et al., 2022; Piva et al., 2023a; Hutchison et al., 2024a, 2024b; Innes et al., 2025). The detection, extraction, and analysis of volcanic glass shards is a useful tool for chemically fingerprinting large and distant eruptions that can transport trace amounts of glass over long distances to the poles (e.g., Piva et al., 2023a; Plunkett et al., 2023; Abbott et al., 2024; Harlan et al., 2026). Locating specific eruption deposits across multiple cores through glass shard geochemistry allows more confidence in matching volcanic signatures between cores (volcanic synchronisation) and can also provide insights into the variability of volcanic signals at different ice core sites (e.g., high versus low altitude, coastal versus continental). The detection of volcanic horizons across multiple ice cores, particularly those with the largest sulfate concentration anomalies, also offers unique insights into the timing and climate forcing of large magnitude volcanic events up to supereruption scale.

The Ōruanui event is the most recent supereruption on Earth at ~25.3 ka (Vandergoes et al., 2013; Dunbar et al., 2017; Wilson et al., 2021), originating from New Zealand's Taupō Volcanic Zone (TVZ) (**Fig. 1**). The Ōruanui eruption ejected ~530 km³ of rhyolitic magma (~1150 km³ of pumice and ash) in a complex phreatoplinian eruption, resulting in the caldera collapse of Taupō volcano (Wilson, 2001; Van Eaton & Wilson, 2013; Barker et al., 2021). The eruption occurred during the Last Glacial Maximum (LGM) and spread ash widely across New Zealand and the South Pacific region (Wilson 2001; Wilson et al., 2006; Vandergoes et al., 2013; Dunbar et al.,

https://doi.org/10.5194/egusphere-2026-3434
Preprint. Discussion started: 9 September 2026

2017; Barker et al., 2021). The largest and final eruptive phase produced voluminous pyroclastic density currents and associated coignimbrite fall deposits (unit 10). Based on its inferred volume (~365 km^3 bulk) and thickness at ultra distal sites more than 800 km from source (Wilson, 2001), this unit likely supplied the majority of ash transported to Antarctica. Through a petrological assessment, it is estimated that >130 Tg S was released over the total eruption sequence as well as up to 1800 Tg of chlorine release, suggesting a major potential for global climate impact (Sharpe et al., 2022). Distal pollen records show that vegetation changes occurred in direct response to ashfall and environmental changes (Piva et al., 2023b; Miller et al., 2026), but most sedimentary records do not provide high enough resolution to assess or deconvolve short-term (less than decadal) climate impacts. However, a compilation of high-resolution Antarctic ice cores offers a new opportunity to assess and quantify the climatic and environmental impacts of the Ōruanui eruption (Fig. 1).

Dunbar et al. (2017) first identified Ōruanui-derived glass shards in Antarctica at the WAIS Divide site, associated with the largest sulfate concentration anomaly over the past 67 ka in the WDC06A core (Sigl et al., 2016). The presence of material from this event provides an important time marker in ice core chronologies for the LGM. Building on these findings, our study analyses existing published and unpublished glaciochemical records of volcanic tracers from nine Antarctic ice cores, and further investigates six of these for physical evidence of the Ōruanui deposit to provide insights into the variable preservation of this event at different ice core sites. By integrating these measurements with modeling of volcanic ashfall and climate impacts, we re-estimate the total sulfate deposition from Ōruanui over Antarctica, and evaluate its effects on AOD, stratospheric ozone, and climate forcing. This work establishes Ōruanui as a robust chronological horizon across ice cores at a critical climate interval and refines the transport, deposition, and preservation of Ōruanui glaciochemical deposits across the Southern Ocean to Antarctica, to ultimately build a better understanding of the broader impacts of supereruptions.

https://doi.org/10.5194/egusphere-2026-3434
Preprint. Discussion started: 9 September 2026

2 Methods

2.1 Ice cores used in this study

Published and unpublished volcanogenic glaciochemical data (e.g., sulfate and insoluble particle concentrations, electrical conductivity) were compiled from nine ice cores across Antarctica (**Fig. 1**) over age intervals covering the Ōruanui eruption layer-counted ice core date of 25,318 ± 253 years BP from the WD2014 chronology (Sigl et al., 2016; Dunbar et al., 2017) to identify potential candidate anomalies. The glaciochemical data obtained also vary with different analysis types, sample resolution, and methods used by the different research groups. **Table 1** reports the ice cores, datasets, measurement systems, and data resolution used in this study. Non-sea-salt (nss) sulfate, calculated by correcting sulfate concentrations for the sea-salt-derived contribution estimated from sodium concentrations (further information in **Sect. 2.3**), is commonly used as a volcanic proxy in ice cores as it removes the marine contribution to sulfate concentration. However, nss sulfate cannot be calculated for some ice core records where sodium data are unavailable. Therefore, to enable consistent comparison across all ice cores, this study presents uncorrected sulfate concentration data.

The nine ice core sites are distributed across Antarctica, including both coastal and continental regions, with varying snow accumulation rates. At coastal sites such as RICE, high dust, sea-salt and marine biogenic input means volcanic signals are masked, but these can be enhanced using the close similarity of the liquid conductivity and largely sea-salt-derived calcium records. This is achieved by removing the calcium concentrations - from the conductivity record, which is measured through either liquid conductivity or using probes on solid ice samples (see **Table 1**). This yields a conductivity-to-calcium excess, or non-sea-salt (nss) conductivity (Kjær et al., 2016; Winstrup et al., 2019). Volcanic anomalies of interest were targeted based on the ice age of Ōruanui glass identified in the WDC06A ice core by Dunbar et al. (2017). This targeting was assisted by several cores having been already linked to the WD2014 age scale via synchronisation, including EPICA Dronning Maud Land

https://doi.org/10.5194/egusphere-2026-3434
Preprint. Discussion started: 9 September 2026

(EDML) (Buizert et al., 2018), South Pole Core (SPC-14) (Winski et al., 2019), EPICA Dome C (EDC) (Buizert et al., 2018), TALos Dome Ice CorE (TALDICE) (Buizert et al., 2018), and Skytrain (Mulvaney et al., 2023). The DF2 core was synchronised to the WD2014 chronology through volcanic matching of tie points between the DF2 DEP and the sulfur concentrations of the WDC06A core in the target interval. Ages between tie points were linearly interpolated with respect to depth. The Roosevelt Island Climate Evolution (RICE) core was examined using its independent age scale, which is in excellent agreement with WD2014 (RICE17: Lee et al., 2020) and the Vostok ice core was examined using the AICC2023 age scale (Bouchet et al., 2023). Some of these cores have also been synchronised with the EDC record, including EDML (Severi et al., 2007), DF1 (Fujita et al., 2015), Vostok (Parrenin et al., 2012), and TALDICE (Severi et al., 2012). Of the nine selected records, six were analysed in detail in this work: WDC06A, EDML, SPC-14, DF2, RICE, and Skytrain.

https://doi.org/10.5194/egusphere-2026-3434
Preprint. Discussion started: 9 September 2026

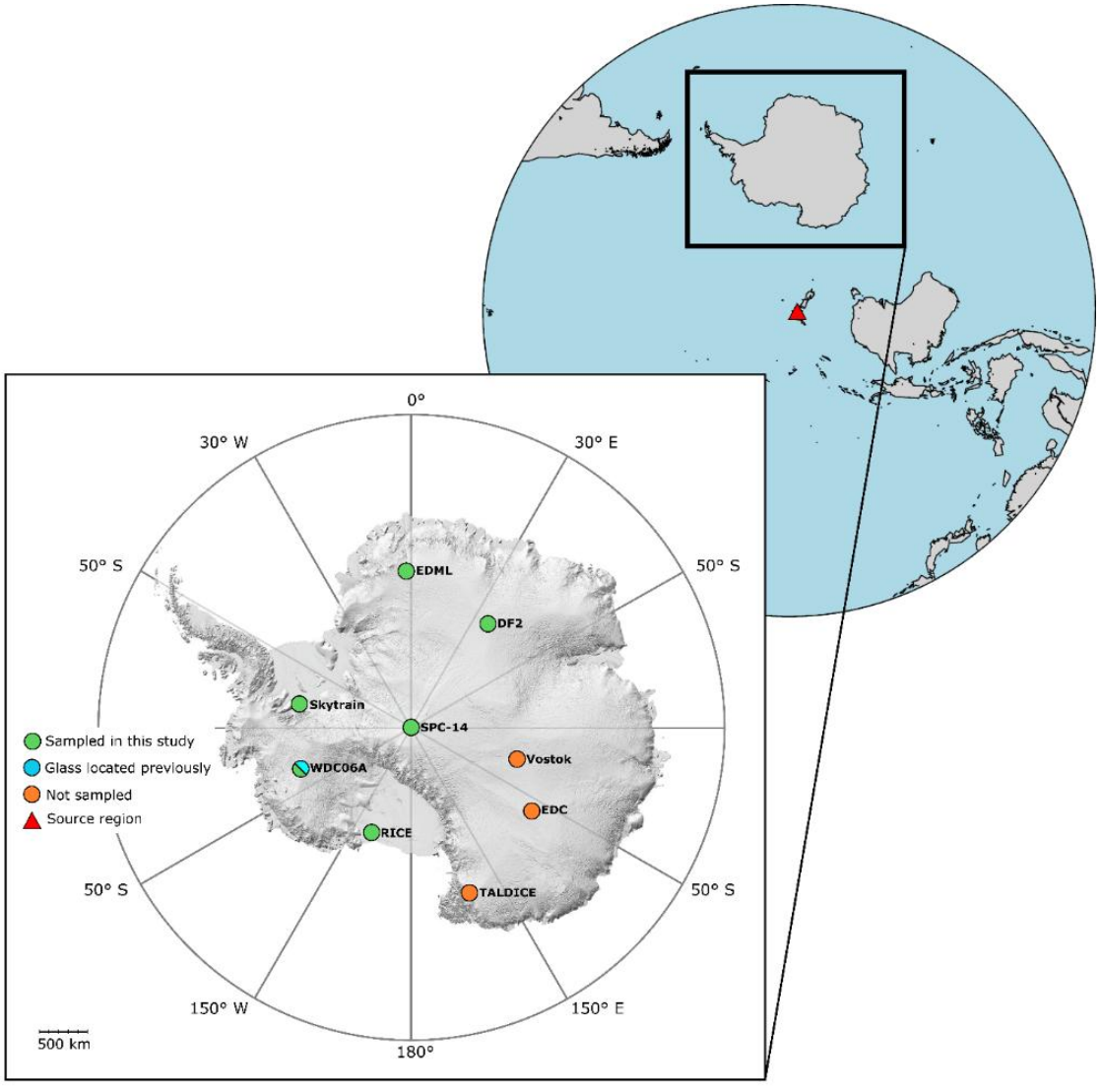

Figure 1: *Map showing the locations of the nine deep ice cores studyied in this paper. Basemap from Howat et al. (2019).*

https://doi.org/10.5194/egusphere-2026-3434
Preprint. Discussion started: 9 September 2026

Unpublished data from five cores used to identify signals over the eruption are summarised below and in **Table 1**.

- In the SPC-14 core, Electrical Conductivity Measurements (ECM) in the frozen core were made at the National Science Foundation Ice Core Facility with alternating-current ECM and direct-current ECM via a robotically controlled system consisting of two electrodes (Souney et al., 2021). Sulfate concentrations were analysed by ion chromatography on discrete samples using a Thermo Fisher Dionex ICS-5000 capillary ion chromatograph (Winski et al., 2019). Insoluble particles (1 – 5.7 µm) were measured as part of a Continuous Flow Analysis (CFA), using a Klotz Abakus particle counter after Winski et al. (2019) and Souney et al. (2021). Both sulfate concentrations and insoluble particle measurements were made at Dartmouth College, New Hampshire, USA.
- In the RICE core, liquid conductivity (3082 with micro flow cell 829, Amber Science) and calcium (Ca^{2+}) data (Traversi, 2007) were measured via CFA at the National Ice Core Facility at Earth Sciences New Zealand, Lower Hutt, New Zealand as described in Winstrup et al. (2019). The system used was a modified version of the Copenhagen CFA system (Bigler et al., 2011; Kjær et al., 2022).
- In the DF2 core, DiElectric Profiling (DEP) measurements were conducted using electrodes with a 2 cm resolution following Moore and Paren, (1987) and insoluble particles (0.79 – 10.62 µm) were analysed with a particle counter Abakus (Klotz) connected to a CFA system following Goto-Azuma et al. (2024) at the National Institute of Polar Research, Tokyo, Japan.
- In the Skytrain core, sulfate concentrations were measured continuously at the British Antarctic Survey, Cambridge, UK, by fast ion chromatography using a Dionex ICS-6000, following Hoffmann et al. (2022) and Grieman et al. (2022). DEP measurements were made on solid ice prior to processing, using the methods of Wilhelms et al. (1998).

https://doi.org/10.5194/egusphere-2026-3434
Preprint. Discussion started: 9 September 2026

- EDML liquid conductivity was measured continuously using a conductometer from Radiometer (CDM230) and a flow-through cell from Microelectrodes connected to a CFA at the Alfred Wegener Institute (AWI), Germany, following Röthlisberger. et al. (1999); Ruth et al. (2007). Insoluble particles were measured as particles per mL using a CFA melting system with two Abakus laser particle detectors following Wegner et al. (2015).
- In the TALDICE core, sulfate concentrations were measured by continuously by CFA-Fast Ion Chromatography (FIC) using two coupled Dionex DX-120 ion chromatographs with a flow analysis device at AWI, Bremerhaven, Germany, following Severi et al. (2015).

Table 1: *Details of the nine ice cores used in this study, including their location, age scale, types of volcanogenic glaciochemical data used to identify Ōruanui (McConnell et al., 2002) for each core and the resolution and sources of these data. DEP: Dielectric Profiling; CFA: Continuous Flow Analysis; ICP-MS: Inductively Coupled Plasma Mass Spectrometry; ECM: Electrical Conductivity Measurement; IC: Ion Chromatography; FIC: Fast Ion Chromatography.*

Ice core	Volcanic tracer data used to identify Ōruanui	Depth interval of interest (m)	Age interval of interest (years BP 1950), and age scale	Measurement system	Reported data resolution (cm)	Reported data resolution (yrs)	Location of measurement/s	References
WDC06A	Non-sea-salt sulfur Liquid conductivity Insoluble particles	2659.6 – 2660.9	25296.8 - 25336.8, WD2014	CFA-ICP-MS CFA-liquid conductivity meter CFA-Abakus	1 1 1	0.34 0.34 0.34	Desert Research Institute, Nevada, USA	McConnell (2017)
SPC-14	Sulfate Electrical conductivity Insoluble particles	1190.7 - 1191.6	25289.2 - 25341.1, WD2014	IC (discrete samples) ECM probe on solid ice CFA-Abakus	2 0.3 average Variable, 0.3 average	1.12 0.17 average 0.17 average	Dartmouth College, New Hampshire, USA	This study
RICE	Liquid conductivity Calcium ion Nss conductivity (calculated using data above)	710.61 - 712.38	24988.7 – 26262.3, RICE17	CFA-liquid conductivity meter CFA-fluorescence	1 1 1	0.64 0.64 0.64	Earth Sciences New Zealand, Lower Hutt, New Zealand	This study; Ulayottil Venugopal et al., 2023
DF2	DEP Insoluble particles	579.43 - 589.72	25160.5 – 26022.4, WD2014	DEP scanning CFA-Abakus	2 1	1.54 0.77	National Institute of Polar Research, Tokyo, Japan	This study
Skytrain	Sulfate DEP	479 - 480	24987.1 - 25555.2, WD2014	CFA-FIC DEP scanning	4 0.5	28 3.55	British Antarctic Survey, UK	This study
EDML	Sulfate Liquid conductivity Insoluble particles	1069.1 – 1070.4	25290.0 - 25346.1, WD2014	CFA-FIC CFA- liquid conductivity meter CFA-Abakus	1.7 - 1.8 0.7 0.7	0.74 – 0.78 0.3 0.3	Alfred Wegener Institute, Bremerhaven, Germany	Severi et al. (2007); Buizert et al. (2018) Ruth et al. (2007) Fischer et al. (2023)
EDC99	Sulfate Insoluble particles	561.1 - 561.5	25288.7 - 25328.1, WD2014	CFA-FIC Coulter counter (discrete samples)	Variable, down to 2 1	Down to 1.92 0.96	Measured in the field	Severi et al. (2007) Lambert et al. (2012)
Vostok	Electrical conductivity	423 - 432	24663.9 – 25635.1, AICC2023	ECM probe on solid ice	1	1.11	Measured in the field	Parrenin et al. (2012); Bouchet et al. (2023)
TALDICE	Sulfate	905.6 - 906.3	25275.6 - 25349.2, WD2014	CFA-FIC	2 average	2.12	Alfred Wegener Institute, Bremerhaven, Germany	This study; Severi et al. (2012)

245

https://doi.org/10.5194/egusphere-2026-3434
Preprint. Discussion started: 9 September 2026

2.2 Glass shard sampling, extraction, and analysis

Volcanic anomaly records were examined in the nine cores, and selected sulfate, conductivity, and insoluble particle anomalies were identified as potential Ōruanui candidates based on the following criteria: (1) existing volcanic synchronisation records, (2) proximity of the anomaly in age to the known Ōruanui deposit in WDC06A, and (3) magnitude of the sulfate anomaly. Where all three criteria agreed, we suggested a candidate anomaly for the Ōruanui event. In some cases, multiple candidate anomalies around the expected age were investigated. In addition, we re-assessed samples from WDC06A at a higher sampling resolution across the previously identified eruption interval to validate our extraction technique, and further refine the location and number of glass particles preserved within the core. A total of six cores were investigated or reinvestigated for glass shards at candidate anomalies: WDC06A, EDML, SPC-14, DF2, RICE, and Skytrain **(Fig. 1)**. Samples for glass shard extraction (**Table 2**) were either the outer wings of ice cores or refrozen melt water vials collected from CFA.

Most samples were prepared at Victoria University of Wellington (VUW), New Zealand, in a laboratory space dedicated solely to ice core tephra work. Glass shard extraction followed a modified version of methods used by Piva et al. (2023a) to minimise the risk of external particle contamination and to ensure maximum glass shard retention for glass major element geochemical analysis **(Fig. 2)**. Inside a HEPA-filtered laminar flow hood, a hotplate was set at ~80ºC and a Kapton-taped hard drive disk, with pre-drilled, pre-polished and pre-cleaned four-hole epoxy mounts attached, placed on top. Meltwater samples were centrifuged in 15 mL centrifuge tubes at 3000 rpm for 3 minutes to concentrate particulate matter. Using a 10-100 µL pipettor with a 3x Milli-Q rinsed long pipette tip attached, a 20 µL sample aliquot was extracted from the base of the tube and pipetted into the corresponding hole in the mount. This process was repeated six times per sample (for a total of 120 µL), with centrifuging in between each pipetting round. The disks were allowed to dry, then cool before the mount holes were backfilled with freshly made Epoxy resin mixture. Mounts were cured for >48 hours before removal from

https://doi.org/10.5194/egusphere-2026-3434
Preprint. Discussion started: 9 September 2026

the disks, then re-polished using 6, 3, and 1 µm diamond suspension pastes, and carbon coated. Blank samples of Milli-Q water were pipetted into some holes to test for any lab-related contaminants or particulates, although none were found to be present in any of our samples. The only samples not to follow this method were those sampled from the 479.5 m Skytrain sample interval, which were prepared at the University of St Andrews following the methods of Innes et al. (2024). Briefly, ~1 mL of centrifuged meltwater was dried in the centre of a 1-inch stub, with the entire stub then being back-filled with a freshly made Epoxy resin mixture. The mounts were then cured, polished, and carbon coated in the same way.

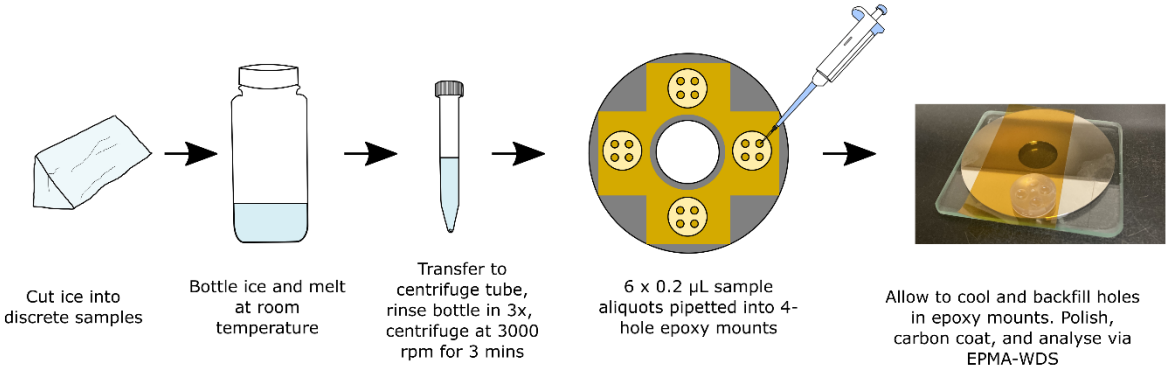

***Figure 2**: Schematic demonstrating our new glass shard extraction methodology using four-hole mounts.*

Sample mounts were visually scanned during Electron Probe MicroAnalysis (EPMA) using backscattered electron (BSE) and secondary electron (SEI) images to search for glass shards. Once shards were identified visually and confirmed by semi-quantitative EPMA-EDS (Energy Dispersive Spectrometry) analysis, major element geochemical characterisation was carried out using EPMA-WDS (Wavelength-Dispersive Spectrometry) to identify potential Ōruanui-derived shards. Most samples were analysed at VUW using a JEOL JXA-8230 electron microprobe, with the only exception being the 479.5 m Skytrain sample interval, which was analysed at the University of St Andrews using methods of Innes et al. (2024). Briefly, at the University of St Andrews, beam sizes of 10 µm were analysed on a JEOL JXA-isp100 electron microprobe using a 5 nA current and 15 kV

https://doi.org/10.5194/egusphere-2026-3434
Preprint. Discussion started: 9 September 2026

accelerating voltage. Smaller beam sizes of 5 µm and 3 µm were analysed using currents of 5 nA and 1 nA, respectively. Various minerals were used as primary standards, while the secondary standards were ML3B basaltic glass, StHs6/80-G andesitic glass, and Lipari rhyolitic glass. At VUW, two analytical routines were applied due to the EPMA software being upgraded during the study. Routine 1 was used for the initial DF2 analysis and the Skytrain visible tephra. Large glass shards (>20 µm) were analysed under 10 nA current and 15 kV accelerating voltage, using beam sizes of 20 µm. Smaller glass shards were measured under 8 and 5 nA currents, using beam sizes of 10 µm or 5 µm, respectively. Primary standards were VG-568 rhyolitic glass and VG-A-99 basaltic glass and secondary standards were KN-18 and ATHO-G rhyolite glasses. Count times were reduced for Na to 10 s with no peak search to minimise migration. Routine 2 was used for WDC06A, EDML, and second round of DF2 analyses. This routine used updated Probe for EPMA software, incorporating a zero-time correction for Na loss. Shards were measured at 8 nA and 15 kV regardless of beam size (5 to 20 µm), using the same primary and secondary standards and with Si, K and Na measured first. Both techniques show similar accuracy and precision for the secondary standards (**Table S1**). Where shards were irregularly shaped or smaller than the minimum beam size, the broad beam overlap method was employed (Iverson et al., 2017a), involving the beam diameter overlapping on to the host epoxy, resulting in lower analytical totals. We employ a cutoff of 80% for totals in this work (e.g., Innes et al., 2024) as due to the small shard sizes, conventionally acceptable (>93%: Miller et al., 2026) totals were challenging to obtain. All analyses were normalised to 100 wt. % for intercomparison of data. This should not impact analytical accuracy but may affect precision (Iverson et al., 2017a). Laser Ablation Inductively Coupled Plasma Mass Spectrometry (LA-ICP-MS) was also attempted on larger shards; however, due to the shards being extremely thin, only a few seconds of counts were possible during ablation and analyses were unsuccessful.

https://doi.org/10.5194/egusphere-2026-3434
Preprint. Discussion started: 9 September 2026

After geochemical characterisation, detailed image analysis of glass shard populations was undertaken to investigate their particle size distribution. Maximum Feret diameters of the particles (defined as the distance between two parallel planes restricting the object perpendicular to that direction) and particle areas (μm^2) were measured in BSE compositional imagery taken on the probe, using ImageJ (Schneider et al., 2012) following the methods of Van Eaton (2012). In WDC06A, where an image of the entire mount surface was obtained with a large number of glass shards exposed, we only counted glass shards in BSE images on high contrast, ignoring <4 μm^2 features to remove small pixel clusters not clearly recognisable as glass. All resulting particle sizes carry a degree of uncertainty, as the separation of particle boundaries in images are manually controlled through adjustments to threshold conditions. As a result, the finest particles may be under-represented. In EDML and DF2, shards were measured from individual imagery of single shards after analysis and confirmation of correct composition. Shard counts were too sparse in these cores for particles to be confidently identified from whole mount imagery. There is therefore an inherent bias towards larger shards in EDML and DF2 because shards <~5 μm^2 were not analysed. Number and area particle size plots are therefore only presented and discussed for WDC06A.Shape factors utilised in Ash3d model simulations (described further in **Sect. 2.5**) were measured using WDC06A BSE imagery, as (b + c)/2a, where a, b and c are the maximum, intermediate and minimum diameters of the particle (assumed to be an ellipsoid).

Table 2: *Details of glass shard sampling intervals, including their resolution and sample type used. Sampling resolution is described across the peak (the centre of the eruptive interval) and the background (samples offset from the eruptive interval).*

Ice core	Depths sampled (m)	Ages sampled (interpolated, years BP 1950)	Age scale used	Sampling resolution (cm)	Sample type	Cross-sectional area sampled (cm^2)	Preparation method
WDC06A	2660.205 - 2661.096	25316.1 - 25343.0	WD2014	2 cm peak Variable background (> 4 cm)	Fresh ice	2.2 - 8.8	This study, after Piva et al. (2023a)
SPC-14	1191.0 - 1191.3	25306.8 – 25323.7	WD2014	10 cm	Fresh ice, filter papers	~2.5	After Dunbar et al. (2003); Dunbar et al. (2017), filter papers reinvestigated in this study
RICE	710.6095 - 710.9611; 711.3060 - 712.0484; 712.0713 - 712.3794	24988.7 - 25214.0; 25435.0 - 25986.6; 26005.7 - 26262.3	RICE17	2-3 cm	Refrozen meltwater vials from CFA	N/A	This study, after Piva et al. (2023a)
DF2	580.95 - 581.5; 582.48 - 583.03; 584.65 - 585.38; 579.43 - 580.14; 585.61 - 586.18; 589.08 - 589.72	25293.84 - 25336.27; 25411.87 - 25454.30; 25579.27 - 25635.59; 25176.59 - 25231.36; 25653.33 - 25697.30; 25921.01 - 25970.39	WD2014	7 cm (average)	Fresh ice	4.3	This study, after Piva et al. (2023a)
Skytrain	[1] 479.26 - 479.86; [2] 480.84 - 481.26	25,122.8 - 25,462.4; 26,087 - 26,405	WD2014	2 cm peak 4 cm background	Fresh ice	~6.8	[1] Innes et al. (2025) [2] This study, after Piva et al. (2023a)
EDML	1069.484 - 1069.944	25306.48 - 25326.36	WD2014	2 cm peak 4 cm background	Fresh ice	3.0	This study, after Piva et al. (2023a)

https://doi.org/10.5194/egusphere-2026-3434
Preprint. Discussion started: 9 September 2026

2.3 Volcanic sulfate deposition

The total sulfate deposition from the Ōruanui eruption over Antarctica was recalculated following the methods of Lin et al. (2022), using data from the WDC06A, EDML, EDC, and newly included SPC-14 core. Corrections are applied to each ice core dataset for non-volcanic background sulfate using a running median, contemporaneous site-specific accumulation rates, and layer thinning with depth as per Lin et al. (2022). The calculation for removing the sea salt component from sulfate concentration to isolate potential volcanic signals is:

$$non - sea - salt\ sulfate = [SO_4] - (0.25 * [Na]) , \quad (1)$$

with the 0.25 ratio from Bonsang et al. (1980).

The Ōruanui-derived cumulative volcanic sulfate deposition (often referred to as 'flux') is calculated for each ice core record by integrating sulfate concentration with respect to depth, to compare signal strength across Antarctica, following the calculation method of Lin et al. (2022). Details of parameters, including filter lengths, detection thresholds, and integration window lengths for sulfate deposition are presented in **Table S2**. WDC06A, EDML, and SPC-14 were fairly high accumulation ice cores at the time of eruption, and therefore typically record higher than average volcanic sulfate deposition compared to the Antarctic mean (e.g., Toohey et al., 2013; Sigl et al., 2014). EDC on the other hand is excluded in our estimate due to its non-representative Ōruanui sulfate deposition. The Ōruanui sulfate deposition values at WDC06A, EDML, and SPC-14 were rescaled to estimate the average sulfate deposition across Antarctica, using a scaling factor as described in Sigl et al. (2022) and Innes et al. (2025). For 41 common large volcanic eruptions (400 – 2,000 CE), we compared the mean volcanic sulfate depositions of stacked ($n \geq 2$) ice cores from those three sites (WAIS Divide, Dronning Maud Land, South Pole) in which we identified volcanic sulfate associated with Ōruanui to the corresponding values from the comprehensive ($n \geq 12$) Antarctic Volcanic (AVS2K) stack over the past 2,000 years (**Fig. S1**) (Sigl et al., 2014, 2022; Innes et al., 2025).

https://doi.org/10.5194/egusphere-2026-3434
Preprint. Discussion started: 9 September 2026

This three-site mean is, on average, 15 % higher than the AVS2K stack, likely due to the overrepresentation of some high accumulation sites in our dataset relative to the range of sites in the AVS2K stack. We therefore apply a scaling factor of 0.85 to reduce our average sulfate deposition by 15%. Using this correction, the total volcanic sulfate deposition for Antarctica for the Ōruanui eruption is estimated at ~270 kg km^{-2}. The volcanic sulfate deposition uncertainty estimate for Antarctica is derived from the standard deviation of the rescaled volcanic sulfate depositions for all three Antarctic sites as per Lin et al. (2022). Average Greenland deposition values and their uncertainties are defined in Lin et al. (2022) based on Svensson et al. (2020), and are used unchanged in our recalculation.

2.4 Volcanic stratospheric sulfur injection (VSSI) and climate forcing

The mass of sulfur injected into the stratosphere (VSSI; Tg S) was estimated using transfer functions – scaling factors that account for the uneven hemispheric distribution of volcanic sulfate from an extra-tropical eruption latitude, such as ~39 °S for Ōruanui. For this calculation, we use the extra-tropical transfer function of 0.57×10^9 km^2 (Gao et al., 2007) for Antarctic deposition and tropical transfer function 1×10^9 km^2 for Greenland deposition (as per Toohey & Sigl, 2017), along with our updated Antarctic deposition average, and previous Greenland estimate (Lin et al., 2022). This is in contrast to previous work, where Lin et al. (2022) calculated for Ōruanui using tropical transfer functions for both Antarctica and Greenland. Uncertainty on the VSSI value is quantified following Toohey and Sigl (2017). No glass shards from the Ōruanui eruption have been identified in Greenland, raising uncertainty about the bipolar link proposed by Svensson et al. (2020). This suggests that the Greenland sulfate contribution could be lower than estimated by Lin et al. (2020). To address this, we present an alternative scenario assuming zero Greenland sulfate deposition, providing a lower boundary estimate for VSSI **(Table S3).** This allows us to assess how the resulting VSSI estimates vary depending on the assigned anomaly in Greenland, which is arguably the largest source of uncertainty in these estimates. To estimate radiative forcing from the eruption, first we calculated the global mean (monthly) stratospheric aerosol optical depth (SAOD) using the

https://doi.org/10.5194/egusphere-2026-3434
Preprint. Discussion started: 9 September 2026

EVA_H volcanic stratospheric aerosol forcing emulator (Aubry et al., 2020). Parameters used in the model are described in **Table S4**. We then apply the exponential transformation between the volcanic SAOD, expressed as an anomaly relative to the non-volcanic background, and the Effective Radiative Forcing (ERF) from Marshall et al. (2020) as per **Eq. (2)**:

$$ERF = \alpha(1 - e^{-SAOD}) \quad (2)$$

where $\alpha = -20.7$ W m^{-2}.

2.5 Geologic constraints on Ash3d simulations

To simulate the variability in Ōruanui volcanic ash deposition to the Antarctic Ice Sheet and to assess the controls of particle size and shape on dispersal and deposition, a sensitivity study of plume parameters was carried out using the 3-D Eulerian atmospheric transport model Ash3d (Schwaiger et al., 2012). The range of parameters were informed by field characteristics of the eruption (Wilson, 2001; Van Eaton and Wilson, 2013), previous numerical simulations (Dunbar et al., 2017; Barker et al., 2019), and new observations from this study (**Table S5**). Focusing on characteristics of Ōruanui phase 10, the final and most voluminous phase of the eruption, we use a bulk volume of 365 km^3 (Wilson, 2001) and assume continuous eruption over 72 hours. The Ash3d model does not explicitly resolve processes that accelerate ash fallout, such as particle aggregation, wet deposition, or gravitational instabilities, all of which were active and important during this water-rich eruption (Wilson, 2002; Van Eaton and Wilson, 2013). Instead, these effects were simplified by assuming rapid fallout of 95% of the total erupted mass and injection of the remaining 5% into the umbrella cloud. We modeled plume heights of 24 km and 35 km above sea level. In Ash3d, these heights do not represent the absolute maximum height of the eruption column, which was likely much greater, but assume that the overshooting top collapsed into a laterally spreading umbrella cloud at the neutral buoyancy height, where most lateral transport occurred. We constrained the level of neutral buoyancy from large-eddy simulations of the Ōruanui volcanic plumes from Van Eaton et al. (2012) and

https://doi.org/10.5194/egusphere-2026-3434
Preprint. Discussion started: 9 September 2026

from observations of the water-rich eruption of Hunga volcano, Tonga, in 2022, which produced long-distance transport layers in the mid-stratosphere despite a maximum overshooting height of 58 km (e.g., Kahn et al., 2024).

For constraints on grain size, we consider that unit 10 is predominantly coignimbrite ash and exceptionally fine grained, dominated by mean grain sizes of 20–65 μm (Wilson, 2001). These particle sizes are consistent with deposits from other Ōruanui units - for example, unit 3 contains ~40 wt.% <32 μm ash 175 km from source (Van Eaton and Wilson, 2013) and basal Ōruanui ash 820 km from source (likely unit 9), contains 46% <32 μm ash (Matthews et al., 2012). We used 40 μm as a single particle size class for the simulations, with an assumed density of 2.4 g cm^{-3} for rhyolite glass (Durant, 1989). We also included simulations using a single particle size of 80 μm diameter (at the high end of our observed particles at WDC06A). The model used particle shape factors of 0.3 based on our measurements. Settling velocities were calculated using the method of Wilson and Huang (1979). The 2.5 degree NCEP/NCAR Reanalysis2 dataset was to provide 3-D time-varying wind inputs to the model. We used to method of Dunbar et al. (2017) to account for weather patterns during the LGM by running simulations during 80 time periods that correspond to northwesterly flow over New Zealand and strong circumpolar westerlies surrounding Antarctica. This combination of eruption source parameters and weather inputs resulted in 640 simulations (found in Mastin et al., 2026), which were combined to show the spatial probability of fallout within the given range of wind fields in **Fig. 10**. Given the simplifying assumptions described here, the model results do not exclude the possibility of deposition at greater or lesser distances than shown in **Fig. 10**; however, they do provide an indication of the expected transport distance of different-sized particles. Full details of parameters used for the simulations can be found in **Table S5**.

https://doi.org/10.5194/egusphere-2026-3434
Preprint. Discussion started: 9 September 2026

2.6 Community Earth System Modelling

To further evaluate the climatic and environmental impacts of the Ōruanui eruption, including model changes in temperature, precipitation, AOD, and ozone, we performed a series of 5-year climate simulations for an Ōruanui-like event under pre-industrial conditions due to uncertainties regarding LGM conditions. We used the Community Earth System Model (CESM2) (Danabasoglu et al., 2020) with the Whole Atmosphere Community Climate Model component (WACCM6) (Gettelman et al., 2019), incorporating fully coupled atmosphere-ocean dynamics, prognostic aerosols (simulating active growth, transport, and decay), and comprehensive atmospheric chemistry. Simulations were conducted with stratospheric injections of ~260 Tg SO_2 as constrained by petrological considerations (Sharpe et al., 2022), and within the range of our new ice core estimates (~228 ± 66 Tg SO_2). Petrological values from Sharpe et al. (2022) were selected to represent a maximum injection scenario. We ran multiple scenarios with variable HCl and HBr injection efficiency into the stratosphere (1% and 10% of total from magma), reflecting uncertainties in the pre-eruptive HCl content of Ōruanui magma (Sharpe et al., 2022) and the highly variable amounts of halogens that reach the stratosphere in large explosive eruptions (Textor et al., 2003; Kutterolf et al., 2013; Krüger et al., 2015) (**Table 3**). HBr values were scaled from petrological HCl estimates according to Bureau et al. (2000) and Unni and Schilling (1978). The eruption scenario was prescribed as occurring in the SH summer, lasting six days (i.e., reflecting the later, most vigorous and voluminous stages of the eruption: Wilson, 2001), with an injection altitude of 24 km based on an unsaturated Plinian column with 10% surface water input (Van Eaton et al., 2012). Initial atmospheric conditions included a Westerly Quasi-biennial Oscillation (QBO) and neutral El Niño-Southern Oscillation (ENSO) state following Brenna et al. (2020), providing a baseline for assessing atmospheric responses under realistic seasonal and dynamical conditions. Preindustrial 1850 conditions were used throughout the simulations. While these do not represent glacial conditions, they are the closest available alternative.

https://doi.org/10.5194/egusphere-2026-3434
Preprint. Discussion started: 9 September 2026

450

Table 3: *Simulation set-up for the CESM2/WACCM model, run for an Ōruanui-like eruption.*

Simulation	Height (km)	Eruption month	Duration (days)	SO_2 (Tg)	HCl (Tg)	HBr (Tg)	Halogen injection efficiency (%)
Sulfur only	24	March	6	260	0	0	0
1% halogens	24	March	6	260	18	0.06	1
10% halogens	24	March	6	260	180	0.6	10

3 Results

3.1 Glaciochemical tracers of the Ōruanui eruption

455 The magnitude of glaciochemical volcanogenic anomalies attributed to the Ōruanui eruption vary considerably across Antarctica in the cores investigated. Sulfate concentration records have been supplemented with conductivity and insoluble particle data to identify candidate eruption anomalies at nine core sites (**Table 4; Fig. 3**). Where we provide the depths and ages of candidate Ōruanui anomalies, we report the values at the centre of the sulfate or conductivity anomaly as the reference position. Typically, the position of glass on the older shoulder
460 of the sulfate anomaly represents the onset of volcanic deposition (e.g., Dunbar et al., 2017; Piva et al., 2023a) which then lasts for several years, but this information is not consistently available for every site and the position can also vary depending on diffusion of the anomaly over time.

We use WDC06A, a relatively high accumulation (0.11 m a^{-1} ice equivalent at the time of eruption, i.e.: Fudge et
465 al., 2016) West Antarctic ice core, as the exemplar site, given the previous identification of glass shards associated

https://doi.org/10.5194/egusphere-2026-3434
Preprint. Discussion started: 9 September 2026

with large sulfate (1800 ppb, 16x background sulfate concentration: **Fig. 3a**) and conductivity anomalies (Dunbar et al., 2017). At this site, the glass shard horizon is represented by a large insoluble particle anomaly at 2660.3 m depth. The WD2014 ice age of the Ōruanui eruption, 25,318 ± 253 years BP (1950) (Sigl et al., 2016; Dunbar et al., 2017), provides an important chronological tie-point, as many Antarctic ice cores are aligned to this age scale. This age is within 2σ error of the revised radiocarbon-age from proximal deposits of 25,335 - 25,800 cal BP using the latest calibration curve for the SH (SHCal20) (Muscheler et al., 2020).

Drilled in Dronning Maud Land, East Antarctica, EDML was a moderate accumulation-rate site at the time of eruption (0.037 m a^{-1} i.e.: Bazin et al., 2013a). Based on volcanic synchronisation between WDC06A and EDML (Buizert et al., 2018), the targeted depth of the Ōruanui anomaly in EDML is 1069.71 m, corresponding to a WD2014 age of 25,316 years BP. At this depth, a prominent sulfate anomaly occurs, with concentrations rising tenfold above background (100-year running mean centred on 25,316 years BP) to a discrete peak of 2600 ppb (**Fig. 3b**). No significant insoluble particle anomaly is observed at this site, although the background signal is highly variable. The sulfate anomaly has been previously attributed to Ōruanui by previous work and represents the second largest sulfate anomaly in the past 68.5 ka of the EDML record (Severi et al., 2007; Buizert et al., 2018; Lin et al., 2022).

The SPC-14 ice core drill site sits at an elevation of 2835 m (Casey et al., 2014) and had moderate snow accumulation rates at the time of eruption (0.033 m a^{-1}, i.e.: Kahle et al., 2020). Using volcanic synchronisation with WDC06A (Winski et al., 2019), a sulfate anomaly is identified in the SPC-14 core at 1191.12 m (25,313 years BP) with a highest concentration of ~3600 ppb, ~18 times above the 100-year background (**Fig. 3c**). The SPC-14 core has a distinct insoluble particle peak; however, unlike in WDC06A this occurs on the younger shoulder of the sulfate anomaly. This sulfate anomaly, which represents the most likely candidate for Ōruanui, is

https://doi.org/10.5194/egusphere-2026-3434
Preprint. Discussion started: 9 September 2026

one of the largest anomalies in the entire ~54 ka SPC-14 record.

Dome Fuji represents the second highest dome summit in Antarctica, located on the East Antarctic Plateau at an elevation of ~3810 m (Motoyama, 2007). Synchronisation of DF1 with WDC06A (Oyabu et al., 2022) places the Ōruanui target depth at 582.17 m, which translates to 581.23 m in DF2 (25,315 years). Both depths coincide with a large conductivity anomaly (**Fig. 3d**), with the close age overlap with WDC06A suggesting that it is a good candidate for the Ōruanui. No distinct insoluble particle anomalies are detected at this site. Five additional glaciochemical anomalies were also investigated for glass shards between 579.48 and 589.72 m.

https://doi.org/10.5194/egusphere-2026-3434
Preprint. Discussion started: 9 September 2026

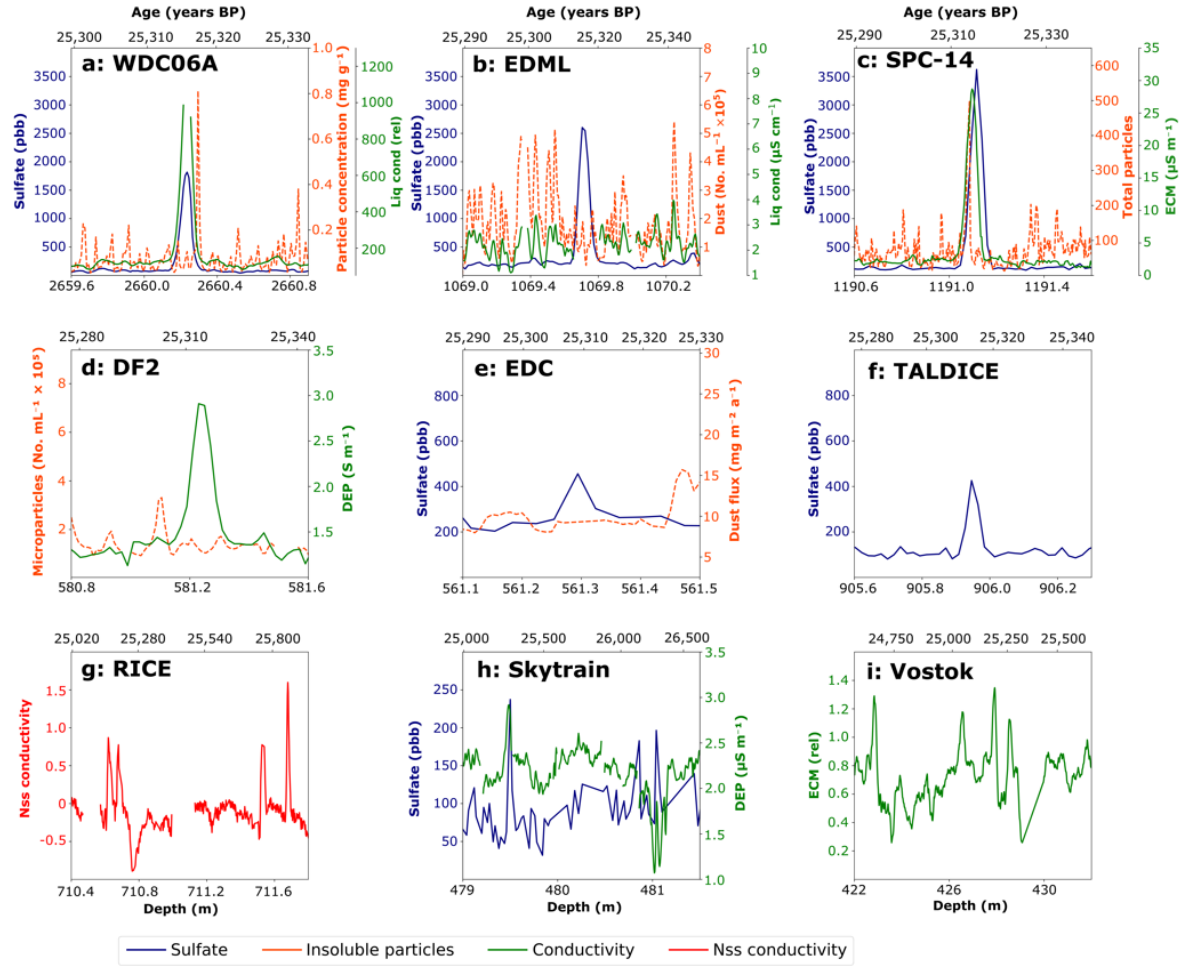

Figure 3: *Volcanic anomalies in each of the nine cores identified as potential candidates for the Ōruanui supereruption using their ice age, magnitude, and presence or lack of glass shards derived from the eruption. The top row shows cores which represent the largest glaciochemical signals related to the eruption. The middle row shows signals which likely represent Ōruanui but are smaller in magnitude. The bottom row shows cores where the presence of Ōruanui remains uncertain. Glaciochemical data sources are referenced in* ***Table 1****. Age models applied in figure: a) WD2014 (Sigl et al., 2016); b) EDML1 (Ruth et al., 2007) mapped to WD2014; c) SP19 (Winski et al., 2019) mapped to WD2014; d) DF2 age scale mapped to WD2014; e) AICC (Bouchet et al., 2023)*

https://doi.org/10.5194/egusphere-2026-3434
Preprint. Discussion started: 9 September 2026

mapped to WD2014; f) TALDICE-1 (Buiron et al., 2011) mapped to WD2014; g) RICE17 (Lee et al., 2020); h) ST22 (Mulvaney et al., 2023); i) AICC2023 Bouchet et al. (2023).

Table 4: *Proposed glaciochemical anomalies in nine deep Antarctic ice cores representing the Ōruanui supereruption. *Maximum of the sulfate or conductivity peak.*

Ice core	Type of anomaly	*Depth of proposed anomaly (m)	Age of proposed anomaly (yrs BP 1950)	Timescale used	Reference
WDC06A	Insoluble particle	2660.30	25318.81	WD2014	Dunbar et al. (2017)
SPC-14	Sulfate	1191.12	25313.26	WD2014	Winski et al. (2019)
EDML	Sulfate	1069.71	25316.32	WD2014	Buizert et al. (2018)
DF2	Sulfate	581.23	25315.44	WD2014	This study
EDC99	Sulfate	561.30	25316.16	WD2014	Buizert et al. (2018)
Talos Dome	Sulfate	905.95	25314.37	WD2014	Buizert et al. (2018)
Vostok	Conductivity	Unknown	Unknown	VK-5G	This study
RICE	Nss conductivity	Unknown	Unknown	RICE17	This study
Skytrain	Sulfate	Unknown	Unknown	WD2014	This study

https://doi.org/10.5194/egusphere-2026-3434
Preprint. Discussion started: 9 September 2026

The EDC core on the East Antarctic Plateau provides a ~800 kyr record of past Antarctic temperature, chemical impurities and atmospheric composition (Bazin et al., 2013b). Using volcanic synchronisation between WDC06A and EDC (Buizert et al., 2018), a small sulfate anomaly at 561.3 m (25,316 yrs BP) was identified by Lin et al. (2022) as a plausible Ōruanui signal, despite sulfate concentration being low in comparison to other sites (~450 ppb sulfate, 1.7 times the 100-year background: **Fig. 3e**). A number of other sulfate anomalies are also potential candidates, although they do not match as well in terms of age overlap (>75 years difference) or overall volcanic synchronisation of the core.

In the TALDICE core, drilled at the edge of the East Antarctic Plateau in the Ross Sea Sector at an altitude of ~440 m, a volcanic anomaly at 905.95 m (25,314 years BP model age) is identified as the primary Ōruanui target based on synchronisation with WDC06A (Urbini et al., 2006; Buizert et al., 2018). The sulfate anomaly is modest, comparable to that at EDC, with a peak discrete concentration of ~425 ppb (3.5 times the 100-year background: **Fig. 3f**). A number of similar magnitude anomalies are present in TALDICE; however, their age matches are not as strong as the 905.95 m signal, and they are therefore discarded as candidates.

The RICE ice core is unique in this array of ice cores, being a coastal site located on Roosevelt Island in the eastern Ross Sea, with high marine biogenic sulfur inputs (Bertler et al., 2018; Winstrup et al., 2019). The core is dated to 83 kyr (Lee et al., 2020). Here, conductivity is not a reliable proxy for volcanic deposition, because it represents sulfate input from multiple sources. Instead, nss conductivity is used to identify potential volcanic signals (Winstrup et al., 2019; Piva et al., 2023a). Several large nss conductivity anomalies occur between 710.5 and 711.8 m depth (RICE17 model ages: 24,919 to 25,780 years BP); however, the record is highly variable and contains several possible candidates (**Fig. 3g**).

https://doi.org/10.5194/egusphere-2026-3434
Preprint. Discussion started: 9 September 2026

Located inland of the Ronne Ice Shelf in West Antarctica, the Skytrain ice core had a low accumulation rate at the time of eruption (0.023 m a^{-1} i.e., Mulvaney and Wolff., 2023), and sits at low elevation (784 m) (Hoffmann et al., 2022). The core hosts a single sulfate anomaly of ~250 ppb (three times background concentration) at 479.5 m (25,255 years BP) within the ±200-year age uncertainty (ST22 age scale) of the Ōruanui age (**Fig. 3h**). We present this anomaly as a potential target, while noting that the magnitude of the anomaly is smaller than other sites, and the lack of volcanic synchronisation tie-points near this age make this link tentative. We also examine a visible tephra noted at 481.06 m depth (26,242 yrs BP) as a possible tie-point near in age to Ōruanui. Further details are provided in **Sect. 3.2.6**.

Drilled at 3488 m elevation on the central East Antarctic Plateau, the Vostok ice core is volcanically synchronised with EDC (Parrenin et al., 2012), with two published conductivity tie-points close in age to the Ōruanui eruption date but not directly marking the anomaly itself. These tie-points occur at 553.12 m (24,519 years BP, WD2014) and 564.39 m (25,620 years BP, WD2014) in EDC, corresponding to 422.85 m (24,648 years BP, AICC2023) and 432.36 m (25,675 years BP, AICC2023) in Vostok. The proposed Ōruanui anomaly in EDC lies at 561.3 m, between these two tie-points, implying that the equivalent depth in Vostok is between 422.85 and 432.36 m (**Fig. 3i**). Within this interval, several conductivity anomalies rise above a very variable background, one of which may represent the eruption horizon. However, this site was not further investigated due to the large age uncertainties (>2,000 years: Veres et al., 2013).

3.2 Glass shard identification

We selected six sites to further investigate for glass shards that satisfied our sampling criteria as described in **Sect. 2.2**. The results of our particle investigations are presented below.

https://doi.org/10.5194/egusphere-2026-3434
Preprint. Discussion started: 9 September 2026

3.2.1 WDC06A

Original work by Dunbar et al. (2017) located a large population of glass shards in WDC06A, with 19 shards of 5 - 35 µm analysed from two samples between 2660.335 - 2660.000 m (35 cm total in length), which were assumed to be associated with the large insoluble particle anomaly on the leading edge of the sulfate anomaly (**Fig. 3a, 4a**). We re-examined the same interval with higher resolution sampling, and located a large population of Ōruanui glass in a 2 cm sample between 2660.285 – 2660.305 m, confirming the insoluble particle peak represents the eruption. Glass particles across this peak commonly show angular and delicate morphologies, with some appearing platy or cuspate and some being elongate with vesicle bubble wall textures, including tube pumice (**Fig. 5a**). No glass shards were recovered in surrounding samples either side of the insoluble particle anomaly. A total of >10,000 glass particles were identified using ImageJ analysis, ranging in size from 4 - 110 µm Feret diameter (**Fig. 6a, Table S6**). The distribution by percent mass of particles, assuming ellipsoid shapes, thicknesses of 5 µm and density of 2.4 g cm^{-3}, has a mean and mode between 26.3 - 31.3 µm (5.25 – 5 Phi, φ) (**Fig. 6b**), while the distribution by percent area of particles shows the mean falls within 22.1 - 31.3 µm (5.5 - 5 φ) and mode is 22.1 – 26.3 (5.5 - 5.25 φ) (**Fig. 6c**). The number particle size distribution is skewed towards smaller shards, with the mean particle size being ~13 µm, and mode being 6.6 – 7.8 µm (7.25 – 7 φ). Considering the total meltwater volume of the sample, we calculate a glass concentration of ~460 shards/mL of meltwater. We consider this to be a minimum estimate given that particles may not be fully exposed on the surface of the epoxy mount, and particles <4 μm^2 are excluded in the counting process as below this size they are below analytical limits, and also not confidently identifiable as glass using ImageJ. The <4 μm^2 cutoff also influences the range of particle sizes, which may have otherwise been lower. Our EPMA analysis of glass from WDC06A (n = 47, totals >90%) shows good consistency with published values from ice, marine core, and terrestrial samples of distal tephra from the Ōruanui eruption (Dunbar et al., 2017) (**Fig. 7**).

https://doi.org/10.5194/egusphere-2026-3434
Preprint. Discussion started: 9 September 2026

3.2.2 EDML

We investigated the EDML ice core for glass particles across the 1069.71 m sulfate anomaly. EDML had a relatively high and variable dust background during the LGM (Wegner et al., 2015) therefore insoluble particle data show multiple peaks. Many of the samples contained abundant dust and fine insoluble particles, making glass particle identification challenging. However, when sampling at 2 cm resolution, a small population of volcanic glass was located within a single sample between 1069.744 - 1069.764 m depth (**Fig. 3b**). We analysed ten of these shards: seven had analytical totals over 90%, and three had lower totals (80 - 90%). The latter were normalised using the broad beam overlap method (Iverson et al., 2017a) and all shards fell within the same rhyolitic geochemical population. Glass chemistry from these EDML shards show strong similarity with published Ōruanui values, including from the WDC06A ice core, confirming that the sulfate anomaly is from this eruption (**Fig. 7**). Analysed shards were typically platy or cuspate in morphology, and are between 9 and 26 μm in diameter (longest axis) (**Fig. 6b**). Tens to hundreds of smaller shards of similar greyscale shade in BSE images were evident during imaging but were too small (<4 μm^2) for quantitative chemical analysis (**Fig. S2a**).

https://doi.org/10.5194/egusphere-2026-3434
Preprint. Discussion started: 9 September 2026

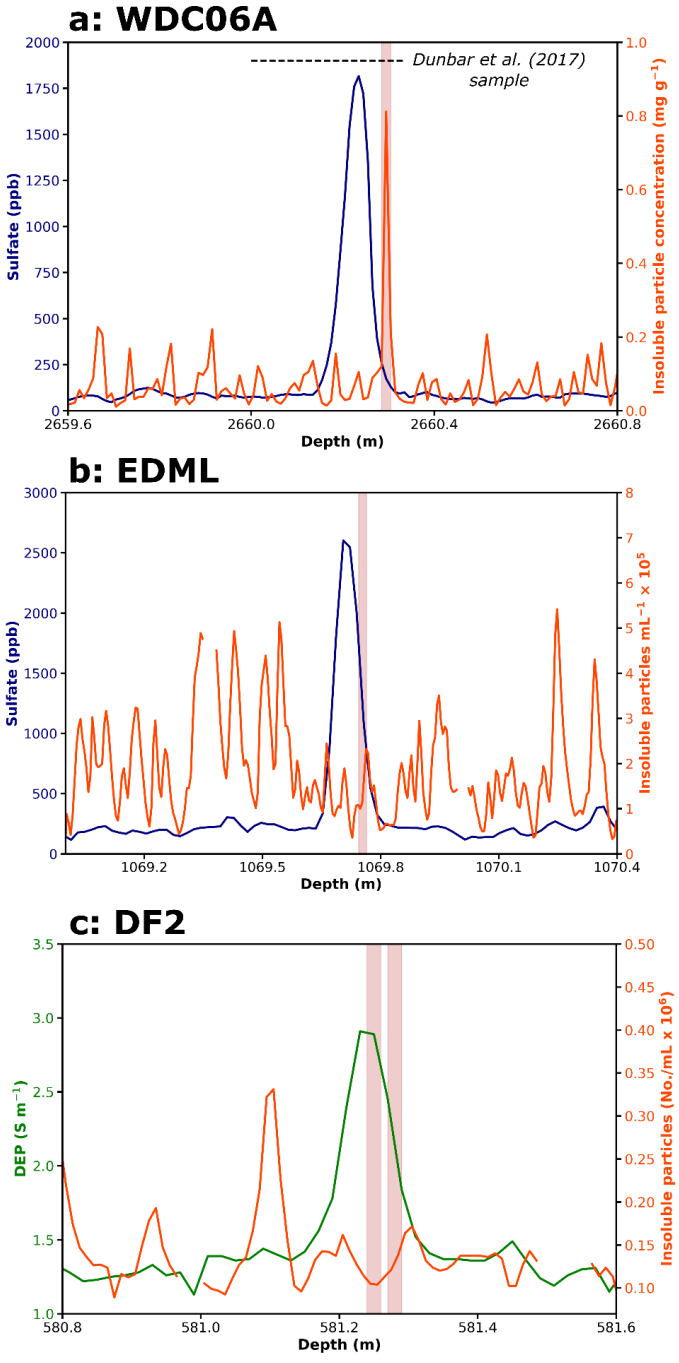

***Figure 4**: The locations of glass shard horizons in (a) WDC06A, (b) EDML, and (c) DF2 relative to their respective volcanic anomaly records. The red shaded areas represent the glass shard horizons. See **Table 1** for data sources.*

https://doi.org/10.5194/egusphere-2026-3434
Preprint. Discussion started: 9 September 2026

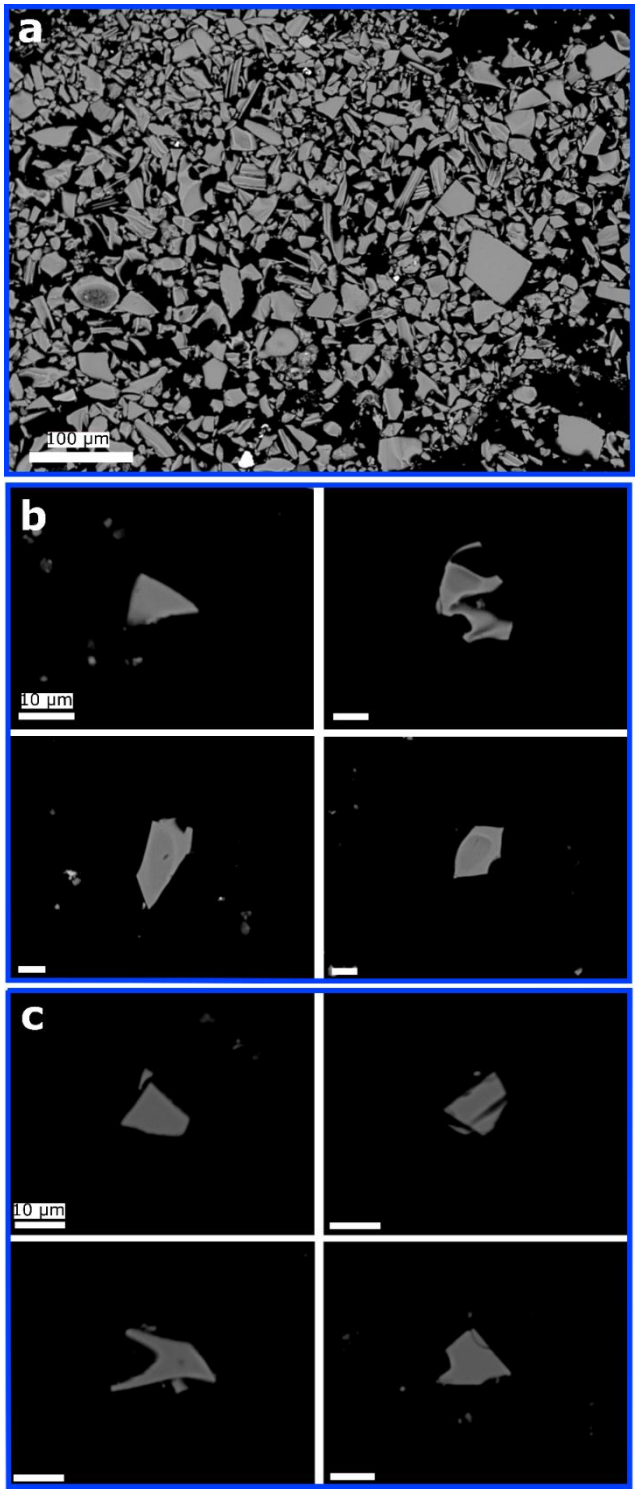

Figure 5: *Representative morphology of glass shards from (a) WDC06A, (b) EDML, and (c) DF2 cores.*

https://doi.org/10.5194/egusphere-2026-3434
Preprint. Discussion started: 9 September 2026

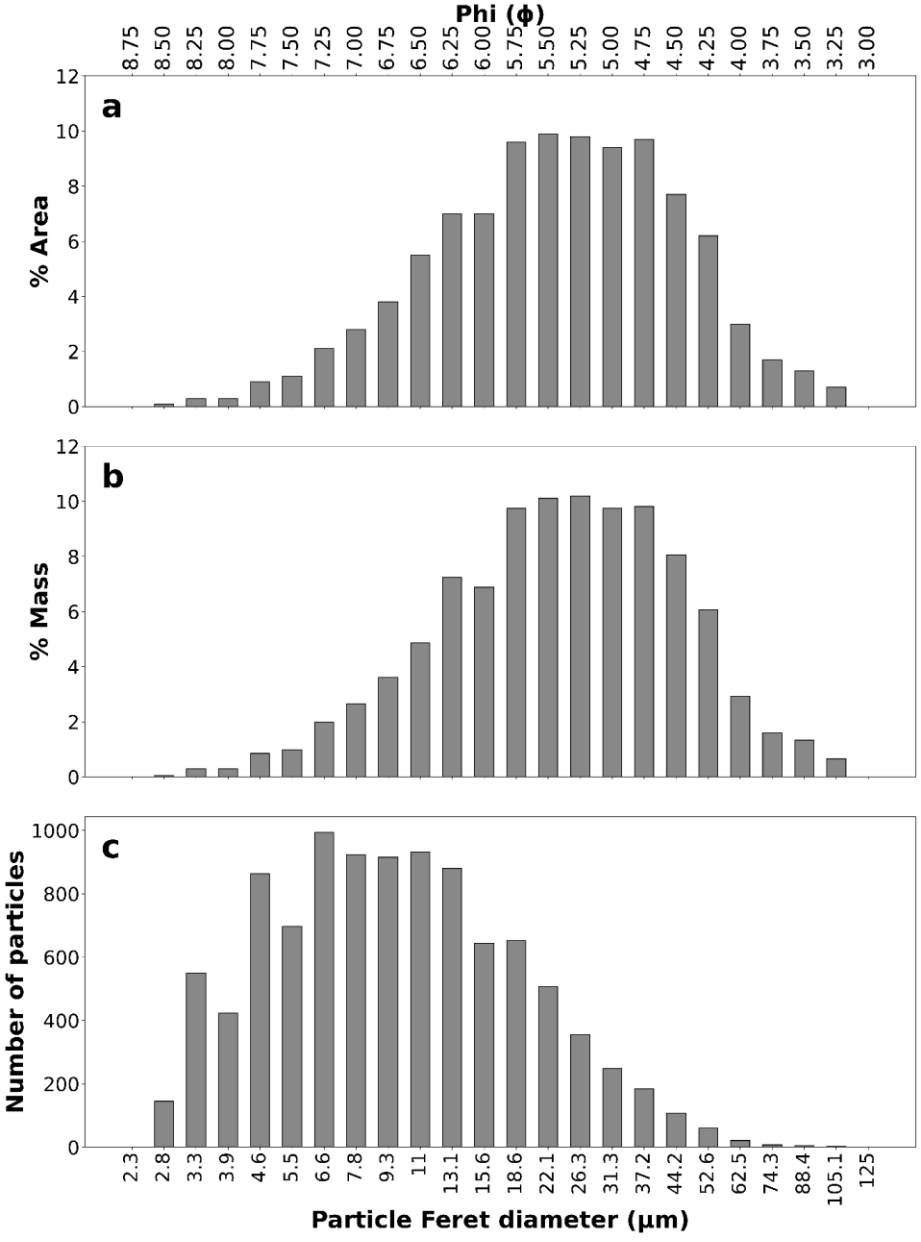

Figure 6: *Plot (a) shows WDC06A Feret diameter of glass particles against the percent area of particles, Plot (b) shows WDC06A Feret diameter against the percent mass of particles (assuming all particles as ellipsoids, with thickness 5 µm and density 2.4 g cm^{-3}), and Plot (c) shows WDC06A Feret diameter against the total number of particles quantified by ImageJ. Phi = -log$_2$ size in millimetres.*

https://doi.org/10.5194/egusphere-2026-3434
Preprint. Discussion started: 9 September 2026

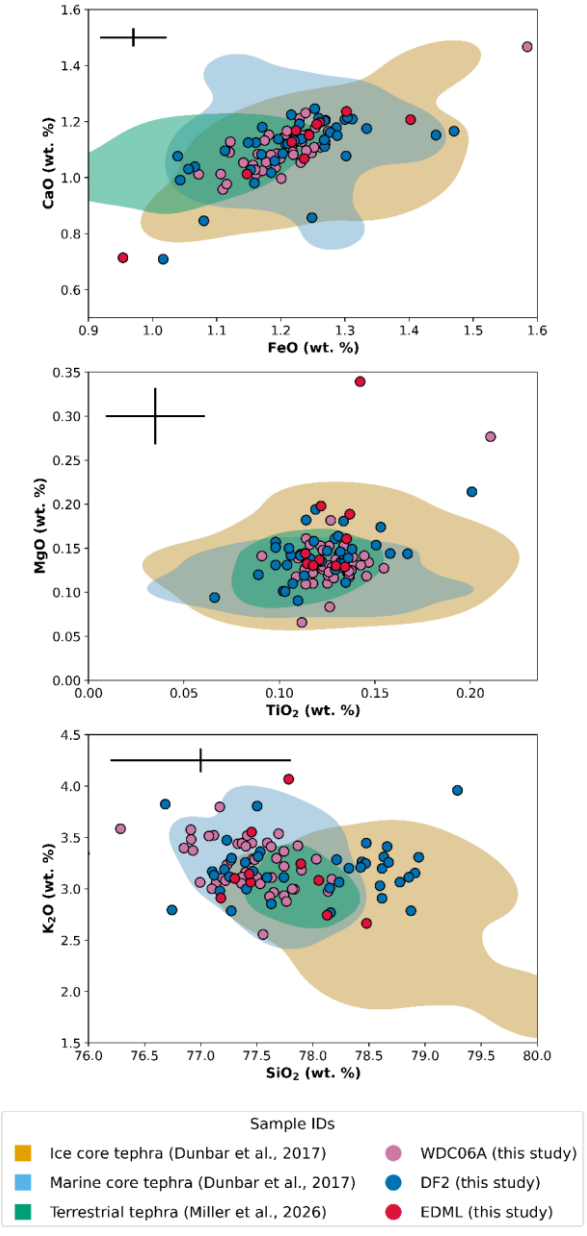

Figure 7: *Glass shard compositions from the WDC06A, EDML, and DF2 ice cores showing geochemical correlations with reference fields to ice core and terrestrial Ōruanui samples. Reference marine and ice core data from Dunbar et al. (2017), terrestrial data from Miller et al. (2026). Standard deviation bars represent measured ATHO-G standard values during the initial DF2 run (the run with the highest 2SD%), and display 2SD each side of centre point.*

https://doi.org/10.5194/egusphere-2026-3434
Preprint. Discussion started: 9 September 2026

3.2.3 DF2

Six significant conductivity peaks above background were identified in the DF2 ice core as potential Ōruanui tracers, based on their magnitudes and/or proximity in age to the glass shards discovered in WDC06A. These signals were ranked from 1 - 6 in priority order for further investigation. The priority 1 peak, spanning depths 580.95 – 581.5 m contained a single distinct population of 19 analysable glass shards covering 581.21 – 581.28 m depth (corresponding to 25,313.9 to 25,319.4 years BP 1950 WD2014), along with potentially tens to hundreds of glass fragments too small for EPMA analysis (**Fig. S2b**). Out of these 19 shards, 17 returned analytical totals >90%, and two returned totals between 80 - 90%, all with rhyolitic compositions consistent with the Ōruanui field (**Fig. 7**). To further refine the position of the glass within this 7 cm sample, we reinvestigated fresh ice samples at 1 cm intervals and located two clusters of glass, one covering two samples between 581.24 – 581.26 m (five shards with >90 % totals, and a further six of 80 - 90%) and one covering two samples between 581.27 – 581. 29 m (eight shards >90 % and an additional two of 80 - 90%). Shards exhibit angular, platy and cuspate morphologies, with elongated vesicles present in just over a quarter of shards **(Fig. 6c).** Analysable shards were rhyolitic and geochemically consistent with the original population and also with Ōruanui-derived glass shards found in WDC06A and EDML in this study **(Fig. 7)**. Geochemical analyses confirm chemical uniformity among the population, and show that key oxides for fingerprinting such as CaO, FeO, and TiO_2 match those of ice core, terrestrial, and offshore tephra from the Ōruanui supereruption (Vandergoes et al., 2013; Allan et al., 2017; Dunbar et al., 2017, Miller et al., 2026). We analysed the particle size distribution of analysed shards across both suites of samples (n = 40) using ImageJ, with sizes ranging from 6 to 36 µm diameter. This population is located on the rising limb of the sulfate anomaly, although slightly closer to the peak compared to WDC06A and EDML (**Fig. 4c**). No glass shards were found in any subsidiary anomalies investigated.

https://doi.org/10.5194/egusphere-2026-3434
Preprint. Discussion started: 9 September 2026

3.2.4 SPC-14

SPC-14 was originally investigated for Ōruanui glass shards between 1191.0 and 1191.3 m using the filtration methods of Iverson et al. (2017a). However, no glass shards were recovered in the targeted interval using this technique. We reinvestigated remaining filter papers from initial analyses to attempt further recovery, by placing the filters in an ultrasonic bath to remove particles and applying subsequent centrifugation methods. However, no analysable glass shards were recovered and the targeted insoluble particle peak at 1191.09 m consisted of fine grained (<5 µm) dust. Most were too small to analyse using a 5 µm spot on the EPMA, but sparse larger particles had feldspar and quartz compositions.

3.2.5 RICE

Guided by earlier work that identified glass particles in RICE including rhyolites, depth intervals of interest (710.61 - 710.96, 711.31 - 712.05, 712.07 - 712.38 m) were resampled using refrozen meltwater vials. Analysis of these samples revealed several small (1 - 2 shard) groups of predominantly trachytic glass particles, <5 µm in size, consistent with previous findings. In addition, a single rhyolitic shard with a composition comparable to Ōruanui was identified; however, this particle yielded a low analytical total (74%), introducing uncertainty to the measurement. Overall, these results do not provide evidence for a distinct Ōruanui glass population within the investigated intervals.

3.2.6 Skytrain

Two distinct primary populations of glass shards were present in the proposed Ōruanui sampling interval for the Skytrain ice core (479.256 – 479.856 m; 25,120 – 25483 years BP ST2022_WD2014). However, these shards were of andesitic and trachytic composition with no rhyolitic particles indicative of the Ōruanui supereruption. The andesitic glass may have been derived from the South Sandwich Islands, ~2000 km from Skytrain core site, based on geochemical data from Pearce et al. (1995) (**Fig. 8**). However, the exact source volcano remains unclear

https://doi.org/10.5194/egusphere-2026-3434
Preprint. Discussion started: 9 September 2026

due to a lack of historic and geological data on South Sandwich Islands eruption chronology and composition (Pearce et al., 1995). The trachyte is a close match to compositions erupted from Mount Berlin (Iverson et al., 2017b), a coalescence of two shield volcanoes in Marie Byrd Land, Antarctica **(Fig. 8)**. An additional, minor population is present and consists of just two small shards of dacitic composition, one of which shows signs of abrasion and has a low total (<80 %). These particles are unlikely to represent a primary glass shard horizon and have therefore not been attributed a source. A second sulfate anomaly at 481.06 m (~26.242 ka) coinciding with a 5 mm visible tephra horizon was targeted as a potential local eruption marker horizon. Analysis of glass from this tephra also shows a strong Mount Berlin compositional match and is further discussed in **Sect. 4.2 (Fig. 9)**.

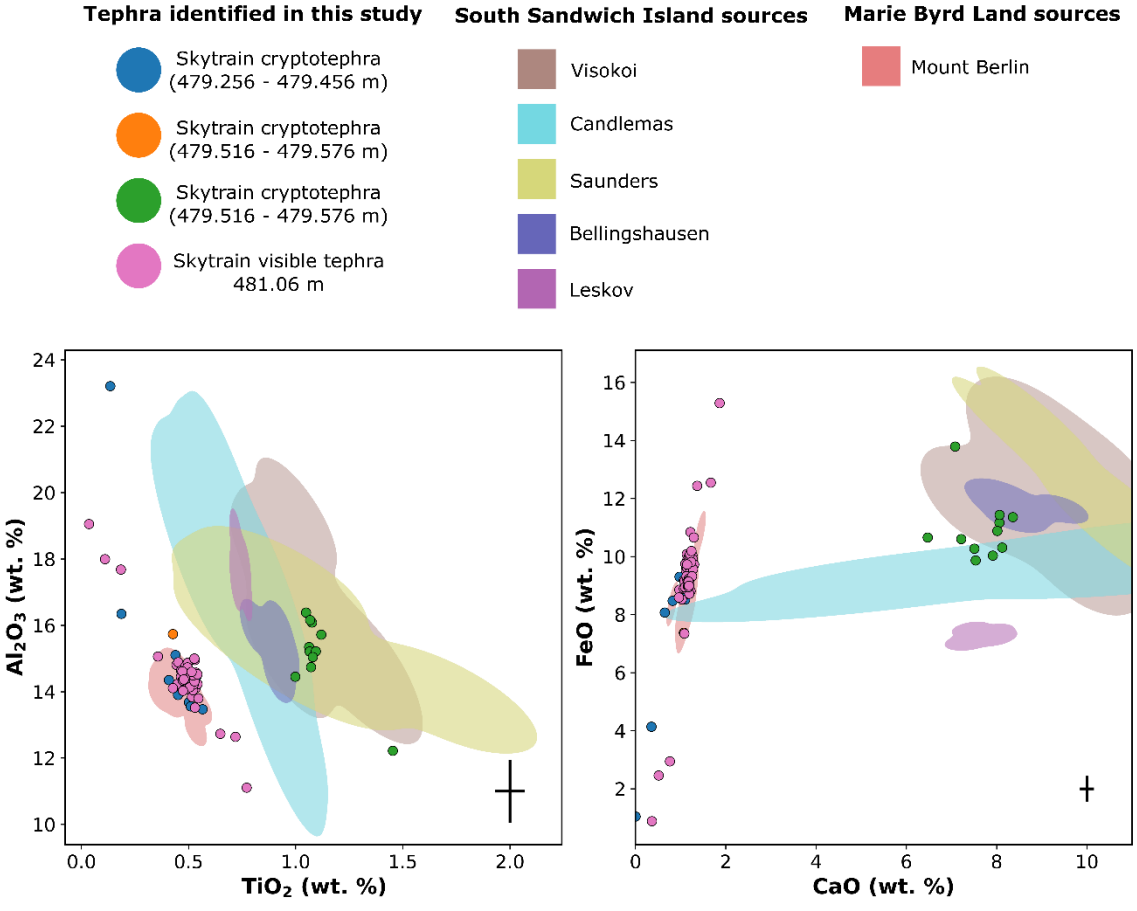

https://doi.org/10.5194/egusphere-2026-3434
Preprint. Discussion started: 9 September 2026

790 ***Figure 8:*** *Geochemical biplots showing the correlation between new Skytrain cryptotephra and Skytrain visible tephra samples (Skytrain_26.2), and Mount Berlin (red KDE field, threshold 0.01, data from Iverson et al. (2017b)) and the most compositionally similar South Sandwich Islands volcanic centres (Pearce et al., 1995). Only shards with >90% analytical totals were plotted. 2SDs plotted on ML3B standard values.*

795

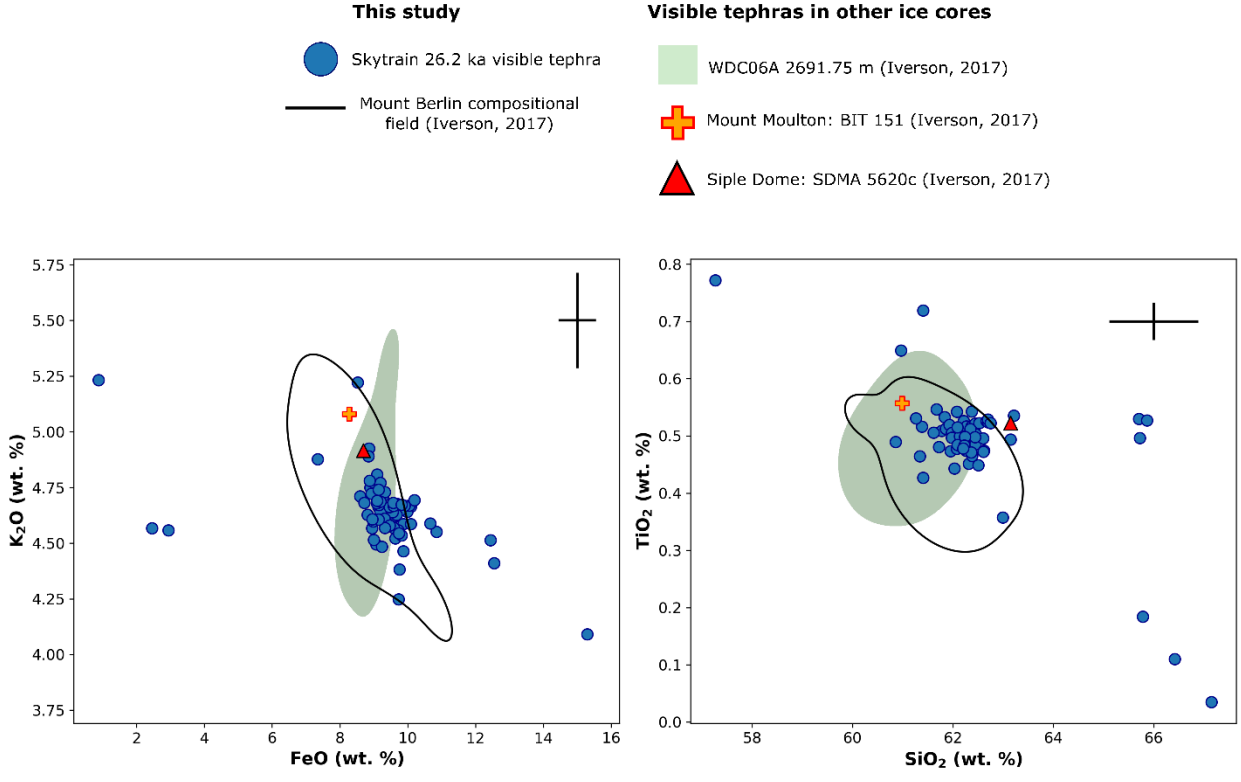

800

805

810 ***Figure 9:*** *Skytrain ~26.2 ka visible tephra composition compared with similarly ages tephras in WDC06A, Mount Moulton (BIT-151), and Siple Dome (SDMA-5620c) (Iverson, 2017). 2SD bars for measured KN18 standard values.*

https://doi.org/10.5194/egusphere-2026-3434
Preprint. Discussion started: 9 September 2026

3.3 Sulfate deposition

Our identification and confirmation of the Ōruanui eruption signature in multiple cores (WDC06A, EDML, DF2) allows us to revise estimates of cumulative sulfate deposition over Antarctica. Despite a lack of glass particles, the size and excellent age match of the SPC-14 sulfate anomaly indicates that Ōruanui sulfate deposition occurred at South Pole. A lack of published sulfate data from the DF2 record means that we were unable to incorporate this core in loading calculations, despite glass being located at this site. Using WDC06A, EDML, and SPC-14 sulfate deposition values (**Table 5**; Lin et al. (2022)), the average Antarctic Ōruanui-derived sulfate deposition is ~270 kg km^{-2}. This is a ~40% increase from original estimates by Lin et al. (2022), and the average Greenland deposition from Lin et al. (2022) is ~190 kg km^{-2}, consistent with expectations of asymmetry between the poles for a SH mid-latitude eruption. Note that we exclude EDC from our revised Antarctic estimate, due to suspected wind erosion that reworks and occasionally removes volcanic signals at this site even under recent climate conditions (Gautier et al., 2016), and no current identification of glass at the site to confirm the assigned anomaly is correct. Using WDC06A, EDML, and SPC-14 we recalculated a VSSI of 114 ± 33 Tg S (342 ± 99 Tg SO_4^{2-}) for the Ōruanui supereruption, a value that is within error of that estimated from petrological techniques (~390 Tg sulfate: Sharpe et al., 2022). To estimate radiative forcing potential of the Ōruanui eruption using VSSI, the observationally constrained volcanic forcing emulator EVA_H (Aubry et al., 2020) was utilised. Following Verkerk et al. (2025), a 1000-member ensemble was generated by sampling eruptive parameters, including SO_2 mass and injection height, within their respective uncertainty range (**Table S4**). Using this model, we estimate a global mean (monthly) SAOD value of 0.56 (0.28 to 0.88, 95% confidence interval). A global mean ERF value of -8.6 W m^{-2} (-4.9 to -12 W m^{-2}, 95% confidence interval) was calculated for the Ōruanui eruption using an exponential transformation from Marshall et al. (2020) (**Eq. 2**), suggesting that the eruption would have had substantial impacts on global climate.

https://doi.org/10.5194/egusphere-2026-3434
Preprint. Discussion started: 9 September 2026

Table 5: *New sulfate deposition estimates for the Ōruanui supereruption.*

Core	Depth (m)	Sulfate deposition (kg km^{-2}) Lin et al. (2022)	Sulfate deposition (kg km^{-2}) This study
WDC06A	2660.23	370.1	350.3
EDML	1069.71	265.7	264.1
EDC	561.29	7.2	6.1
SPC-14	1191.12	N/A	332.5

3.4 Volcanic ash dispersion model sensitivity tests

Existing simulations of ash deposition from an Ōruanui-like eruption suggest that an eruption of this magnitude from the TVZ would have produced variable deposition across Antarctica. On average, simulations indicate greater mass loading to West Antarctica (consistent with the high shard counts recovered from WDC06A) and lower mass-load "fingers" of ash dispersed over parts of East Antarctica, leaving some regions largely ash-free (Dunbar et al., 2017). The Ash3d model scenarios (**Fig. 10, Table S5**) show that, for the same grain size, the higher-altitude plume dispersed much more widely. However, particle size (40 or 80 μm) exerted a first-order control on dispersal patterns. Notably, only 1–3% of the simulations could reproduce the observed fallout of 80 μm particles in Antarctica, even with a higher-altitude plume (**Fig. 10d**). Particles >80 microns comprise only 2% of our measured size distribution by mass in the WDC06A ice core.

https://doi.org/10.5194/egusphere-2026-3434
Preprint. Discussion started: 9 September 2026

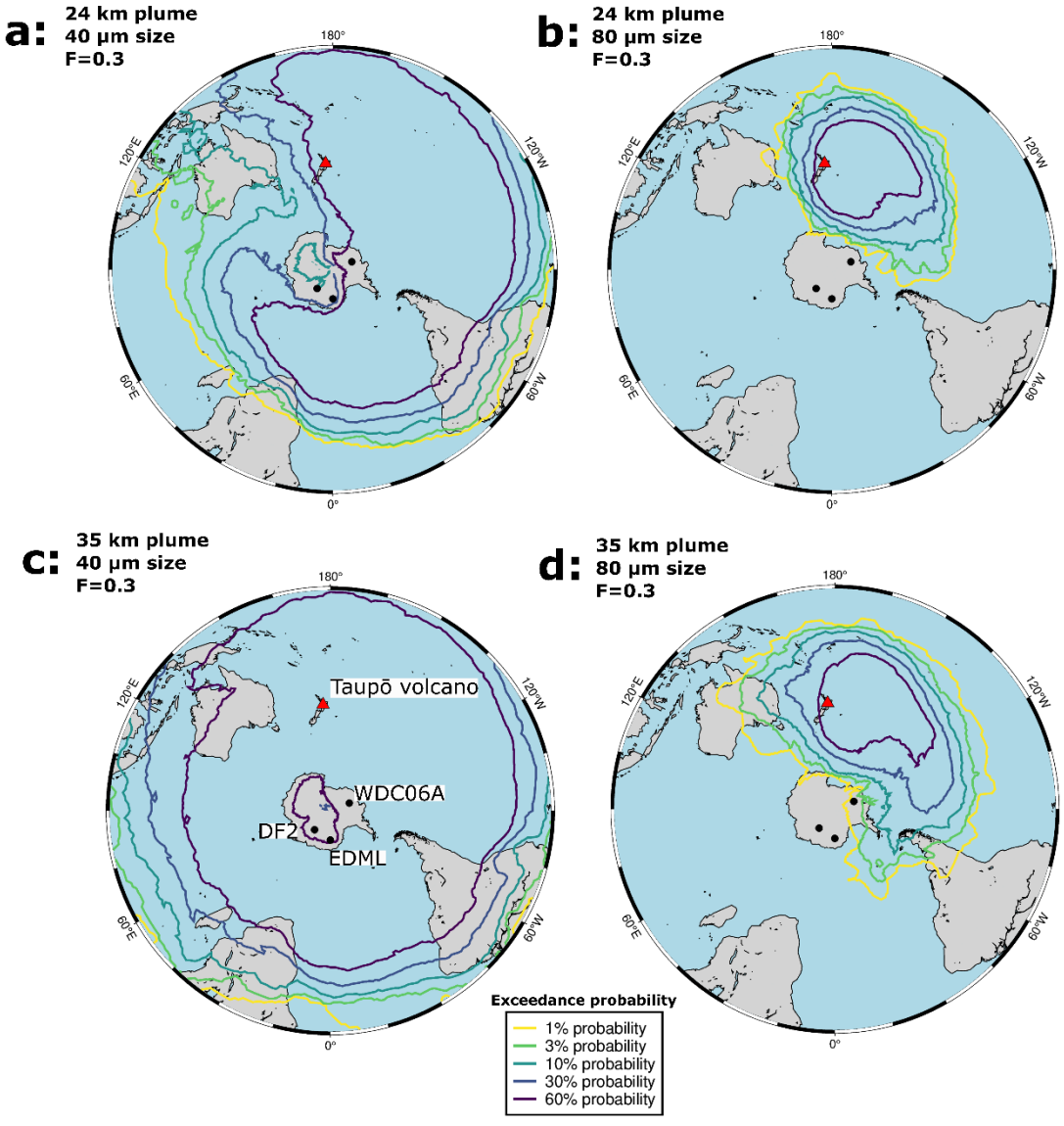

Figure 10: *Summary Ash3d simulation maps showing the percentage of 80 runs in each scenario that deposited >1 g m^2 ash over regions of Antarctica. Map (a) shows a summary of simulations run with 24 km plume height, 40 µm particle size, and particle shape factor F=0.3. Map (b) shows 24 km plume height, 80 µm particle size, and particle shape factor F=0.3. Map (c) shows 35 km plume height, 40 µm particle size, and particle shape factor F=0.3. Map (d) shows 35 km plume height, 80 µm particle size, and particle shape factor F=0.3.*

https://doi.org/10.5194/egusphere-2026-3434
Preprint. Discussion started: 9 September 2026

3.5 CESM2 model outputs

Climate simulations using the CESM2 model indicate that the Ōruanui eruption likely induced significant hemispheric cooling, with the SH experiencing peak surface temperature reductions of 2.5 – 3 K approximately one year after the event, most pronounced at 30 – 40° S (Australia/New Zealand) and in the simulation with the 1% halogen scenario (**Figs. 11 & 12**). In the Northern Hemisphere (NH), peak cooling of a similar magnitude occurred 1.5 – 2 years post-eruption, and was strongest in the 10% halogen scenario with some areas in continental regions experiencing up to 10 K cooling. A reduction in precipitation is evident in the SH and peaks after 1 year, whereas precipitation increases slightly in the NH. Model results suggest that climatic anomalies would have persisted for at least the 5-year duration of the simulations, but with temperatures on a trajectory to likely recover within a decade. Changes in AOD peak in the SH at ~2.7 – 3.7 and are smaller in the NH (~1), with perturbations largely returning to baseline after ~4 years (**Fig. 13a**). The simulations also reveal pronounced strong ozone column reduction in both 1% and 10% halogen scenarios, with the sulfur only scenario conversely showing slight ozone enrichment (**Fig. 13b**). Simulations with 1% halogens are close to recovery to baseline ozone levels after 5 years, however, 10% halogen injection shows a major decline of column ozone beyond the model run timeframe, in line with previous sulfur- and halogen-rich model simulations for very large eruptions (e.g., Cadoux et al., 2015; Brenna et al., 2019, 2020; Fuglestvedt et al., 2025).

https://doi.org/10.5194/egusphere-2026-3434
Preprint. Discussion started: 9 September 2026

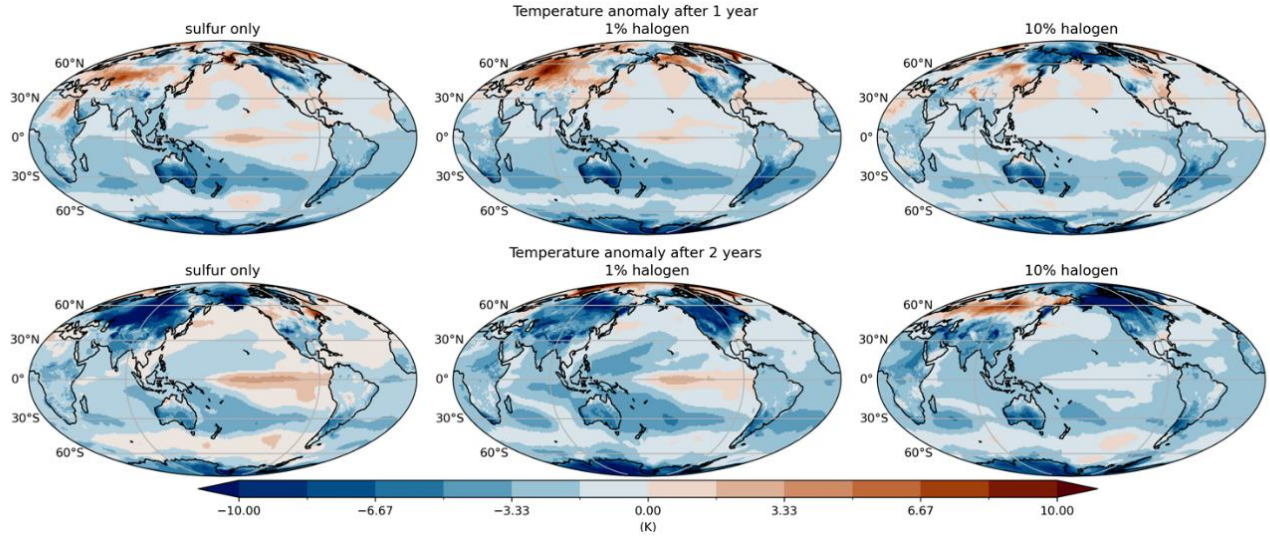

Figure 11: *CESM2/WACCM modelled surface temperature anomalies after 1 and 2 years of eruption onset, for three scenarios: sulfur only, 1% halogen, and 10% halogen injection.*

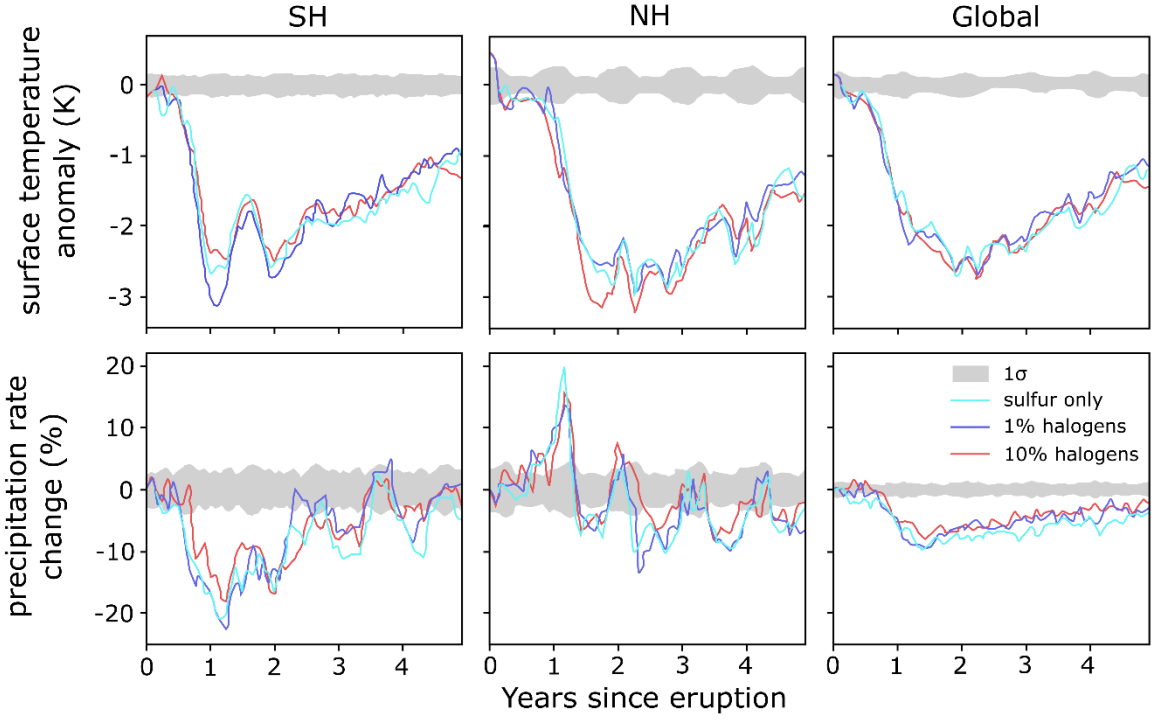

Figure 12: *Modelled surface air temperature anomalies and precipitation rate change over 5 years post-eruption for sulfur only, 1% halogen, and 10% halogen scenarios.*

https://doi.org/10.5194/egusphere-2026-3434
Preprint. Discussion started: 9 September 2026

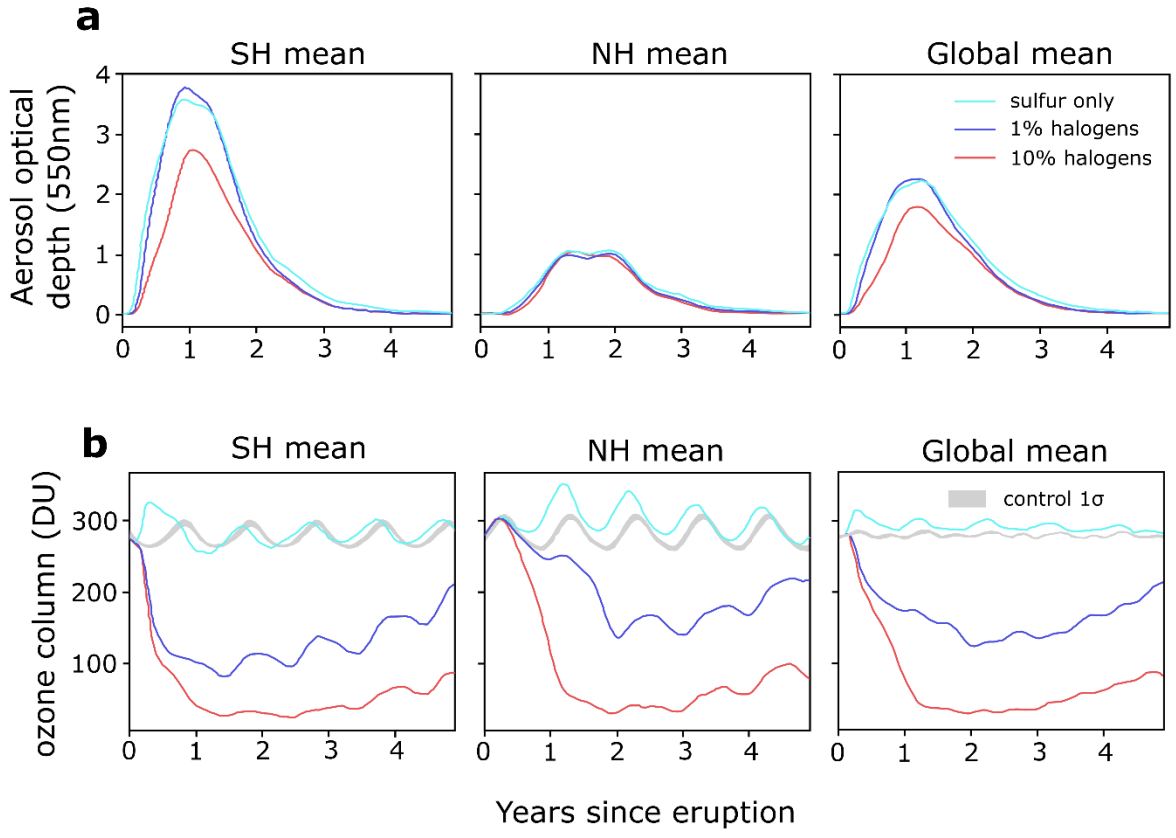

Figure 13: ***(a)*** *Mean aerosol optical depth (550nm) for the Southern Hemisphere (SH), Northern Hemisphere (NH), and the global mean under three emission scenarios.* ***(b)*** *Post-eruption ozone depletion in the Southern Hemisphere (SH), Northern Hemisphere (NH), and the global mean under three emission scenarios.*

https://doi.org/10.5194/egusphere-2026-3434
Preprint. Discussion started: 9 September 2026

4 Discussion

4.1 Variability in preservation of Ōruanui eruption signals across Antarctica

4.1.1 Volcanic ash deposition across Antarctica

We identify Ōruanui glass populations at three out of six investigated core sites: WDC06A, EDML, and DF2. All three populations show strong geochemical compositional similarities to distal ice core glass analysed by Dunbar et al. (2017), and to deposits analysed from terrestrial and marine records of the Ōruanui eruption (e.g., Dunbar et al., 2017; Miller et al., 2026) **(Fig. 7).** While distal Ōruanui tephra deposits show only subtle internal stratigraphy (Allan et al., 2017; Miller et al., 2026), we infer that the glass shards in Antarctica represent the later and most voluminous stages of the Ōruanui eruption, with enough explosivity to transport material to Antarctica (Wilson, 2001).

Based on our new Ash3d simulations of deposited ash onto the Antarctic continent, we establish that plume height, particle size and particle shape are major factors influencing the geographic spread of fine particles from the plume. Through comparison of the Ash3d scenarios with our observations of glass shard number concentrations and particle sizes, and glass shard geochemistry in ice cores across Antarctica, we find that deposition as far south as Antarctica is most effective with a 35 km umbrella cloud height and low shape factor value (0.3), with substantially higher deposition values and coverage across the SH from 40 µm compared to 80 µm shards, i.e., Scenarios C and D (**Figs. 10c and d, Table S5)**. Our simulations show that under the right conditions (e.g., for shards with shape factors ≤ 0.3), shards >80 µm may reach Antarctica (e.g., 1% of shards, in Scenario D), consistent with our observations of shards up to 110 µm at WDC06A. The overall simulated trend of deposition onto Antarctica shows higher probability of glass particles reaching West Antarctica and the Antarctic Peninsula, and lower probability of deposition of East Antarctica or the South Pole **(Fig. 10)**, which supports our findings of a more numerous, coarser shard population at WDC06A, compared to smaller sparse populations in EDML and

https://doi.org/10.5194/egusphere-2026-3434
Preprint. Discussion started: 9 September 2026

DF2, and no apparent shard populations at other investigated sites. However, we note that greater aeolian reworking in East Antarctica could also be a reason for the difference between cores. Based on visual inspection of shards under transmitted light, we infer that most particles are cuspate in shape, with many exhibiting shard thicknesses of <5 µm and therefore shape factors averaging 0.3. Such thin shard morphologies would have helped facilitate long-range transport, since particles can behave like microscopic umbrellas (Stevenson et al., 2015). In Scenario A (**Fig. 10a**), using 24 km plume height (Van Eaton et al., 2012), 40 µm particle size (Matthews et al., 2012), and a shape factor of 0.3 from our BSE observations, we note that out of 80 simulations run, >1 g m^{-2} ash deposition occurred in 60 % of these at WDC06A, whereas at EDML and DF2 this value falls to between 10 – 30 %, in line with our observations of higher glass deposition in WDC06A and lower counts in EDML and DF2. Scenario C shows an additional isopleth within the 60% area, suggesting a reduced likelihood of glass deposition across the central Antarctic continent. This may represent a high-pressure polar system that inhibits the advection of ash towards the pole. This could also explain the lower shard abundances and smaller shard sizes observed at EDML and DF2, which are located within the additional isopleth, compared with WDC06A, which lies outside this area.

Historic volcanic eruptions such as the 2010 Eyjafjallajökull and 2011 Puyehue-Cordón Caulle events highlight that ash can have multiple tropospheric transport routes and demonstrate how natural variability in atmospheric transport can produce heterogeneous ash deposition at both regional and distal scales, including to the polar regions (Gudmundsson et al., 2012; Koffman et al., 2017). Westerly winds and synoptic circulation patterns around Antarctica are a key driver of the particle size distribution and insoluble particle concentrations in ice cores, and may influence the distribution of volcanic material during settling through the troposphere. Koffman et al. (2013) and Neff and Bertler (2015) suggest that such pathways control tropospheric dust deposition, often with higher loading in West Antarctica, and lower loading in East Antarctica, a trend also demonstrated by our

https://doi.org/10.5194/egusphere-2026-3434
Preprint. Discussion started: 9 September 2026

glass abundance and particle size data. Integrating the Ash3d modelling and ice core observations, suggest that ash from Ōruanui would have settled out from the stratosphere through the troposphere en-route to ice sheets, with regional atmospheric circulation processes in the lower atmosphere also influencing the spatial distribution patterns of glass shard concentration and particle size across Antarctica. Post-depositional processes likely also influenced the preservation of Ōruanui glass deposits in ice. For example, volcanic glass in WDC06A and EDML occurs within single-sample horizons, whereas in DF2 it is found in two non-adjacent sample intervals. This pattern likely reflects partial erosion or surface reworking at DF2, enhanced by the low snow accumulation rate.

4.1.2 Variability in glaciochemical anomalies across Antarctica

Glaciochemical anomalies preserved in ice cores, such as sulfate and conductivity, provide key evidence of past volcanic eruptions. These proxies are more widely preserved and easily detected via continuous chemical analysis techniques compared to volcanic glass shards, which require intensive manual investigation (e.g., Legrand, 1997; Cole-Dai et al., 2021; Plunkett et al., 2023). However, the magnitude of these anomalies can vary substantially between sites for the same eruption, and such variability can occur even between ice cores located within close spatial proximity (e.g., Dunbar et al., 2003; Wolff et al., 2005; Gfeller et al., 2014; Gautier et al., 2016; Kjær et al., 2022). Understanding the reasons for this variability is important, as it impacts estimates of volcanic forcing using sulfate signals in ice, offers insights into aerosol atmospheric transport pathways to Antarctica, as well as the depositional and post-depositional processes that may influence the preservation of glaciochemical volcanic signals in ice cores.

The glaciochemical data presented in **Fig. 3** and **Table 5** demonstrate that volcanic proxies for Ōruanui vary considerably in both preservation and signal strength across the range of investigated ice cores. Strong sulfate anomalies are recorded in WDC06A, SPC-14, and EDML, with very high sulfate concentrations up to several thousand ppb, whereas DF2, EDC, and TALDICE preserve weaker signals (<500 ppb sulfate, where reported). In

https://doi.org/10.5194/egusphere-2026-3434
Preprint. Discussion started: 9 September 2026

Vostok, Skytrain, and RICE no specific candidate horizons satisfied our Ōruanui identification criteria. The Ōruanui event is considered to have produced largely stratospheric sulfate transport to the pole (given the large sulfate output of the event: Sharpe et al., 2022, the power of the eruption plume: Wilson, 2001; and the potential for a lowered tropopause over New Zealand during the LGM: Ladstädter et al., 2025), with the variability in magnitude and presence of glaciochemical signals suggested to reflect processes affecting sulfate transport while settling through the troposphere above Antarctica in the months to years following the eruption. In addition to atmospheric processes, local depositional factors and site-specific processing may also influence sulfate deposition and the strength of the anomaly. In general, ice cores with relatively high accumulation rates and located further inland provide the most reliable records for preserving volcanic anomalies in the case of Ōruanui. For example, the WDC06A, EDML, and SPC-14 cores meet these criteria and have the strongest sulfate anomaly preservation of the cores examined. In contrast, cores such as RICE, Skytrain, and TALDICE appear to be less suitable, as their proximity to the ocean introduces stronger marine influence, with volcanic sulfate becoming harder to identify. Some inland cores, including Dome Fuji, EDC, and Vostok, are also problematic despite their distance from the ocean, primarily due to their very low accumulation rates allowing greater snow redistribution effects and erosion of anomalies. However, some sites do not follow this broad pattern. For example, TALDICE preserves a much stronger signal than most East Antarctic sites despite its proximity to the coast, and the Ōruanui sulfate anomaly was successfully identified at DF2 despite its low accumulation rate and potential for reworking.

Post-depositional processes likely also play a role in the preservation of signals at both regional and local scales (e.g., Dunbar et al., 2003; Wolff et al., 2005; Gautier et al., 2016). Previous studies of historic eruption records in polar ice cores such as Laki 1783 (Gao et al., 2007), Tambora 1815 (Gao et al., 2007, 2008; Sigl et al., 2014; Marshall et al., 2018), Katmai 1912 (Gao et al., 2007), Agung 1963 (Gao et al., 2008), Cerro Hudson 1991 (Harlan et al., 2026) and Pinatubo 1991 (Gao et al., 2007, 2008) have documented a similar pattern, with sulfate deposition

https://doi.org/10.5194/egusphere-2026-3434
Preprint. Discussion started: 9 September 2026

records from the same event varying significantly in magnitude and presence across multiple ice cores (Toohey et al., 2013; Sigl et al., 2014; Lin et al., 2022). Snow drift and wind erosion can remove fresh snow layers containing volcanic sulfur before burial, or partially erode deposits, leaving absent or muted anomalies at some core sites, as noted by previous work (Das et al., 2013). For example, Gautier et al. (2016) demonstrated a lack of replication of the Tambora 1815 eruption horizon in two out of five cores drilled just 1 m apart from each other at the EDC site. This site is particularly prone to wind erosion, suggesting that local processes can impact signal preservation from global eruptions. Wolff et al. (2005) demonstrated very similar patterns and conclusions at this site through investigation of 45 kyr of eruptions in two cores spaced at a 10 m distance. It is important to note that sites such as WDC06A, EDML, and SPC-14 have accumulation rates which are 3 to 10 times higher than those at EDC during the LGM, making these records less susceptible to post-depositional alternations.

Our results also infer the timing, transport pathways, and extent of post-depositional processing of volcanic signal deposition. A key observation is that all three Ōruanui glass shard horizons consistently occur on the rising shoulder of the sulfate anomaly (i.e., shards were deposited before the peak sulfate anomaly), suggesting a timing offset between peak sulfate and volcanic glass deposition (**Fig. 4**). Ash3d modelling suggests that glass from Ōruanui would have likely been transported to Antarctic ice sheets within ~2–4 weeks of eruption (Dunbar et al., 2017). In contrast, sulfate aerosols injected into the stratosphere may remain suspended for 2–3 years (depending on injection height at circulation) before being deposited onto ice sheets (Robock, 2000). This decoupled depositional timing between the two volcanic proxies suggests a longer transport and depositional period (i.e., long-range, likely stratospheric transport) when compared to proximal (tropospheric) eruption signals preserved in ice, and creates a distinct and traceable signature that has been used by many to discriminate distal and proximal eruptions in ice core records (e.g., Abbott and Davies, 2012; Dunbar et al., 2017; Abbott et al., 2021; Piva et al., 2023a; Plunkett et al., 2023; Hutchison et al., 2024a). It is worth noting that the sulfate and conductivity anomalies

https://doi.org/10.5194/egusphere-2026-3434
Preprint. Discussion started: 9 September 2026

are likely broader than their original forms due to diffusion in the ice over time, with lower accumulation sites being more severely affected. Eruptive sources close to the poles with lower transport distances often produce coeval sulfate and glass deposits (e.g., Abbott and Davies, 2012). Within this broader context, the pronounced sulfate anomalies and the tightly constrained stratigraphic occurrence of glass particles in WDC06A, EDML, and DF2 imply that the distal Ōruanui aerosol and ash clouds reached Antarctica, depositing glass shards within just a few weeks of eruption onset, and sulfate over the following years.

In summary, the observed patterns of Ōruanui ash deposition are best explained by a combination of atmospheric transport processes and site-specific depositional effects. Variations in shard size and abundance between sites can be explained by spatially heterogeneous dispersal and deposition of the volcanic plume driven by Southern Hemispheric westerly wind patterns and regional circulation, as supported by new Ash3d simulations of deposition across Antarctica. In contrast, the variability in glaciochemical signals between cores is best explained by broadly uniform stratospheric sulfate transport (supported by the offset between glass and sulfate deposition), followed by heterogeneous tropospheric deposition pathways and modification by localised post-depositional processes. Overall, Ōruanui material was likely injected into the stratosphere above New Zealand, before being transported towards Antarctica and settling through the troposphere. During this descent, winds influenced the spatial distribution of glass shards and their particle size distribution across the Antarctic Ice Sheet.

4.1.3 Ōruanui as a tie-point in Antarctic ice cores

The arrival age of Ōruanui-derived eruptive deposits to Antarctic ice sheets (25,318 ± 253 years BP), as determined by Dunbar et al. (2017), is supported by our identification of glass shard populations in EDML and DF2, confirming that the chronologies of these cores are accurate at this time. Because volcanic tie-points are scarce in ice cores during the LGM, Ōruanui now represents a key chronological marker for this interval. We also

https://doi.org/10.5194/egusphere-2026-3434
Preprint. Discussion started: 9 September 2026

identify a visible tephra close in age to Ōruanui that may serve as a further tie-point, aiding identification of the Ōruanui eruption in other ice cores. Analysis of glass from the ~26,242-year-old visible tephra in Skytrain ice (**Fig. 9**) shows a strong compositional match to tephras from Mount Berlin, a volcano in Marie Byrd Land, Antarctica, with only minor differences in NaO and FeO. Another visible tephra at a very similar age ~26,299 years (2691.75 m depth) in WDC06A has also been fingerprinted to Mount Berlin (Iverson, 2017). A comparison of these tephras alongside similarly aged deposits from Mount Moulton (BIT-151), and Siple Dome (SDMA-5620c), indicates strong compositional similarities (Iverson, 2017) (**Fig. 9**). Some of these horizons may therefore represent the same eruptive event; however, the frequent activity of Mount Berlin throughout the last glacial combined with the chemical similarly of its deposits makes definitive correlations difficult (Dunbar and Kurbatov, 2011).

4.2 Challenges in locating global eruptions in ice cores

Our investigation of the Ōruanui eruption signals across multiple ice cores highlights the inherent challenges associated with identifying volcanic anomalies from a single event across diverse datasets with varying resolution and data types. It also provides important new insights into the factors that influence the detectability of eruptions, which may be useful for targeting and interpreting other large volcanic events in Antarctic ice cores in the future. The main difficulties encountered in locating eruptions in Antarctic ice cores are outlined below:

(1) Variability in data availability and type of proxies recorded is a major limitation for comparing ice cores. Some sites (e.g., WDC06A) have detailed glaciochemical records of the Ōruanui interval, whereas others (e.g., Vostok) have limited data availability, hindering a consistent interpretation across cores. Sulfate concentration is one of the most important indicators of volcanic signals; however, its absence at this depth at key sites such as RICE - despite favourable transport pathways and prior identification of the New Zealand Taupō tephra (Piva et al., 2023a) - prevents identification of the eruption horizon. Insoluble

https://doi.org/10.5194/egusphere-2026-3434
Preprint. Discussion started: 9 September 2026

particle records further complicate comparisons between sites due to differences in analytical methods, calibration, and size ranges reported.

(2) Sampling resolution in both time and volume also represents a fundamental limitation in detecting and correlating volcanic signals across ice core records. Volcanic particle deposition typically occurs over short timescales of weeks to months, while sulfate aerosols may be deposited over several years. However, depending on site-specific accumulation rates, individual ice core samples used for particle and sulfate concentration analysis can integrate many years of deposition. For example, in the Skytrain ice core investigated in this study, a single sample represents approximately 13 years of accumulation, greatly increasing the likelihood that short-lived volcanic signals are diluted with background variability, or entirely smoothed out and missed. Further thinning of the ice with depth enhances the risk of entirely missing the few glass shards that were originally deposited in a layer.

(3) The presence of non-volcanic sources of glaciochemical tracers commonly used to identify eruptions, particularly sulfate and insoluble particles. For example, SPC-14 ice core exhibits a pronounced particle peak that does not coincide with the expected stratigraphic position of glass relative to the sulfate anomaly. We found this to reflect enrichment in fine mineral dust, rather than volcanic glass, highlighting that while particle counts are useful in guiding locations to search for particles, they are not always representative of volcanic glass populations or signal eruption timing. In addition, marine biogenic emissions, sea salt, continental dust, and biomass burning can all contribute sulfate and conductivity signals to Antarctic ice (e.g., Sigl et al., 2016; Winstrup et al., 2019), particularly at coastal sites, producing background variability unrelated to volcanism.

(4) Lastly, for distally located eruptions such as Ōruanui, glass shards are often scarce, fine-grained, and unevenly distributed, making their successful recovery and analysis highly dependent on glass extraction methods, and analytical thresholds such as EPMA beam size. This inherent variability means that the

https://doi.org/10.5194/egusphere-2026-3434
Preprint. Discussion started: 9 September 2026

absence of analysable glass at a given site does not necessarily indicate the absence of volcanic deposition, complicating efforts to replicate and correlate eruption horizons across multiple ice cores. We note that locating glass shards using insoluble particle anomalies can be challenging, particularly if particle size bins vary or are not reported. Insoluble particle counts over intervals from this study were typically on the order of 10^5 mL^{-1}, whereas glass shard counts are much lower. It is therefore unsurprising that dust peak positions do not consistently align with glass shard locations. At WDC06A, the eruption horizon coincides with a pronounced insoluble particle anomaly, consistent with the recovery of thousands of glass shards **(Fig. 5).** In contrast, EDML records only a minor increase in insoluble particle flux (**Fig. 3b**), and DF2 shows little deviation from background levels, consistent with shard counts in the tens. These observations indicate that insoluble particle counts and flux can be useful for pinpointing glass populations, but more so in cores with lower particulate backgrounds, and where glass shard counts are high.

Despite challenges arising from dataset variability, sampling resolution, non-volcanic contributions, the low abundance, small size, and uneven preservation of volcanic glass shards, and the risk of incomplete recovery from extraction methods, we pinpoint evidence for the Ōruanui supereruption horizon at multiple Antarctic ice core sites, largely aided by our refined glass shard extraction methodology. Below, we use this critical new information to provide new insights into potential eruption impacts.

4.3 Do supereruptions result in severe climate impacts?

Ice cores preserve both volcanic glass and sulfate, which enables precise eruption identification and high-resolution assessment of post-eruptive climate impacts within well-resolved age models. Here we use the established methods of Lin et al. (2022) to revise and quantify Ōruanui sulfate deposition to Antarctica, infer

https://doi.org/10.5194/egusphere-2026-3434
Preprint. Discussion started: 9 September 2026

stratospheric sulfate injection, to estimate the associated radiative forcing and AOD change (Gao et al., 2007; Toohey and Sigl, 2017; Aubry et al., 2020; Marshall et al.. 2020; Lin et al., 2022).

4.3.1. Sulfate deposition estimates

The injection of large volumes of volcanic sulfur into the stratosphere is known to drive abrupt cooling in the months to years following major eruptions (Rampino and Self, 1984; Robock, 2000). Estimating stratospheric sulfur injection is therefore critical for understanding eruptions in the geological record. Sulfate deposition onto polar ice sheets provides a key tool for this purpose, and has previously been used to calculate the stratospheric injection and radiative forcing of numerous historic and prehistoric eruptions (e.g., Sigl et al., 2015; Toohey and Sigl, 2017; Lin et al., 2022; Sigl et al., 2022; Innes et al., 2025). With the inclusion of the SPC-14 ice core in our calculations, the Antarctic sulfate deposition estimate for Ōruanui increases from initial estimates by Lin et al. (2022) as expected. Lin et al. (2022) applied a tropical transfer function, which led to higher estimates of VSSI and ERF for the eruption. Consequently, our VSSI value of 114 ± 33 Tg S (342 ± 99 Tg SO_4^{2-}) is slightly lower than the previous ice core estimate (127.4 Tg S), but is still within uncertainty of petrological estimates of >130 Tg S ejection (Sharpe et al., 2022). This VSSI is broadly in alignment with estimates for other large eruptions **(Table 6),** with Ōruanui now placing as the sixth largest sulfate-producing event in the past 60 ka (Lin et al., 2022).

Table 6: *Volcanic Stratospheric Sulfur Injection (VSSI) estimates from a selection of large, explosive eruptions in the calculated using ice core records, along with uncertainty on these values (1σ). Where multiple estimates for VSSI exist, the minimum value is displayed.*

Eruption	Latitude	VSSI (Tg S)	1σ	Reference
Pinatubo 1991	15.14	9.0	2	Toohey and Sigl (2017)
Tambora 1815	-8.24	28.1	4	Toohey and Sigl (2017)
Samalas 1257	-8.5	59.4	11	Toohey and Sigl (2017)

https://doi.org/10.5194/egusphere-2026-3434
Preprint. Discussion started: 9 September 2026

Ōruanui 25.5 ka BP	-38.82	114	33	This study
Mazama 7.6 ka BP	42.92	162.0	47	Sigl et al. (2022)
Toba YTT (T2) 74 ka BP	2.62	178.0	32	Lin et al. (2023)
Atitlan LCY 80 ka BP	14.6	226.0	48	Innes et al. (2025)

4.3.2 Climate forcing of the Ōruanui eruption

The ERF value calculated for Ōruanui through EVA_H (-8.6 W m^{-2}) is almost three times more negative than that recorded for the Pinatubo 1991 eruption (Hansen et al., 1992; Schmidt et al., 2018), which itself resulted in ~0.5°C average global cooling in following years (McCormick et al., 1995). However, this model does not fully take into account circulation patterns, precipitation, or depositional processes. As a fully coupled Earth system model, CESM2 has the ability to couple atmosphere, ocean, land, sea-ice, and ice sheet components (Danabasoglu et al., 2020), making it a particularly useful tool for investigating feedback from abrupt climate disruption resulting from the injection of huge volumes of sulfur and halogens into the atmosphere. Our simulations of an Ōruanui-like eruption in CESM2 further highlight the global climatic impacts and indicate that volcanic cooling would have been broadly similar in magnitude between the NH and SH, with peak hemispheric cooling reaching up to 3 K in both hemispheres (**Figs. 11 and 12**). However, peak cooling occurred after approximately one year in the SH, compared to closer to two years in the NH. The onset of cooling occurred sooner in the SH, with a delayed onset in the NH resulting in peak cooling almost a year later, consistent with the source hemisphere of the event. Notably, global surface temperature anomalies persisted for more than five years after the eruption and did not recover before the end of the modelled period, indicating a distinct short-term perturbation of the global climate system, beyond that of other smaller eruptions in historic records. The strongest changes in AOD occurred in the SH, although smaller impacts were also noted in the NH, with a ~4-year recovery period. The difference between AOD, which is much more severely affected in the SH, and the surface temperature response, which is relatively similar between hemispheres, could be explained by the greater continental landmass in the NH, which cools more rapidly than oceanic regions, as shown in **Fig. 11**. Another possible explanation is that an El Niño response may

https://doi.org/10.5194/egusphere-2026-3434
Preprint. Discussion started: 9 September 2026

be simulated following the eruption, resulting in strengthened warming in the NH (e.g., Kim et al., 2025). Interestingly, the SH AOD response was slightly muted in the 10% halogen scenario compared to the 1% halogen and sulfur only scenarios (**Fig. 13a**). We suggest this phenomenon is due to the fact hydroxyl (OH) concentrations were depleted, resulting in delayed conversion of SO_2 to SO_4^{2-}, or alternatively differences in effective aerosol radii sizes leading to more rapid fallout and no longer-lasting anomaly (e.g., Brenna et al., 2019; Osipov et al., 2021). In parallel, stratospheric ozone experienced strong decline extending beyond the polar vortex area, with recovery over a longer period than temperature, likely exceeding >7 years. This longevity agrees with other sulfur and halogen simulations (Cadoux et al., 2015; Brenna et al., 2019, 2020; Ming et al., 2020) and our findings reemphasise the potential for prolonged impacts of volcanic sulfur and halogens (**Fig. 13b**). While the SH was most strongly affected by both scenarios of halogen output, the NH was also projected to have experienced significant ozone decline. These key modelling results using constraints from both petrological and ice core inputs reveal the potential severe short-term (<10 year) global impacts of an Ōruanui-like eruption on temperature, precipitation, and ozone. Precipitation rates also change following the eruption across all three scenarios, with major decreases in the SH during the year after the eruption and recovery over the following 3–4 years. In contrast, the NH shows a different trend, with increased precipitation simulated at approximately one year after the eruption. This may suggest that, following the initial eruption-driven cooling, the Intertropical Convergence Zone (a low-pressure belt that circles the equator) shifted northwards, resulting in enhanced NH precipitation. Such changes could have intensified monsoon systems in regions such as Asia, with potential implications for environment and early societies within this region.

Our models highlight that although the climate impacts of Ōruanui were severe, they lasted less than a decade. Consistent with this, high-resolution $\delta^{18}O$ records from WDC06A, which provide a proxy for temperature and precipitation conditions at the time of snowfall, show a sharp negative shift coincident with Ōruanui sulfate

https://doi.org/10.5194/egusphere-2026-3434
Preprint. Discussion started: 9 September 2026

deposition. However, we note that the record had begun to decline before volcanic deposition commenced, reaching its lowest values within the ±35-year interval, suggesting a possible short-term volcanic cooling signal, although the record may also be partly influenced by a core break (**Fig. 14**). SPC-14 shows a smaller, muted decrease, with overall $\delta^{18}O$ records supporting climate modelling estimates to suggest the eruption did not trigger long-term decadal-scale change. This conclusion is supported by the palynological work of Piva et al. (2023b), who found that sediments directly above the Ōruanui tephra record a decline in the relative abundance of the dominant canopy species *Fuscospora*, with a general recovery occurring over a period of <10 years. Together with recent findings for the Los Chocoyos supereruption (Brenna et al., 2020; Innes et al., 2025), our new results suggest that supereruptions in general may not necessarily produce long-lasting centennial climatic impacts, although their short-term impacts may be much more severe than any historic volcanic events.

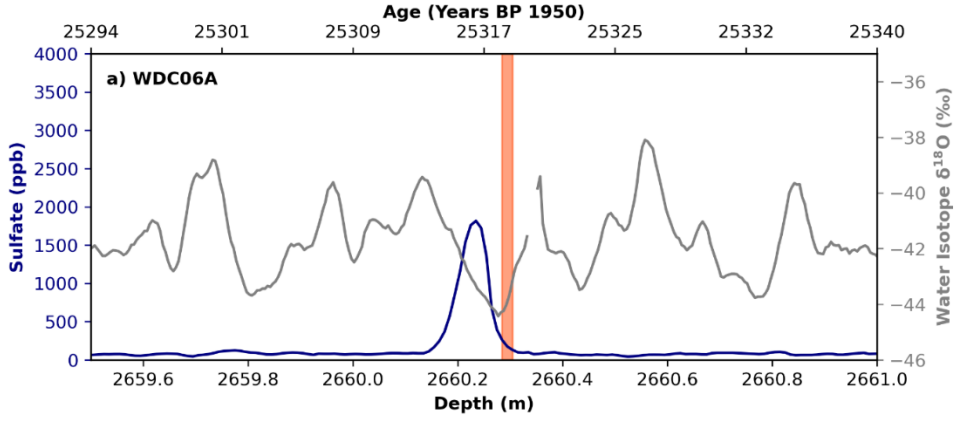

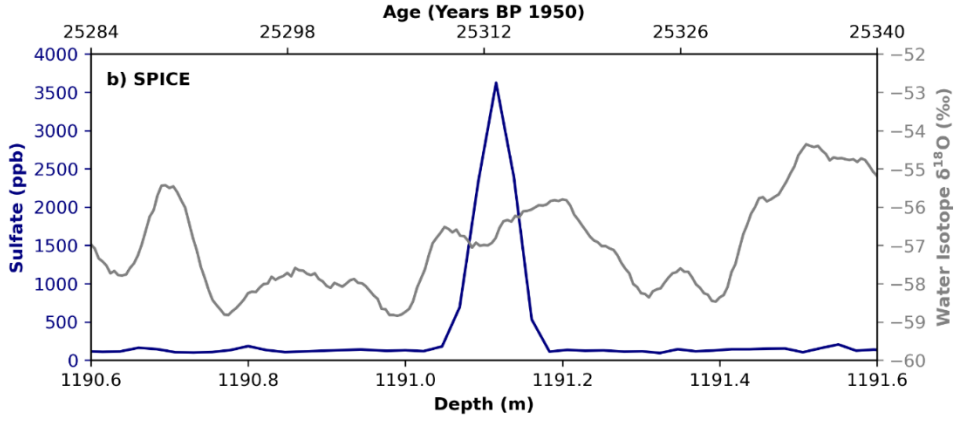

https://doi.org/10.5194/egusphere-2026-3434
Preprint. Discussion started: 9 September 2026

Figure 14: *Published high-resolution oxygen isotope records for WDC06A (Sigl et al., 2016; Jones et al., 2017) and SPC-14 (Steig et al., 2019) covering the Ōruanui event. The red bar shows the location of glass shards in WDC06A.*

4.3.3 Limitations of sulfur estimates, radiative forcing, and modelling, and future work

Several limitations affect the sulfate deposition and ERF calculations presented here that should be considered regarding the model results. Firstly, the geographic coverage and number of ice core sites are limited. With only three Antarctic cores included, large areas of the East Antarctic Plateau in particular remain unquantified. By excluding EDC (a low accumulation rate sites that records minimal deposition), our estimate reflects a maximum scenario that is biased toward higher-deposition sites with well-preserved anomalies. Secondly, all calculations rely on assumptions about deposition pathways and hemispheric distribution. Following existing methods (e.g., Gao et al., 2007; Toohey and Sigl., 2015), we assume that all sulfate deposited on the Antarctic ice sheet from Ōruanui originated from stratospheric injection, neglecting any potential tropospheric component which is yet to be quantified. We also retain the Greenland anomalies identified by Lin et al. (2022) without modification, assuming that these signals correctly represent the Ōruanui eruption rather than unrelated events occurring within the same time interval, although we provide scenarios where Greenland receives no deposition as a sensitivity test (**Table S3**). Future work could assess Greenland anomalies for Ōruanui glass shards, although our Ash3d assessment does not suggest large-scale Northern Hemisphere particle dispersal. Further work on sensitivity testing of Antarctic transfer functions, as was recently done for Greenland, would help evaluate the uncertainties associated with these calculations. Many uncertainties also arise from needing to estimate eruption parameters such as SO_2 injection altitude and eruption timing (start and duration). EVA_H is calibrated against the satellite era (1979 - 2015) record (Aubry et al., 2020), which is not an ideal analogue for an eruption of the magnitude of Ōruanui, and also does not consider dynamical circulation, precipitation, or deposition processes.

https://doi.org/10.5194/egusphere-2026-3434
Preprint. Discussion started: 9 September 2026

There are also a number of uncertainties associated with the CESM2(WACCM6) model which must be noted. In the application of this model to an Ōruanui-like eruption, there is a level of uncertainty in the parameters applied for the eruption scenario, as well as the fact that simulations were conducted under pre-industrial (1850) boundary conditions rather than those of an LGM climate. While historical simulations show improved agreements with present day observations, residual biases in ice sheet extent, precipitation, radiation, and teleconnections, highlight areas of model uncertainty that should be considered when interpreting results. We note that there are also particularly large uncertainties in the choice of halogen contents of the plume and the mass of halogens that reached the stratosphere. Estimation of original HCl contents of the Ōruanui magma and associated fluid phases are highly sensitive to pressure and vary over an order of magnitude (Sharpe et al., 2022). Bromine (Br) can have major impacts on climate and ozone (von Glasow et al., 2009; Kutterolf et al., 2013; Krüger et al., 2015; Brenna et al., 2019; Waelkens et al., 2021) and has not been directly measured for the Ōruanui magma body, but has been scaled to Cl content (Unni and Schilling, 1978; Bureau et al., 2000). Therefore, further measurements are required to fully derive the total Br output of the Ōruanui eruption. The portion of the halogens erupted at the vent that reach the stratosphere is also not well constrained as halogens may be scavenged by water, ice and ash in the plume (Halmer et al., 2002). Given the water-rich nature of the Ōruanui plume (Wilson, 2001; Van Eaton et al., 2012), significant amounts of halogen removal may have occurred. Despite efficient scavenging, it is often suggested that around 10 % of the HCl emitted at the vent of large explosive eruptions in the tropics could reach the stratosphere (Textor et al., 2003; Krüger et al., 2015; Vidal et al., 2016; Brenna et al., 2020; Staunton-Sykes et al., 2021) whereas up to 75% may reach the stratosphere for high-latitude eruptions (Fuglestvedt et al 2025). While we have run a range of scenarios for halogen injection, further work could help refine the nature of the Ōruanui plume and the impact of such large-scale events on ozone levels, including the effects of ozone depletion on surface UV radiation levels (Brenna et al 2019, 2020). Ash3d also has several limitations that affect the reliability of its simulations. The model depends heavily on input data that are not well constrained, such as plume

https://doi.org/10.5194/egusphere-2026-3434
Preprint. Discussion started: 9 September 2026

height, particle size, and particle shape. Sensitivity testing shows that changing these parameters can dramatically influence the resulting ash deposition distribution across Antarctica (**Fig. 10**). In addition, the wind field data used to drive the model is based on pre-industrial conditions rather than LGM conditions. For example, Antarctic ice sheet and sea ice extent would have been much larger during the LGM, altering the position of the SH westerlies (Sime et al., 2013), which could have impacted atmospheric transport pathways introducing further uncertainty to modelling simulations. Despite these limitations, these model simulations used the most up-to-date petrological and ice core data to provide the best available estimates of climatic and stratospheric changes resulting from the Ōruanui eruption, as well as the extent of ash deposition, yielding results that align with our new evidence of physical deposits in Antarctica.

5 Conclusions

We present the first continent-scale compilation of nine Antarctic ice core signals from the ~25.3 ka Ōruanui supereruption, integrating glaciochemical records with new cryptotephra analyses and volcanic ash deposition modelling to constrain its timing, transport pathways, and climatic relevance. We document Ōruanui glass shards in three Antarctic ice cores from West and East Antarctica, demonstrating that the eruption was able to disperse volcanic material across the continent. Despite a coherent geochemical fingerprint, glass records exhibit pronounced spatial heterogeneity in particle abundances and sizes. Volcanic ash deposition simulations suggest that this variability likely reflects differing deposition across the continent, strongly influenced by atmospheric pathways, plume height, average particle size, and particle shape. The recovery of unusually abundant and coarse glass shards (>50 μm) in WDC06A highlights improvements in glass extraction methodology, and implies efficient long-range transport of thin cuspate ash particles >5000 km from source. Glaciochemical records show variable preservation of the Ōruanui eruption signal across Antarctica, with strong sulfate anomalies in some cores (WDC06A, SPC-14, EDML) and weak or absent signals in others. This variability reflects a combination of

https://doi.org/10.5194/egusphere-2026-3434
Preprint. Discussion started: 9 September 2026

Southern Hemispheric westerly wind circulation during tropospheric settling and to a lesser extent site-specific post-depositional processes such as wind erosion and snow redistribution. Sites most favourable for locating volcanic anomalies appear to be those with relatively high accumulation rates, intermediate distance from the ocean, lower thinning rates, and limited post-depositional alteration. Regarding eruption impacts, revised Antarctic sulfate deposition estimates infer a stratospheric sulfur injection of ~114 Tg S (342 Tg SO_4^{2-}), placing Ōruanui among the largest sulfur-emitting eruptions of the Quaternary and implying radiative forcing nearly three times stronger than the Pinatubo 1991 eruption. CESM2(WACCM6) model simulations show cooling of 3 K, and associated severe global climate impacts for >5 years post-eruption. However, our results suggest that an Ōruanui-like eruption in the SH may not necessarily generate climatic shifts or impacts on decadal to centennial timescales. Future work could focus on further exploring the cascading impacts and potential prolongation of the instantaneous volcanic response of Ōruanui via SH oceans and climate, which is critical for global systems including biogeochemical cycling.

https://doi.org/10.5194/egusphere-2026-3434
Preprint. Discussion started: 9 September 2026

Data availability.

The data sets for tephra major oxide geochemistry can be found in the PANGEA data centre: https://doi.pangaea.de/10.1594/PANGAEA.995655. Ash3d simulation data can be found in: Mastin, L. G., Mattin, A., Barker, S.J., and Van Eaton, A.R., 2026, Model simulations of volcanic ash transport from Taupo volcano (New Zealand) during the 25 ka Oruanui eruption: U.S. Geological Survey data release, https://doi.org/10.5066/P149UBKZ.

Supplement.

The supplementary material is provided as separate file with this article.

Author contributions.

Conceptualisation: SJB, VHLW, KK

Data curation: AM, ARVE, AS, HAK, IO, KGA, LGM, MH, MSe, NB, PS, SF

Formal analysis: AM, SJB, AS, DW, HAK, KK, MV, MSi, NAI, PS, SBP, SBP

Funding acquisition: SJB, VHLW

Investigation: AM, SJB, VHLW, KK, MSi, NAI, SBP

Methodology: AM, SJB, VHLW, AB, ARVE, AS, KK, LGM, MV, MSi, PS, WH

Project administration: AM, SJB, VHLW

Resources: SJB, VHLW, AB, ARVE, AVK, HAK, IO, KGA, LGM, MH, PS, SF, WH

Software: AM, ARVE, KK, LGM

Supervision: SJB, VHLW

Validation: AM

Visualization: AM, KK

Writing (original draft preparation): AM

Writing (review and editing): SJB, VHLW, AB, WH, PS, KK, ARVE, LGM, MSi, EWW, SF, KGA, IO, AS, MV, CJNW, NWD, HAK, NB, MSe, AVK, DW

Competing interests.

Some authors are members of the editorial board of journal *Climate of the Past*.

Acknowledgments.

We thank the British Antarctic Survey (BAS) for providing access to ice core facilities, particularly Jack Humby and Shaun Miller for their assistance with Skytrain ice core cutting. We also thank the Alfred Wegener Institute (AWI) for providing sampling facilities, especially Johannes Freitag and Piers Larkman for EDML sample preparation assistance. We would like to thank Rebecca Pyne from the National Ice Core Facility at Earth Sciences New Zealand for her support in RICE sample

https://doi.org/10.5194/egusphere-2026-3434
Preprint. Discussion started: 9 September 2026

preparation. We would also like to thank Kerstin Gruender for assistance with microprobe work at Victoria University of Wellington. We would like to thank Christoph Kern and Tyler Paladino for contributing insightful comments through their USGS reviews of the manuscript.

Financial support.

This work was supported by the Marsden Fund of the Royal Society of New Zealand (RSNZ) Te Apārangi (21-VUW-233: SJB). SJB also acknowledges ongoing support through an RSNZ Rutherford Discovery Fellowship (VUW2302). This project has received funding from the European Research Council under the Horizon 2020 research and innovation programme (grant agreement No 742224, WACSWAIN). This material reflects only the authors' views and the Commission is not liable for any use that may be made of the information contained therein. EWW was funded by the Leverhulme Trust through an Emeritus Fellowship. Funding for related RICE work was provided by the New Zealand Ministry of Business, Innovation, and Employment Grants RDF-VUW-1103, 15-VUW-131, MFP-GNS-1901. HAK was funded by Horizon Europe (P2F 101184070, Icelink 101184621) and the Danish Research foundation (DFF 1131-00007B). KK and MSi would like to acknowledge their work contribution towards the University Oslo Energy and Environment Convergence Environment project "ClimSHOCK". The CESM2(WACCM6) model simulations were initiated by KK, carried out by Christina Brodowsky, and performed on resources provided by Sigma2 - the National Infrastructure for High-Performance Computing and Data Storage in Norway. AS was funded by the European Union (ERC, Green2Ice, 101072180). Views and opinions expressed are however those of the author(s) only and do not necessarily reflect those of the European Union or the European Research Council Executive Agency. Neither the European Union nor the granting authority can be held responsible for them. IO and MH were funded by Japan Society for the Promotion of Science (JSPS) and Ministry of Education, Culture, Sports, Science and Technology-Japan (MEXT) KAKENHI Grant Numbers 24H02345. SPICEcore research was funded by US National Science Foundation grant #1443336.

Disclaimer.

Any use of trade, firm, or product names is for descriptive purposes only and does not imply endorsement by the U.S. government.

https://doi.org/10.5194/egusphere-2026-3434
Preprint. Discussion started: 9 September 2026

References

Abbott, P. M., and Davies, S. M.: Volcanism and the Greenland ice-cores: the tephra record. Earth-Sci. Rev., 115, 173-191, https://doi.org/10.1016/j.earscirev.2012.09.001, 2012.

Abbott, P. M., Plunkett, G., Corona, C., Chellman, N. J., McConnell, J. R., Pilcher, J. R., Stoffel, M., and Sigl, M.: Cryptotephra from the Icelandic Veiðivötn 1477 CE eruption in a Greenland ice core: confirming the dating of volcanic events in the 1450s CE and assessing the eruption's climatic impact. Clim. Past, 17, 565-585, https://doi.org/10.5194/cp-17-565-2021, 2021.

Abbott, P. M., McConnell, J. R., Chellman, N. J., Kipfstuhl, S., Hörhold, M., Freitag, J., Cook, E., Hutchison, W., and Sigl, M.: Mid-to Late Holocene East Antarctic ice-core tephrochronology: implications for reconstructing volcanic eruptions and assessing their climatic impacts over the last 5,500 years, Quat. Sci. Rev., 329, 108544, https://doi.org/10.1016/j.quascirev.2024.108544, 2024.

Allan, A. S. R., Barker, S. J., Millet, M.-A., Morgan, D. J., Rooyakkers, S. J., Schipper, C. I., and Wilson, C. J. N.: A cascade of magmatic events during the assembly and eruption of a super-sized magma body, Contrib. Mineral. Petrol., 172, 49, https://doi.org/10.1007/s00410-017-1367-8, 2017.

Aubry, T. J., Toohey, M., Marshall, L., Schmidt, A., and Jellinek, A. M.: A new volcanic stratospheric sulfate aerosol forcing emulator (EVA_H): comparison with interactive stratospheric aerosol models, J. Geophys. Res.: Atmos., 125, e2019JD031303, https://doi.org/10.1029/2019JD031303, 2020.

Barker, S. J., Van Eaton, A. R., Mastin, L. G., Wilson, C. J. N., Thompson, M. A., Wilson, T. M., Davis, C., and Renwick, J. A.: Modeling ash dispersal from future eruptions of Taupo supervolcano, Geochem. Geophys. Geosyst., 20, 3375–3401, https://doi.org/10.1029/2018GC008152, 2019.

Barker, S. J., Wilson, C. J. N., Illsley-Kemp, F., Leonard, G. S., Mestel, E. R. H., Mauriohooho, K., and Charlier, B. L. A.: Taupō: an overview of New Zealand's youngest supervolcano, N.Z. J. Geol. Geophys., 64, 320–346, https://doi.org/10.1080/00288306.2020.1792515, 2021.

Bazin, L., Landais, A., Lemieux-Dudon, B., Toyé Mahamadou Kele, H., Veres, D., Parrenin, F., Martinerie, P., Ritz, C., Capron, E., Lipenkov, V. Y., Loutre, M.-F., Raynaud, D., Vinther, B. M., Svensson, A. M., Rasmussen, S. O., Severi, M., Blunier, T., Leuenberger, M. C., Fischer, H., Masson-Delmotte, V., Chappellaz, J. A., Wolff, E. W.: AICC2012 chronology for ice core EDML [dataset], accessed on 17/01/2024, https://doi.org/10.1594/PANGAEA.824866, 2013a.

Bazin, L., Landais, A., Lemieux-Dudon, B., Toyé Mahamadou Kele, H., Veres, D., Parrenin, F., Martinerie, P., Ritz, C., Capron, E., Lipenkov, V. Y., Loutre, M.-F., Raynaud, D., Vinther, B. M., Svensson, A. M., Rasmussen, S. O., Severi, M., Blunier, T., Leuenberger, M. C., Fischer, H., Masson-Delmotte, V., Chappellaz, J. A., and Wolff, E. W.: AICC2012 chronology for ice core EDC [dataset], accessed on 17/01/24, https://doi.org/10.1594/PANGAEA.824865, 2013b.

Bertler, N. A. N., Conway, H., Dahl-Jensen, D., Emanuelsson, D. B., Winstrup, M., Vallelonga, P. T., Lee, J. E., Brook, E. J., Severinghaus, J. P., Fudge, T. J., Keller, E. D., Baisden, W. T., Hindmarsh, R. C. A., Neff, P. D., Blunier, T., Edwards, R., Mayewski, P. A., Kipfstuhl, S., Buizert, C., Canessa, S., Dadic, R., Kjær, H. A., Kurbatov, A., Zhang, D., Waddington, E. D., Baccolo, G., Beers, T., Brightley, H. J., Carter, L., Clemens-Sewall, D., Ciobanu, V. G., Delmonte, B., Eling, L., Ellis, A., Ganesh, S., Golledge, N. R., Haines, S., Handley, M., Hawley, R. L., Hogan, C. M., Johnson, K. M., Korotkikh, E., Lowry, D. P., Mandeno, D., McKay, R. M., Menking, J. A., Naish, T. R., Noerling, C., Ollive, A., Orsi, A., Proemse, B. C., Pyne, A. R., Pyne, R. L., Renwick, J., Scherer, R. P., Semper, S., Simonsen, M., Sneed, S. B., Steig, E. J., Tuohy, A., Venugopal, A. U., Valero-Delgado, F., Venkatesh, J., Wang, F., Wang, S., Winski, D. A., Winton, V. H. L., Whiteford, A., Xiao, C., Yang, J., and Zhang, X.: The Ross Sea Dipole – temperature, snow accumulation and sea ice variability in the Ross Sea region, Antarctica, over the past 2700 years, Clim. Past., 14(2), 193-214. https://doi.org/10.5194/cp-14-193-2018. 2018.

Bigler, M., Svensson, A., Kettner, E., Vallelonga, P., Nielsen, M., and Steffensen, J.: Optimization of high-resolution continuous flow analysis for transient climate signals in ice cores, Env. Sci. Technol., 45, 4483–4489, https://doi.org/10.1021/es200118, 2011.

Bluth, G. J. S., Doiron, S. D., Schnetzler, C. C., Krueger, A. J., and Walter, L. S.: Global tracking of the SO_2 clouds from the June, 1991 Mount Pinatubo eruptions. Geophys. Res. Lett., 19, 151-154. https://doi.org/10.1029/91GL02792, 1992.

https://doi.org/10.5194/egusphere-2026-3434
Preprint. Discussion started: 9 September 2026

Bonsang, B., Nguyen, B. C., Gaudry, A., and Lambert, G.: Sulfate enrichment in marine aerosols owing to biogenic gaseous sulfur compounds, J. Geophys. Res.: Oceans, 85, 7410–7416, https://doi.org/10.1029/JC085iC12p07410, 1980.

Bouchet, M., Landais, A., Grisart, A., Parrenin, F., Prié, F., Jacob, R., Fourré, E., Capron, E., Raynaud, D., Lipenkov, V. Y., Loutre, M.-F., Extier, T., Svensson, A., Legrain, E., Martinerie, P., Leuenberger, M., Jiang, W., Ritterbusch, F., Lu, Z.-T., and Yang, G.-M.: The Antarctic Ice Core Chronology 2023 (AICC2023) chronological framework and associated timescale for the European Project for ice coring in Antarctica (EPICA) Dome C ice core. Clim. Past, 19, 2257–2286, https://doi.org/10.5194/cp-19-2257-2023, 2023.

Brenna, H., Kutterolf, S., Krüger, K., Brenna, H., Kutterolf, S., and Krüger, K.: Global ozone depletion and increase of UV radiation caused by pre-industrial tropical volcanic eruptions. Sci. Rep., 9, 9435, https://doi.org/10.1038/s41598-019-45630-0, 2019.

Brenna, H., Kutterolf, S., Mills, M. J., and Krüger, K.: The potential impacts of a sulfur- and halogen-rich supereruption such as Los Chocoyos on the atmosphere and climate, Atmos. Chem. Phys., 20, 6521–6539, https://doi.org/10.5194/acp-20-6521-2020, 2020.

Buiron, D., Chappellaz, J., Stenni, B., Frezzotti, M., Baumgartner, M., Capron, E., Landais, A., Lemieux-Dudon, B., Masson-Delmotte, V., Montagnat, M., Parrenin, F., and Schilt, A.: TALDICE-1 age scale of the Talos Dome deep ice core, East Antarctica, Clim. Past, 7, 1–16, https://doi.org/10.5194/cp-7-1-2011, 2011.

Buizert, C., Sigl, M., Severi, M., Markle, B. R., Wettstein, J. J., McConnell, J. R., Pedro, J. B., Sodemann, H., Goto-Azuma, K., Kawamura, K., Fujita, S., Motoyama, H., Hirabayashi, M., Uemura, R., Stenni, B., Parrenin, F., He, F., Fudge, T. J., Steig, E. J.: Abrupt ice-age shifts in southern westerly winds and Antarctic climate forced from the north, Nature, 563, 681–685, https://doi.org/10.1038/s41586-018-0727-5, 2018.

Büntgen, U., Arseneault, D., Boucher, É., Churakova (Sidorova), O. V., Gennaretti, F., Crivellaro, A., Hughes, M. K., Kirdyanov, A. V., Klippel, L., Krusic, P. J., Linderholm, H. W., Ljungqvist, F. C., Ludescher, J., McCormick, M., Myglan, V. S., Nicolussi, K., Piermattei, A., Oppenheimer, C., Reinig, F., Sigl, M., Vaganov, E. A., and Esper, J.: Prominent role of volcanism in Common Era climate variability and human history. Dendrochronologia, 64, 125757, https://doi.org/10.1016/j.dendro.2020.125757, 2020.

Bureau, H., Keppler, H., and Métrich, N.: Volcanic degassing of bromine and iodine: Experimental fluid/melt partitioning data and applications to stratospheric chemistry. Earth Planet. Sci. Lett., 183(1–2), 51–60. https://doi.org/10.1016/s0012-821x(00)00258-2, 2000.

Cadoux, A., Scaillet, B., Bekki, S., Oppenheimer, C., and Druitt, T. H.: Stratospheric Ozone destruction by the Bronze-Age Minoan eruption (Santorini Volcano, Greece). Sci. Rep., 5, 12243, https://doi.org/10.1038/srep12243, 2015.

Casey, K. A., Fudge, T. J., Neumann, T. A., Steig, E. J., Cavitte, M. G. P., and Blankenship, D. D.: The 1500 m South Pole ice core: recovering a 40 ka environmental record, Ann. Glaciol., 55, 137–146, https://doi.org/10.3189/2014AoG68A016, 2014.

Cole-Dai, J., Ferris, D. G., Kennedy, J. A., Sigl, M., McConnell, J. R., Fudge, T. J., Geng, L., Maselli, O. J., Taylor, K. C., and Souney, J. M.: Comprehensive record of volcanic eruptions in the Holocene (11,000 years) from the WAIS Divide, Antarctica ice core, J. Geophys. Res.: Atmos., 126, e2020JD032855, https://doi.org/10.1029/2020JD032855, 2021.

Cook, E., Abbott, P. M., Pearce, N. J. G., Mojtabavi, S., Svensson, A., Bourne, A. J., Rasmussen, S. O., Seierstad, I. K., Vinther, B. M., Harrison, J., Street, E., Steffensen, J. P., Wilhelms, F., and Davies, S. M.: Volcanism and the Greenland ice cores: a new tephrochronological framework for the last glacial-interglacial transition (LGIT) based on cryptotephra deposits in three ice cores. Quat. Sci. Rev., 292, 107596, https://doi.org/10.1016/j.quascirev.2022.107596, 2022.

Danabasoglu, G., Lamarque, J.-F., Bacmeister, J., Bailey, D. A., DuVivier, A. K., Edwards, J., Emmons, L. K., Fasullo, J., Garcia, R., Gettelman, A., Hannay, C., Holland, M. M., Large, W. G., Lauritzen, P. H., Lawrence, D. M., Lenaerts, J. T. M., Lindsay, K., Lipscomb, W. H., Mills, M. J., Neale, R., Oleson, K. W., Otto-Bliesner, B., Phillips, A. S., Sacks, W., Tilmes, S., van Kampenhout, L., Vertenstein, M., Bertini, A., Dennis, J., Deser, C., Fischer, C., Fox-Kemper, B., Kay, J. E., Kinnison, D., Kushner, P. J., Larson, V. E., Long, M. C., Mickelson, S., Moore, J. K., Nienhouse, E., Polvani, L., Rasch, P. J., and Strand, W. G.: The Community Earth System Model Version 2 (CESM2), J. Adv. Model. Earth Syst., 12, e2019MS001916, https://doi.org/10.1029/2019MS001916, 2020.

Das, I., Bell, R. E., Scambos, T. A., Wolovick, M., Creyts, T. T., Studinger, M., Frearson, N., Nicolas, J. P., Lenaerts, J. T. M., and van den Broeke, M. R.: Influence of persistent wind scour on the surface mass balance of Antarctica, Nat. Geosci., 6, 367–371, https://doi.org/10.1038/ngeo1766, 2013.

https://doi.org/10.5194/egusphere-2026-3434
Preprint. Discussion started: 9 September 2026

Dunbar, N. W., Zielinski, G. A., and Voisins, D. T.: Tephra layers in the Siple Dome and Taylor Dome ice cores, Antarctica: sources and correlations, J. Geophys. Res.: Sol. Earth, 108, 2374, https://doi.org/10.1029/2002JB002056, 2003.

Dunbar, N. W., Iverson, N. A., Van Eaton, A. R., Sigl, M., Alloway, B. V., Kurbatov, A. V., Mastin, L. G., McConnell, J. R., and Wilson, C. J. N.: New Zealand supereruption provides time marker for the Last Glacial Maximum in Antarctica, Sci. Rep., 7, 12238, https://doi.org/10.1038/s41598-017-11758-0, 2017.

Dunbar, N. W., and Kurbatov, A. V.: Tephrochronology of the Siple Dome ice core, West Antarctica: correlations and sources. Quat. Sci. Rev., 30(13-14), 1602-1614. https://doi.org/10.1016/j.quascirev.2011.03.015, 2011.

Durant, G. P.: Rhyolite. In D. R. Bowes (Ed.), Encyclopedia of igneous and metamorphic petrology (pp. 512–513), Springer, https://doi.org/10.1007/0-387-30845-8_216, 1989.

Esper, J., Schneider, L., Krusic, P. J., Luterbacher, J., Büntgen, U., Timonen, M., Sirocko, F., and Zorita, E.: European summer temperature response to annually dated volcanic eruptions over the past nine centuries, Bull. Volcanol., 75, 736, https://doi.org/10.1007/s00445-013-0736-z, 2013.

Fasullo, J. T., Tomas, R., Stevenson, S., Otto-Bliesner, B., Brady, E., and Wahl, E.: The amplifying influence of increased ocean stratification on a future year without a summer, Nat. Commun., 8, 1236, https://doi.org/10.1038/s41467-017-01302-z, 2017.

Fischer, H., Wegner, A., Delmonte, B., Petit, J. R., Erhardt, T., Ruth, U., Svensson, A. M., Vinther, B. M., and Miller, H.: Particulate dust concentrations and coarse particle percentage from EPICA ice core EDML [dataset], PANGAEA, https://doi.org/10.1594/PANGAEA.955821, 2023.

Fudge, T. J., Markle, B. R., Cuffey, K. M., Buizert, C., Taylor, K. C., Steig, E. J., Waddington, E. D., Conway, H., and Koutnik, M.: Variable relationship between accumulation and temperature in West Antarctica for the past 31,000 years, Geophys. Res. Lett., 43, 3795–3803, https://doi.org/10.1002/2016GL068356, 2016.

Fuglestvedt, H. F., Gabriel, I., Sigl, M., Thordarson, T., and Krüger, K.: Revisiting the 10th-century Eldgjá eruption: modeling the climatic and environmental impacts, Geophys. Res. Lett., 52, e2024GL110507, https://doi.org/10.1029/2024GL110507, 2025.

Fujita, S., Parrenin, F., Severi, M., Motoyama, H., and Wolff, E. W.: Volcanic synchronization of Dome Fuji and Dome C Antarctic deep ice cores over the past 216 kyr, Clim. Past, 11, 1395–1416, https://doi.org/10.5194/cp-11-1395-2015, 2015.

Gao, C., Oman, L., Robock, A., and Stenchikov, G. L.: Atmospheric volcanic loading derived from bipolar ice cores: accounting for the spatial distribution of volcanic deposition, J. Geophys. Res.: Atmos., 112, D09109, https://doi.org/10.1029/2006JD007461, 2007.

Gao, C., Robock, A., and Ammann, C.: Volcanic forcing of climate over the past 1500 years: an improved ice core-based index for climate models, J. Geophys. Res.: Atmos., 113, D23111. https://doi.org/10.1029/2008JD010239, 2008.

Gautier, E., Savarino, J., Erbland, J., Lanciki, A., and Possenti, P.: Variability of sulfate signal in ice core records based on five replicate cores, Clim. Past, 12, 103–113, https://doi.org/10.5194/cp-12-103-2016, 2016.

Gettelman, A., Mills, M. J., Kinnison, D. E., Garcia, R. R., Smith, A. K., Marsh, D. R., Tilmes, S., Vitt, F., Bardeen, C. G., McInerny, J., Liu, H.-L., Solomon, S. C., Polvani, L. M., Emmons, L. K., Lamarque, J.-F., Richter, J. H., Glanville, A. S., Bacmeister, J. T., Phillips, A. S., Neale, R. B., Simpson, I. R., DuVivier, A. K., Hodzic, A., and Randel, W. J.: The Whole Atmosphere Community Climate Model Version 6 (WACCM6), J. Geophys. Res.: Atmos., 124, 12380–12403, https://doi.org/10.1029/2019JD030943, 2019.

Gfeller, G., Fischer, H., Bigler, M., Schüpbach, S., Leuenberger, D., and Mini, O.: Representativeness and seasonality of major ion records derived from NEEM firn cores, The Cryosphere, 8, 1855–1870, https://doi.org/10.5194/tc-8-1855-2014, 2014.

Goto-Azuma, K., Dallmayr, R., Ogawa-Tsukagawa, Y., Moteki, N., Mori, T., Ohata, S., Kondo, Y., Koike, M., Hirabayashi, M., Ogata, J., Kitamura, K., Kawamura, K., Fujita, K., Matoba, S., Nagatsuka, N., Tsushima, A., Fukuda, K., and Aoki, T.: High-resolution analyses of concentrations and sizes of refractory black carbon particles deposited in northwestern Greenland over the past 350 years – Part 1: continuous flow analysis of the SIGMA-D ice core using the wide-range Single-Particle Soot Photometer and a high-efficiency nebulizer, Atmos. Chem. Phys., 24, 12985–13000, https://doi.org/10.5194/acp-24-12985-2024, 2024.

https://doi.org/10.5194/egusphere-2026-3434
Preprint. Discussion started: 9 September 2026

Grieman, M. M., Hoffmann, H. M., Humby, J. D., Mulvaney, R., Nehrbass-Ahles, C., Rix, J., Thomas, E. R., Tuckwell, R., and Wolff, E. W.: Continuous flow analysis methods for sodium, magnesium and calcium detection in the Skytrain ice core, J. Glaciol., 68, 90–100, https://doi.org/10.1017/jog.2021.75, 2022.

Gudmundsson, M. T., Thordarson, T., Höskuldsson, A., Larsen, G., Björnsson, H., Prata, F. J., Oddsson, B., Magnússon, E., Högnadóttir, T., Petersen, G. N., Hayward, C. L., Stevenson, J. A., and Jónsdóttir, I.: Ash generation and distribution from the April-May 2010 eruption of Eyjafjallajökull, Iceland, Sci. Rep., 2, 572, https://doi.org/10.1038/srep00572, 2012.

Guo, S., Bluth, G. J. S., Rose, W. I., Watson, I. M., and Prata, A. J.: Re-evaluation of SO_2 release of the 15 June 1991 Pinatubo eruption using ultraviolet and infrared satellite sensors, Geochem. Geophys. Geosyst., 5, Q04001, https://doi.org/10.1029/2003GC000654, 2004.

Halmer, M. M., Schmincke, H.-U., Graf, H.-F.: The annual volcanic gas input into the atmosphere, in particular into the stratosphere: a global data set for the past 100 years, J. Volcanol. Geotherm. Res., 115, 511–528, https://doi.org/10.1016/S0377-0273(01)00318-3, 2002.

Hansen, J., Lacis, A., Ruedy, R., and Sato, M.: Potential climate impact of Mount Pinatubo eruption, Geophys. Res. Lett., 19, 215–218, https://doi.org/10.1029/91GL02788, 1992.

Harlan, M. M., Fox, J., Kjær, H. A., Vance, T. R., Svensson, A., and Cook, E.: Cryptotephra in the East Antarctic Mount Brown South ice core, Clim. Past Discuss., 22(5), 1057–1083, https://doi.org/10.5194/cp-2024-64, 2026.

Hoffmann, H. M., Grieman, M. M., King, A. C. F., Epifanio, J. A., Martin, K., Vladimirova, D., Pryer, H. V., Doyle, E., Schmidt, A., Humby, J. D., Rowell, I. F., Nehrbass-Ahles, C., Thomas, E. R., Mulvaney, R., and Wolff, E. W.: The ST22 chronology for the Skytrain Ice Rise ice core – Part 1: a stratigraphic chronology of the last 2000 years, Clim. Past, 18, 1831–1847, https://doi.org/10.5194/cp-18-1831-2022, 2022.

Howat, I. M., Porter, C., Smith, B. E., Noh, M.-J., and Morin, P.: The reference elevation model of Antarctica, Cryosphere, 13, 665–674, https://doi.org/10.5194/tc-13-665-2019, 2019.

Hutchison, W., Gabriel, I., Plunkett, G., Burke, A., Sugden, P., Innes, H., Davies, S., Moreland, W. M., Krüger, K., Wilson, R., Vinther, B. M., Dahl-Jensen, D., Freitag, J., Oppenheimer, C., Chellman, N. J., Sigl, M., and McConnell, J. R.: High-resolution ice-core analyses identify the Eldgjá eruption and a cluster of Icelandic and trans-continental tephras between 936 and 943 CE, J. Geophys. Res.: Atmos., 129,e2023JD040142, https://doi.org/10.1029/2023JD040142, 2024a.

Hutchison, W., Sugden, P., Burke, A., Abbott, P., Ponomareva, V. V., Dirksen, O., Portnyagin, M. V., MacInnes, B., Bourgeois, J., Fitzhugh, B., Verkerk, M., Aubry, T. J., Engwell, S. L., Svensson, A., Chellman, N. J., McConnell, J. R., Davies, S., Sigl, M., and Plunkett, G.: The 1831 CE mystery eruption identified as Zavaritskii caldera, Simushir Island (Kurils), Proc. Natl. Acad. Sci. U.S.A., 122, e2416699122, https://doi.org/10.1073/pnas.2416699122, 2024b.

Innes, H. M., Hutchison, W., and Burke, A.: Geochemical analysis of extremely fine-grained cryptotephra: new developments and recommended practices, Quat. Geochron., 83, 101553, https://doi.org/10.1016/j.quageo.2024.101553, 2024.

Innes, H. M., Hutchison, W., Sigl, M., Crick, L., Abbott, P. M., Bigler, M., Chellman, N. J., Davies, S. M., Kutterolf, S., McConnell, J. R., Severi, M., Sparks, R. S. J., Svensson, A., Wolff, E. W., Rae, J. W. B., and Burke, A.: Ice core evidence for the Los Chocoyos supereruption disputes millennial-scale climate impact, Comm. Earth Environ., 6, 137, https://doi.org/10.1038/s43247-025-02095-6, 2025.

Iverson, N. A.: Characterization and correlation of englacial tephra from blue ice areas and ice cores, Antarctica, PhD thesis, New Mexico Institute of Mining and Technology, New Mexico, 2017.

Iverson, N. A., Kalteyer, D., Dunbar, N. W., Kurbatov, A., and Yates, M.: Advancements and best practices for analysis and correlation of tephra and cryptotephra in ice, Quat. Geochron., 40, 45–55, https://doi.org/10.1016/j.quageo.2016.09.008, 2017a.

Iverson, N. A., Lieb-Lappen, R., Dunbar, N. W., Obbard, R., Kim, E., and Golden, E.: The first physical evidence of subglacial volcanism under the West Antarctic Ice Sheet, Sci. Rep., 7, 11457, https://doi.org/10.1038/s41598-017-11515-3, 2017b.

Jones, T. R., White, J. W. C., Steig, E. J., Vaughn, B. H., Morris, V., Gkinis, V., Markle, B. R., and Schoenemann, S. W.: Improved methodologies for continuous-flow analysis of stable water isotopes in ice cores. Atmos. Meas. Tech., 10, 617–632, https://doi.org/10.5194/amt-10-617-2017, 2017.

Kahn, R. A., Limbacher, J. A., Junghenn Noyes, K. T., Flower, V. J. B., Zamora, L. M., & McKee, K. F.: Evolving particles in the 2022 Hunga Tonga—Hunga Ha'apai volcano eruption plume. Journal of Geophysical Research: Atmospheres, 129, e2023JD039963, https://doi.org/10.1029/2023JD039963, 2024.

https://doi.org/10.5194/egusphere-2026-3434
Preprint. Discussion started: 9 September 2026

Kim, H., Kang, S. M., Pendergrass, A. G., Lehner, F., Shin, Y., Ceppi, P., Yeh, S-W., Song, S-Y.: Higher precipitation in East Asia and western United States expected with future Southern Ocean warming, Nat. Geosci, 18, 313–321, https://doi.org/10.1038/s41561-025-01669-5, 2025.

Kjær, H. A., Vallelonga, P., Svensson, A., Elleskov L. Kristensen, M., Tibuleac, C., Winstrup, M., and Kipfstuhl, S.: An optical dye method for continuous determination of acidity in ice cores, Env. Sci. Technol., 50, 10485–10493, https://doi.org/10.1021/acs.est.6b00026, 2016.

Kjær, H.A., Zens, P., Black, S., Lund, K.H., Svensson, A., Vallelonga, P.: Canadian forest fires, Icelandic volcanoes and increased local dust observed in six shallow Greenland firn cores. Clim. Past 18(10), 2211-2230. https://doi.org/10.5194/cp-18-2211-2022, 2022.

Koffman, B. G., Kreutz, K. J., Kurbatov, A. V., and Dunbar, N. W.: Impact of known local and tropical volcanic eruptions of the past millennium on the WAIS Divide microparticle record, Geophys. Res. Lett., 40, 4712-4716, https://doi.org/10.1002/grl.50822, 2013.

Koffman, B. G., Dowd, E. G., Osterberg, E. C., Ferris, D. G., Hartman, L. H., Wheatley, S. D., Kurbatov, A. V., Wong, G. J., Markle, B. R., Dunbar, N. W., Kreutz, K. J., and Yates, M.: Rapid transport of ash and sulfate from the 2011 Puyehue-Cordón Caulle (Chile) eruption to West Antarctica, J. Geophys. Res.: Atmos., 122, 8908–8920, https://doi.org/10.1002/2017JD026893, 2017.

Krüger, K., Kutterolf, S., and Hansteen, T. H.: Halogen release from Plinian eruptions and depletion of stratospheric ozone, in: Volcanism and Global Environmental Change, edited by: Schmidt, A., Fristad, K. E., and Elkins-Tanton, L. T., Cambridge Univ. Press, New York, USA, 244–259, 2015.

Kutterolf, S., Hansteen, T. H., Appel, K., Freundt, A., Krüger, K., Pérez, W., and Wehrmann, H.: Combined bromine and chlorine release from large explosive volcanic eruptions: a threat to stratospheric ozone?, Geology, 41, 707–710, https://doi.org/10.1130/G34044.1, 2013.

Ladstädter, F., Stocker, M., Scher, S., & Steiner, A. K.: Observed changes in the temperature and height of the globally resolved lapserate tropopause. Atmospheric Chemistry and Physics, 25(22), 16053–16062. https://doi.org/10.5194/acp-25-16053-2025, 2025.

Lambert, F., Bigler, M., Steffensen, J. P., Hutterli, M. A., and Fischer, H.: EDC dust flux 800 kyr (full resolution) [dataset], PANGAEA, accessed on 17/07/2023, https://doi.org/10.1594/PANGAEA.779310, 2012.

Lee, J. E., Brook, E. J., Bertler, N. A. N., Buizert, C., Baisden, T., Blunier, T., Ciobanu, V. G., Conway, H., Dahl-Jensen, D., Fudge, T. J., Hindmarsh, R., Keller, E. D., Parrenin, F., Severinghaus, J. P., Vallelonga, P., Waddington, E. D., and Winstrup, M.: An 83 000-year-old ice core from Roosevelt Island, Ross Sea, Antarctica, Clim. Past, 16, 1691–1713, https://doi.org/10.5194/cp-16-1691-2020, 2020.

Legrand, M.: Ice-core records of atmospheric sulphur, Philos. Trans. R. Soc. Lond. B Biol. Sci., 352, 241–250, https://doi.org/10.1098/rstb.1997.0019, 1997.

Lemieux-Dudon, B., Blayo, E., Petit, J.-R., Waelbroeck, C., Svensson, A., Ritz, C., Barnola, J.-M., Narcisi, B. M., and Parrenin, F.: Consistent dating for Antarctic and Greenland ice cores, Quat. Sci. Rev., 29, 8–20, https://doi.org/10.1016/j.quascirev.2009.11.010, 2010.

Lin, J., Svensson, A., Hvidberg, C. S., Lohmann, J., Kristiansen, S., Dahl-Jensen, D., Steffensen, J. P., Rasmussen, S. O., Cook, E., Kjær, H. A., Vinther, B. M., Fischer, H., Stocker, T., Sigl, M., Bigler, M., Severi, M., Traversi, R., and Mulvaney, R.: Magnitude, frequency and climate forcing of global volcanism during the last glacial period as seen in Greenland and Antarctic ice cores (60–9 ka), Clim. Past, 18, 485–506, https://doi.org/10.5194/cp-18-485-2022, 2022.

Lin, J., Abbott, P. M., Sigl, M., Steffensen, J. P., Mulvaney, R., Severi, M., and Svensson, A.: Bipolar ice-core records constrain possible dates and global radiative forcing following the ~74 ka Toba eruption, Quat. Sci. Rev., 312, 108162, https://doi.org/10.1016/j.quascirev.2023.108162, 2023.

Marshall, L. R., Schmidt, A., Toohey, M., Carslaw, K. S., Mann, G. W., Sigl, M., Khodri, M., Timmreck, C., Zanchettin, D., Ball, W. T., Bekki, S., Brooke, J. S. A., Dhomse, S., Johnson, C., Lamarque, J.-F., LeGrande, A. N., Mills, M. J., Niemeier, U., Pope, J. O., Poulain, V., Robock, A., Rozanov, E., Stenke, A., Sukhodolov, T., Tilmes, S., Tsigaridis, K., and Tummon, F.: Multi-model comparison of the volcanic sulfate deposition from the 1815 eruption of Mt. Tambora, Atmos. Chem. Phys., 18, 2307–2328, https://doi.org/10.5194/acp-18-2307-2018, 2018.

https://doi.org/10.5194/egusphere-2026-3434
Preprint. Discussion started: 9 September 2026

Marshall, L. R., Smith, C. J., Forster, P. M., Aubry, T. J., Andrews, T., and Schmidt, A.: Large variations in volcanic aerosol forcing efficiency due to eruption source parameters and rapid adjustments, Geophys. Res. Lett., 47, e2020GL090241, https://doi.org/10.1029/2020GL090241, 2020.

Marshall, L.R., Maters, E.C., Schmidt, A., Timmreck, C., Robock, A., Toohey, M.: Volcanic effects on climate: recent advances and future avenues, Bull Volcanol., 84(54). https://doi.org/10.1007/s00445-022-01559-3, 2022.

Mastin, L.G., Mattin, A., Barker, S., and Van Eaton, A.R.: Model simulations of volcanic ash transport from Taupo volcano (New Zealand) during the 25 ka Oruanui eruption. U.S. Geological Survey data release, https://doi.org/10.5066/P149UBKZ, 2026.

Matthews, N. E., Smith, V. C., Costa, A., Durant, A. J., Pyle, D. M., and Pearce, N. J. G.: Ultra-distal tephra deposits from super-eruptions: examples from Toba, Indonesia and Taupo Volcanic Zone, New Zealand, Quat. Intl., 258, 54–79, https://doi.org/10.1016/j.quaint.2011.07.010, 2012.

McConnell, J. R.: WAIS Divide ice-core aerosol records from 1300 to 3404 m, U.S. Antarctic Program (USAP) Data Center, accessed on 17/07/23, https://doi.org/10.15784/601008, 2017.

McCormick, M. P., Thomason, L. W., and Trepte, C. R.: Atmospheric effects of the Mt Pinatubo eruption, Nature, 373, 399–404, https://doi.org/10.1038/373399a0, 1995.

Miller, A. L., Barker, S. J., Holt, K. A., Piva, S. B., and Wilson, C. J. N.: Origins and environmental impacts of rhyolitic tephra layers on Chatham Island, New Zealand. J. Quat. Sci., 41, 361–379, https://doi.org/10.1002/jqs.70046, 2026.

Ming, A., Winton, V. H. L., Keeble, J., Abraham, N. L., Dalvi, M. C., Griffiths, P., Caillon, N., Jones, A. E., Mulvaney, R., Savarino, J., Frey, M. M., and Yang, X.: Stratospheric ozone changes from explosive tropical volcanoes: modeling and ice core constraints, J. Geophys. Res. Atmos., 125, e2019JD032290, https://doi.org/10.1029/2019JD032290, 2020.

Moore, J.C. and Paren, J.G.: A new technique for dielectric logging of Antarctic ice cores, J. Phys. Colloques, 48 (C1), 155-160, https://doi.org/10.1051/jphyscol:1987123, 1987.

Motoyama, H.: The second deep ice coring project at Dome Fuji, Antarctica, Sci. Drill., 5(5), 41–43, https://doi.org/10.2204/iodp.sd.5.05.2007, 2007.

Mulvaney, R., Wolff, E. W., Grieman, M. M., Hoffmann, H. H., Humby, J. D., Nehrbass-Ahles, C., Rhodes, R. H., Rowell, I. F., Parrenin, F., Schmidely, L., Fischer, H., Stocker, T. F., Christl, M., Muscheler, R., Landais, A., and Prié, F.: The ST22 chronology for the Skytrain Ice Rise ice core – Part 2: an age model to the last interglacial and disturbed deep stratigraphy, Clim. Past, 19, 851–864, https://doi.org/10.5194/cp-19-851-2023, 2023.

Muscheler, R., Adolphi, F., Heaton, T. J., Ramsey, C. B., Svensson, A., Plicht, J. v. d., and Reimer, P. J.: Testing and improving the IntCal20 calibration curve with independent records, Radiocarbon, 62, 1079-1094, https://doi.org/10.1017/RDC.2020.54, 2020.

Neff, P. D. and Bertler, N. A. N.: Trajectory modeling of modern dust transport to the Southern Ocean and Antarctica, J. Geophys. Res.: Atmos., 120, 9303–9322, https://doi.org/10.1002/2015JD023304, 2015.

Oppenheimer, C.: Climatic, environmental and human consequences of the largest known historic eruption: Tambora volcano (Indonesia) 1815, Prog. Phys. Geogr.: Earth Environ., 27, 230–259, https://doi.org/10.1191/0309133303pp379ra, 2003.

Osipov, S., Stenchikov, G., Tsigaridis, K., LeGrande, A. N., Bauer, S. E., Fnais, M., and Lelieveld, J.: The Toba supervolcano eruption caused severe tropical stratospheric ozone depletion, Commun. Earth Environ., 2, 71, https://doi.org/10.1038/s43247-021-00141-7, 2021.

Oyabu, I., Kawamura, K., Buizert, C., Parrenin, F., Orsi, A., Kitamura, K., Aoki, S., and Nakazawa, T.: The Dome Fuji ice core DF2021 chronology (0–207 kyr BP), Quat. Sci. Rev., 294, 107754, https://doi.org/10.1016/j.quascirev.2022.107754, 2022.

Parker, D. E., Wilson, H., Jones, P. D., Christy, J. R., and Folland, C. K.: The impact of Mount Pinatubo on world-wide temperatures, Int. J. Climatol., 16, 487–497, https://doi.org/10.1002/(SICI)1097-0088(199605)16:5<487::AID-JOC39>3.0.CO;2-J, 1996.

Parrenin, F., Petit, J.-R., Masson-Delmotte, V., Wolff, E., Basile-Doelsch, I., Jouzel, J., Lipenkov, V., Rasmussen, S. O., Schwander, J., Severi, M., Udisti, R., Veres, D., and Vinther, B. M.: Volcanic synchronisation between the EPICA Dome C and Vostok ice cores (Antarctica) 0-145 kyr BP, Clim. Past, 8, 1031–1045, https://doi.org/10.5194/cp-8-1031-2012, 2012.

https://doi.org/10.5194/egusphere-2026-3434
Preprint. Discussion started: 9 September 2026

Pearce, J. A., Baker, P. E., Harvey, P. K., and Luff, I. W.: Geochemical evidence for subduction fluxes, mantle melting and fractional crystallization beneath the South Sandwich island arc, J. Petrol., 36, 1073–1109, https://doi.org/10.1093/petrology/36.4.1073, 1995.

Piva, S. B., Barker, S. J., Iverson, N. A., Winton, V. H. L., Bertler, N. A. N., Sigl, M., Wilson, C. J. N., Dunbar, N. W., Kurbatov, A. V., Carter, L., Charlier, B. L. A., and Newnham, R. M.: Volcanic glass from the 1.8 ka Taupō eruption (New Zealand) detected in Antarctic ice at ~ 230 CE, Sci. Rep., 13, 16720, https://doi.org/10.1038/s41598-023-42602-3, 2023a.

Piva, S. B., Barker, S. J., Newnham, R. M., Rees, A. B. H., Wilson, C. J. N., Carter, L., Iverson, N. A., Läuchli, B., and Augustinus, P. C.: Millimetre-scale pollen analysis of non-varved lacustrine sediments from Onepoto maar palaeolake, Auckland, reveals distal vegetation responses and landscape recovery following the 25.5-ka Ōruanui supereruption, New Zealand, J. Quat. Sci., 38, 613–628, https://doi.org/10.1002/jqs.3506, 2023b.

Plunkett, G., Sigl, M., McConnell, J. R., Pilcher, J. R., and Chellman, N. J.: The significance of volcanic ash in Greenland ice cores during the Common Era, Quat. Sci. Rev., 301, 107936, https://doi.org/10.1016/j.quascirev.2022.107936, 2023.

Raible, C. C., Brönnimann., S., Auchmann., R., Brohan., P., Frölicher., T., L,, Graf., H., F, Jones., P., Luterbacher., J., Muthers., S., Neukom., R., Robock., A., Self., S., Sudrajat., A., Timmreck., C., and Wegmann., M.: Tambora 1815 as a test case for high impact volcanic eruptions: Earth system effects. WIREs Clim. Change., 7, 569-589, https://doi.org/10.1002/wcc.407, 2016.

Rampino, M. R. and Self, S.: Historic eruptions of Tambora (1815), Krakatau (1883), and Agung (1963), their stratospheric aerosols, and climatic impact, Quat. Res., 18, 127–143, https://doi.org/10.1016/0033-5894(82)90065-5, 1982.

Rampino, M. R. and Self, S.: Sulphur-rich volcanic eruptions and stratospheric aerosols, Nature, 310, 677–679, https://doi.org/10.1038/310677a0, 1984.

Robock, A.: Volcanic eruptions and climate, Rev. Geophys., 38, 191–219, https://doi.org/10.1029/1998RG000054, 2000.

Robock, A., Ammann, C. M., Oman, L., Shindell, D., Levis, S., and Stenchikov, G.: Did the Toba volcanic eruption of ~74 ka B.P. produce widespread glaciation? J. Geophys. Res. Atmos., *114*, D10107. https://doi.org/10.1029/2008JD011652, 2009.

Röthlisberger., R., Bigler., M., Hutterli., M., Sommer., S., Stauffer., B., Junghans., H. G., and Wagenbach., D.: Technique for continuous high-resolution analysis of trace substances in firn and ice cores, Environ. Sci. Technol., 34, 338–342, https://doi.org/10.1021/es9907055, 1999.

Ruth, U., Barnola, J.-M., Beer, J., Bigler, M., Blunier, T., Castellano, E., Fischer, H., Fundel, F., Huybrechts, P., Kaufmann, P., Kipfstuhl, S., Lambrecht, A., Morganti, A., Oerter, H., Parrenin, F., Rybak, O., Severi, M., Udisti, R., Wilhelms, F., and Wolff, E.: "EDML1": a chronology for the EPICA deep ice core from Dronning Maud Land, Antarctica, over the last 150 000 years, Clim. Past, 3, 475–484, https://doi.org/10.5194/cp-3-475-2007, 2007.

Schmidt, A., Mills, M. J., Ghan, S., Gregory, J. M., Allan, R. P., Andrews, T., Bardeen, C. G., Conley, A., Forster, P. M., Gettelman, A., Portmann, R. W., Solomon, S., and Toon, O. B.: Volcanic radiative forcing from 1979 to 2015, J. Geophys. Res.: Atmos., 123, 12491–12508, https://doi.org/10.1029/2018JD028776, 2018.

Schneider, C. A., Rasband, W. S., and Eliceiri, K. W.: NIH Image to ImageJ: 25 years of image analysis, Nat. Meth., 9, 671–675, https://doi.org/10.1038/nmeth.2089, 2012.

Schwaiger, H. F., Denlinger, R. P., and Mastin, L. G.: Ash3d: a finite-volume, conservative numerical model for ash transport and tephra deposition. J. Geophys. Res.: Sol. Earth, 117, B04204, https://doi.org/10.1029/2011JB008968, 2012.

Self, S.: The effects and consequences of very large explosive volcanic eruptions, Philos. Trans. R. Soc. Lond. A Math. Phys. Eng. Sci., 364, 2073–2097, https://doi.org/10.1098/rsta.2006.1814, 2006.

Self, S. and Blake, S.: Consequences of explosive supereruptions, Elements, 4, 41–46, https://doi.org/10.2113/GSELEMENTS.4.1.41, 2008.

Self, S., Zhao, J.-X., Holasek, R. E., Torres, R. C., and King, A. J.: The atmospheric impact of the 1991 Mount Pinatubo eruption, in: Fire and Mud: Eruptions and Lahars of Mount Pinatubo, Philippines, edited by: Newhall, C. G., and Punongbayan R. S., Philippine Institute of Volcanology and Seismology, Queen City, and University of Washington Press, Seattle, 1089–1115, 1996.

Severi, M., Becagli, S., Castellano, E., Morganti, A., Traversi, R., Udisti, R., Ruth, U., Fischer, H., Huybrechts, P., Wolff, E., Parrenin, F., Kaufmann, P., Lambert, F., and Steffensen, J. P.: Synchronisation of the EDML and EDC ice cores for the last 52 kyr by volcanic signature matching, Clim. Past, 3, 367–374, https://doi.org/10.5194/cp-3-367-2007, 2007.

https://doi.org/10.5194/egusphere-2026-3434
Preprint. Discussion started: 9 September 2026

Severi, M., Udisti, R., Becagli, S., Stenni, B., and Traversi, R.: Volcanic synchronisation of the EPICA-DC and TALDICE ice cores for the last 42 kyr BP, Clim. Past, 8, 509–517, https://doi.org/10.5194/cp-8-509-2012, 2012.

Severi, M., Becagli, S., Traversi, R., and Udisti, R.: Recovering paleo-records from Antarctic ice-cores by coupling a continuous melting device and fast ion chromatography, Anal. Chem., 87, 11441–11447, https://doi.org/10.1021/acs.analchem.5b02961, 2015.

Sharpe, M. S., Barker, S. J., Rooyakkers, S. M., Wilson, C. J. N., Chambefort, I., Rowe, M. C., Schipper, C. I., and Charlier, B. L. A.: A sulfur and halogen budget for the large magmatic system beneath Taupō volcano, Contrib. Mineral. Petrol., 177, 95, https://doi.org/10.1007/s00410-022-01959-w, 2022.

Sigl, M., McConnell, J. R., Toohey, M., Curran, M., Das, S. B., Edwards, R., Isaksson, E., Kawamura, K., Kipfstuhl, S., Krüger, K., Layman, L., Maselli, O. J., Motizuki, Y., Motoyama, H., Pasteris, D. R., and Severi, M.: Insights from Antarctica on volcanic forcing during the Common Era, Nat. Clim. Change, 4, 693–697, https://doi.org/10.1038/nclimate2293, 2014.

Sigl, M., Winstrup, M., McConnell, J. R., Welten, K. C., Plunkett, G., Ludlow, F., Büntgen, U., Caffee, M., Chellman, N., Dahl-Jensen, D., Fischer, H., Kipfstuhl, S., Kostick, C., Maselli, O. J., Mekhaldi, F., Mulvaney, R., Muscheler, R., Pasteris, D. R., Pilcher, J. R., Salzer, M., Schüpbach, S., Steffensen, J. P., Vinther, B. M., and Woodruff, T. E.: Timing and climate forcing of volcanic eruptions for the past 2,500 years, Nature, 523, 543–549, https://doi.org/10.1038/nature14565, 2015.

Sigl, M., Fudge, T. J., Winstrup, M., Cole-Dai, J., Ferris, D., McConnell, J. R., Taylor, K. C., Welten, K. C., Woodruff, T. E., Adolphi, F., Bisiaux, M., Brook, E. J., Buizert, C., Caffee, M. W., Dunbar, N. W., Edwards, R., Geng, L., Iverson, N., Koffman, B., Layman, L., Maselli, O. J., McGwire, K., Muscheler, R., Nishiizumi, K., Pasteris, D. R., Rhodes, R. H., and Sowers, T. A.: The WAIS Divide deep ice core WD2014 chronology – Part 2: annual-layer counting (0–31 ka BP), Clim. Past, 12, 769–786, https://doi.org/10.5194/cp-12-769-2016, 2016.

Sigl, M., Toohey, M., McConnell, J. R., Cole-Dai, J., and Severi, M.: Volcanic stratospheric sulfur injections and aerosol optical depth during the Holocene (past 11 500 years) from a bipolar ice-core array, Earth Syst. Sci. Data, 14, 3167–3196, https://doi.org/10.5194/essd-14-3167-2022, 2022.

Sime, L. C., Kohfeld, K. E., Le Quéré, C., Wolff, E. W., de Boer, A. M., Graham, R. M., and Bopp, L.: Southern Hemisphere westerly wind changes during the Last Glacial Maximum: model-data comparison. Quat. Sci. Rev., 64, 104-120, https://doi.org/10.1016/j.quascirev.2012.12.008, 2013.

Souney, J. M., Twickler, M. S., Aydin, M., Steig, E. J., Fudge, T. J., Street, L. V., Nicewonger, M. R., Kahle, E. C., Johnson, J. A., Kuhl, T. W., Casey, K. A., Fegyveresi, J. M., Nunn, R. M., and Hargreaves, G. M.: Core handling, transportation and processing for the South Pole ice core (SPICEcore) project, Ann. Glaciol., 62, 118–130, https://doi.org/10.1017/aog.2020.80, 2021.

Sparks, R. S. J., Self, S., Grattan, J. P., Oppenheimer, C., Pyle, D. M., and Rymer, H.: Super-eruptions: global effects and future threats. Report of a Geological Society of London Working Group, 24 pp., 2005.

Staunton-Sykes, J., Aubry, T. J., Shin, Y. M., Weber, J., Marshall, L. R., Luke Abraham, N., Archibald, A., and Schmidt, A.: Co-emission of volcanic sulfur and halogens amplifies volcanic effective radiative forcing, Atmos. Chem. Phys., 21, 9009–9029, https://doi.org/10.5194/acp-21-9009-2021, 2021.

Steig, E. J., Jones, T. R., Kahle, E., Morris, V., Schauer, A., Vaughn, B., and White, J.: South Pole high resolution ice core water stable isotope record for dD, $d^{18}O$ [dataset], accessed on 25/04/2025, https://doi.org/10.15784/601239, 2019.

Stevenson, J. A., Millington, S. C., Beckett, F. M., Swindles, G. T., and Thordarson, T.: Big grains go far: understanding the discrepancy between tephrochronology and satellite infrared measurements of volcanic ash, Atmos. Meas. Tech., 8, 2069–2091, https://doi.org/10.5194/amt-8-2069-2015, 2015.

Stoffel, M., Khodri, M., Corona, C., Guillet, S., Poulain, V., Bekki, S., Guiot, J., Luckman, B. H., Oppenheimer, C., Lebas, N., Beniston, M., and Masson-Delmotte, V.: Estimates of volcanic-induced cooling in the Northern Hemisphere over the past 1,500 years, Nat. Geosci., 8, 784-788 https://doi.org/10.1038/ngeo2526, 2015.

Stothers, R. B.: The great Tambora eruption in 1815 and its aftermath, Science, 224, 1191–1198, https://doi.org/10.1126/science.224.4654.1191, 1984.

Svensson, A., Dahl-Jensen, D., Steffensen, J. P., Blunier, T., Rasmussen, S. O., Vinther, B. M., Vallelonga, P., Capron, E., Gkinis, V., Cook, E., Kjær, H. A., Muscheler, R., Kipfstuhl, S., Wilhelms, F., Stocker, T. F., Fischer, H., Adolphi, F., Erhardt, T., Sigl, M., Landais, A., Parrenin, F., Buizert, C., McConnell, J. R., Severi, M., Mulvaney, R., and Bigler, M.:

https://doi.org/10.5194/egusphere-2026-3434
Preprint. Discussion started: 9 September 2026

Bipolar volcanic synchronization of abrupt climate change in Greenland and Antarctic ice cores during the last glacial period, Clim. Past., 16, 1565-1580, https://doi.org/10.5194/cp-16-1565-2020, 2020.

Svensson, A., Vettoretti, G., Lin, J.-M., Sinnl, G., Dahl-Jensen, D., Steffensen, J. P., Rasmussen, S. O., Vinther, B., Hvidberg, C., Kjær, H. A., Gkinis, V., Cook, E., Lohmann, J., Melcher, J. O., Halkjær, S., Kipfstuhl, S., Wilhelms, F., Adolphi, F., Fischer, H., Bigler, M., Sigl, M., Landais, A., Bouchet, M., Klüssendorf, A., Parrenin, F., Mulvaney, R., Wolff, E., Burke, A., Innes, H., Severi, M., Buizert, C., McConnell, J. R., Chellman, N., Wensman, S., Beer, J., Oyabu, I., and Muscheler, R.: Bipolar volcanic ice-core synchronization of the entire last glacial period. Quat. Sci. Rev., 375, 109755, https://doi.org/10.1016/j.quascirev.2025.109755, 2026.

Textor, C., Graf, H.-F., Herzog, M., and Oberhuber, J. M.: Injection of gases into the stratosphere by explosive volcanic eruptions, J. Geophys. Res.: Atmos., 108, 4606, https://doi.org/10.1029/2002JD002987, 2003.

Timmreck, C., Graf, H.-F., Lorenz, S. J., Niemeier, U., Zanchettin, D., Matei, D., Jungclaus, J. H., and Crowley, T. J.: Aerosol size confines climate response to volcanic super-eruptions, Geophys. Res. Lett., 37(24), L24705, https://doi.org/10.1029/2010GL045464, 2010.

Toohey, M., Krüger, K., and Timmreck, C.: Volcanic sulfate deposition to Greenland and Antarctica: a modeling sensitivity study, Geophys. Res. Atmos., 118, 4788-4800, https://doi.org/10.1002/jgrd.50428, 2013.

Toohey, M. and Sigl, M.: Volcanic stratospheric sulfur injections and aerosol optical depth from 500 BCE to 1900 CE, Earth Syst. Sci. Data, 9, 809–831, https://doi.org/10.5194/essd-9-809-2017, 2017.

Traversi, R., Becagli, S., Castellano, E., Maggi, V., Morganti, A., Severi, M., and Udisti, R.: Ultra-sensitive Flow Injection Analysis (FIA) determination of calcium in ice cores at ppt level, Anal. Chim. Acta, 594(2), 219–225, https://doi.org/10.1016/j.aca.2007.05.022, 2007.

Ulayottil Venugopal, A., Bertler, N.A., Pyne, R. L., Kjær, H. A., Winton, V. H. L., Mayewski, P. A., Cortese, G.: RICE ice core calcium data for the last glacial period (83-26 ka BP) [dataset], accessed on 13/04/2024. https://doi.org/10.1594/PANGAEA.941413. 2022.

Unni, C., and Schilling, J.: Cl and Br degassing by volcanism along the Reykjanes Ridge and Iceland. Nature, 272(5648), 19–23. https://doi.org/10.1038/272019a0, 1978.

Urbini, S., Cafarella, L., Zirizzotti, A., Bianchi, C., Tabacco, I., and Frezzotti, M.: Location of a new ice core site at Talos Dome (East Antarctica), Ann. Geophys., 49, 1133–1138, 2006.

Van Eaton, A. R.: Dynamics of large, wet volcanic clouds: the 25.4 ka Oruanui eruption of Taupo volcano, New Zealand, Ph.D thesis, Victoria University of Wellington, Wellington, New Zealand, 2012.

Van Eaton, A. R., and Wilson, C. J. N.: The nature, origins and distribution of ash aggregates in a large-scale wet eruption deposit: Oruanui, New Zealand. J. Volcanol. Geotherm. Res., 250, 129-154, https://doi.org/10.1016/j.jvolgeores.2012.10.016, 2013.

Van Eaton, A. R., Herzog, M., Wilson, C. J. N., and McGregor, J.: Ascent dynamics of large phreatomagmatic eruption clouds: the role of microphysics, J. Geophys. Res.: Sol. Earth, 117, B03203, https://doi.org/10.1029/2011JB008892, 2012.

Vandergoes, M. J., Hogg, A. G., Lowe, D. J., Newnham, R. M., Denton, G. H., Southon, J., Barrell, D. J. A., Wilson, C. J. N., McGlone, M. S., Allan, A. S. R., Almond, P. C., Petchey, F., Dabell, K., Dieffenbacher-Krall, A. C., and Blaauw, M.: A revised age for the Kawakawa/Oruanui tephra, a key marker for the Last Glacial Maximum in New Zealand, Quat. Sci. Rev., 74, 195–201, https://doi.org/10.1016/j.quascirev.2012.11.006, 2013.

Veres, D., Bazin, L., Landais, A., Toyé Mahamadou Kele, H., Lemieux-Dudon, B., Parrenin, F., Martinerie, P., Blayo, E., Blunier, T., Capron, E., Chappellaz, J., Rasmussen, S. O., Severi, M., Svensson, A., Vinther, B., and Wolff, E. W.: The Antarctic ice core chronology (AICC2012): an optimized multi-parameter and multi-site dating approach for the last 120 thousand years, Clim. Past, 9, 1733-1748, https://doi.org/10.5194/cp-9-1733-2013, 2013.

Vidal, C. M., Métrich, N., Komorowski, J.-C., Pratomo, I., Michel, A., Kartadinata, N., Robert, V., and Lavigne, F.: The 1257 Samalas eruption (Lombok, Indonesia): the single greatest stratospheric gas release of the Common Era, Sci. Rep. 6, 34868, https://doi.org/10.1038/srep34868, 2016.

von Glasow, R., Bobrowski, N., and Kern, C.: The effects of volcanic eruptions on atmospheric chemistry, Chem. Geol., 263, 131-142, https://doi.org/10.1016/j.chemgeo.2008.08.020, 2009.

Waelkens, C. M., Stix, J., Monteleone, B., and Burckel, P.: Efficient release of bromine by super-eruptions, Geology, 49, 1416–1420, https://doi.org/10.1130/G49114.1, 2021.

https://doi.org/10.5194/egusphere-2026-3434
Preprint. Discussion started: 9 September 2026

Wegner, A., Fischer, H., Delmonte, B., Petit, J.-R., Erhardt, T., Ruth, U., Svensson, A., Vinther, B., and Miller, H.: The role of seasonality of mineral dust concentration and size on glacial/interglacial dust changes in the EPICA Dronning Maud Land ice core, J. Geophys. Res.: Atmos., 120, 9916–9931, https://doi.org/10.1002/2015JD023608, 2015.

Wilhelms, F., Kipfstuhl, J., Miller, H., Heinloth, K., and Firestone, J.: Precise dielectric profiling of ice cores: a new device with improved guarding and its theory, J. Glaciol., 44, 171–174, https://doi.org/10.3189/S002214300000246X, 1998.

Wilson, C. J. N.: The 26.5 ka Oruanui eruption, New Zealand: an introduction and overview, J. Volcanol. Geotherm. Res., 112, 133–174, https://doi.org/10.1016/S0377-0273(01)00239-6, 2001.

Wilson, C.J.N., Blake, S., Charlier, B.L.A., Sutton, A.N. The 26.5 ka Oruanui eruption, Taupo Volcano, New Zealand: development, characteristics and evacuation of a large rhyolitic magma body. J. Petrol., 47(1), 35–69. https://doi.org/10.1093/petrology/egi066, 2006.

Wilson, C. J. N., Cooper, G. F., Chamberlain, K. J., Barker, S. J., Myers, M. L., Illsley-Kemp, F., and Farrell, J.: No single model for supersized eruptions and their magma bodies, Nat. Rev. Earth Environ., 2, 610-627, https://doi.org/10.1038/s43017-021-00191-7, 2021.

Wilson, L. and Huang, T.C.: The influence of shape on the atmospheric settling velocity of volcanic ash particles. Earth Planet. Sci. Lett., 44(2), 311–324, https://doi.org/10.1016/0012-821X(79)90179-1, 1979.

Wilson, R., Anchukaitis, K., Briffa, K. R., Büntgen, U., Cook, E., D'Arrigo, R., Davi, N., Esper, J., Frank, D., Gunnarson, B., Hegerl, G., Helama, S., Klesse, S., Krusic, P. J., Linderholm, H. W., Myglan, V., Osborn, T. J., Rydval, M., Schneider, L., Schurer, A., Wiles, G., Zhang, P., and Zorita, E.: Last millennium northern hemisphere summer temperatures from tree rings: Part I: The long term context, Quat. Sci. Rev., 134, 1-18. https://doi.org/10.1016/j.quascirev.2015.12.005, 2016.

Winski, D. A., Fudge, T. J., Ferris, D. G., Osterberg, E. C., Fegyveresi, J. M., Cole-Dai, J., Thundercloud, Z., Cox, T. S., Kreutz, K. J., Ortman, N., Buizert, C., Epifanio, J., Brook, E. J., Beaudette, R., Severinghaus, J., Sowers, T., Steig, E. J., Kahle, E. C., Jones, T. R., Morris, V., Aydin, M., Nicewonger, M. R., Casey, K. A., Alley, R. B., Waddington, E. D., Iverson, N. A., Dunbar, N. W., Bay, R. C., Souney, J. M., Sigl, M., and McConnell, J. R.: The SP19 chronology for the South Pole Ice Core – Part 1: volcanic matching and annual layer counting, Clim. Past, 15, 1793–1808, https://doi.org/10.5194/cp-15-1793-2019, 2019.

Winstrup, M., Vallelonga, P., Kjær, H. A., Fudge, T. J., Lee, J. E., Riis, M. H., Edwards, R., Bertler, N. A. N., Blunier, T., Brook, E. J., Buizert, C., Ciobanu, G., Conway, H., Dahl-Jensen, D., Ellis, A., Emanuelsson, B. D., Hindmarsh, R. C. A., Keller, E. D., Kurbatov, A. V., Mayewski, P. A., Neff, P. D., Pyne, R. L., Simonsen, M. F., Svensson, A., Tuohy, A., Waddington, E. D., and Wheatley, S.: A 2700-year annual timescale and accumulation history for an ice core from Roosevelt Island, West Antarctica, Clim. Past, 15, 751–779, https://doi.org/10.5194/cp-15-751-2019, 2019.

Wolff, E. W., Cook, E., Barnes, P. R. F., and Mulvaney, R.: Signal variability in replicate ice cores, J. Glaciol., 51, 462–468, https://doi.org/10.3189/172756505781829197, 2005.

Verkerk, M., Aubry, T. J., Smith, C., Hopcroft, P. O., Sigl, M., Tierney, J. E., Anchukaitis, K., Osman, M., Schmidt, A., Toohey, M.: Using reduced-complexity volcanic aerosol and climate models to produce large ensemble simulations of Holocene temperature. Clim. Past, 21(10), 1755–1778, https://doi.org/10.5194/cp-21-1755-2025, 2025.